Implications of Glacier Recession for Water Resources

Christopher D. Frans

A dissertation
submitted in partial fulfillment of the
requirements for the degree of

Doctor of Philosophy

University of Washington
2015

Reading Committee:
Erkan Istanbulluoglu, Chair
Stephen J. Burges
Dennis P. Lettenmaier

Program Authorized to Offer Degree:
Civil and Environmental Engineering

University of Washington

Abstract

Implications of glacier recession for Water Resources

Christopher D. Frans

Chair of the Supervisory Committee:
Associate Professor Erkan Istanbulluoglu
Department of Civil and Environmental Engineering

Numerical simulation models of hydrologic processes can be effective tools for inferring the consequences of environmental change for water resource systems. In river basins that originate in partially glacierized catchments traditional widely used hydrological modeling approaches are not suitable for prediction of these consequences as they lack a representation of the storage and movement of glacier ice reservoirs on the land surface. In the first part of the dissertation, a framework for applying a recently developed complex glacio-hydrological model suitable for these predictions is described. This methodology was applied to a well instrumented heavily glacierized watershed in the Bolivia Andes. Using long-term projections of climate change constructed from CMIP5 Global Climate Model (GCM) outputs using a stochastic weather generator the model framework was applied to predict evolving hydrological processes from 1987-2100. These predictions served as a baseline for testing sensitivities of hydrological response to model structure and parameter selection. The importance of local insitu data to guide calibration and parameter selection of complex glacio-hydrological models is demonstrated.

Debris cover on glaciers can retard ablation on the surface of glaciers, significantly affecting the rate of response to warming temperatures. In the second part of this work, algorithms that represent the storage and conductance of heat through supraglacial debris on glacier surfaces

were developed into the glacio-hydrological model described in part 1. These model developments were tested against point measurement of ablation underneath debris. Model simulations indicate the relative role of debris cover on the evolution of glacier area and summer discharge in upland drainages in the Hood River Basin, OR. Furthermore, this work is used to demonstrate strong inter-decadal patterns of glacio-hydrological processes that are superimposed on the response to a longer term trend from a warming climate. This highlights the timescales of analysis required to evaluate hydrological response to glacier recession.

The third and last topic of this dissertation focuses on regional patterns of glacio-hydrological response in the Pacific Northwest United States. This chapter describes a modeling study with specific emphasis on the following research objectives: (1) characterize how hydrological response to glacier recession varies within the region; (2) identify vulnerable downstream locations in space and time; and (3) quantify at which spatial scales glacier melt is a significant contributor to discharge patterns. The long-term coupled glacio-hydrological response for a sample of watersheds that span sharp climatic gradients (maritime to continental), a range of temperate northern latitudes (45-49°), and varying local physiological attributes (e.g., range of elevations, wind/leeward) in the Pacific Northwestern United States (PNW) is predicted.

ACKNOWLEDGEMENTS

I thank my advisor Dr. Erkan Istanbulluoglu for his mentorship, patience and guidance as I developed as a scientist through the course of my Master's and Doctoral research activities. I am grateful for the many opportunities he provided for my professional and personal development.

I thank Dr. Dennis P. Lettenmaier for his mentorship and guidance as I became a member of the hydrology research community. I am especially grateful for his guidance in the development of my writing style and instruction in maintaining a broader perspective in the scope of research.

I thank Dr. Stephen J. Burges who educated me on aspects of hydrological research that are sometimes overlooked. Notably, these include the value of quality observational data and the consideration of a broader engineering context as a component of critical thinking in applied research.

Thank you to all committee members (Dr. Erkan Istanbulluoglu, Dr. Dennis P. Lettenmaier, Dr. Stephen J. Burges**,** Dr. Andrew Fountain, Dr. Matthew Bachmann, Dr. Michelle Koutnik, and Dr. Howard Conway) for their participation and feedback in this work. Thank you to Dr. Thomas Condom, Dr. Bibi Naz, Dr. Garry Clarke, and Dr. Jon Riedel for their participation and research activities which made this work possible.

Thank you to Homero Flores, Omer Yetemen, Ronda Strauch, Sai Nudurupati, Matt Stumbaugh, Nicoleta Cristea, Christina Bandaragoda, Francisco Munoz, Vimal Mishra, Yegor Malinovskiy, and Xiaochi Zhou for their friendship and endless support through my time at UW. Thank you to all members of the Land Surface Hydrology, Mountain Hydrology, and Computational Hydrology research groups in the Civil Engineering department at UW for making my time in Wilcox Hall enjoyable.

I thank my family for their overwhelming support.

DEDICATION

This dissertation is dedicated to Elise and Frederick.

.

TABLE OF CONTENTS

LIST OF FIGURES

CHAPTER 4

LIST OF TABLES

CHAPTER 1: INTRODUCTION

1.1. Background

Pervasive recession of alpine glaciers has been observed across the globe in recent decades (Kaser et al. 2005; Gardner et al., 2013). This recession is projected to continue throughout the 21st century in response to continued climate warming (Radic and Hock, 2011). Recession of glaciers in partially glacierized headwater catchments has the potential to affect watershed dynamics in a range of ways, including reduced low flows (Stahl and Moore, 2006), rapid erosion of exposed steep soils, increased sediment transport (Moore et al., 2009), and ecosystem succession (Chapin et al., 1994). Moreover, in the context of water resource management, declining glacier area translates to a decrease in seasonal water storage for many populated areas located downstream from these dynamic cryospheric systems (Barnett et al., 2005).

Partially glacierized watersheds redistribute wet season precipitation to streamflow at times of the year when precipitation is at a minimum (Fountain and Tangborn, 1985). This glacier melt buffering of low flows is further enhanced during dry years as a greater area of glacier surfaces is exposed to melting for longer durations during the melt season due to a reduction of and earlier depletion of the seasonal snowpack. As glaciers respond to a warming climate, this contribution is expected to increase initially, however reductions in glacier area will eventually overcome enhanced rates of melting from warmer temperatures. Diagnosing the past and current glacier melt signature in watershed hydrology is complicated by a lack of long-term glaciological and discharge observations. Moreover, discharge observations are often located at significant distances from the glacierized headwaters, providing difficulty for deciphering the glacier melt signal outside of the most extreme years. Furthermore, inter-annual and decadal variability of precipitation presents a challenge in detecting changes in glacier area in response to persistent increasing air temperatures.

Various methods have been applied to describe the role of glaciers in watershed hydrology (La Frenierre and Mark, 2014). The simplest approach, relates discharge volumes measured near the glacier terminus to measurements collected further downstream (e.g., Gascoin et al., 2011; Nolin et al., 2010). This method is limited by the accuracy of discharge measurements in proglacial streams as high sediment loads and dynamic changes to bed and channel geometries

change the relationship between stage and discharge. Methods that utilize geochemical tracers (e.g., Mark and Seltzer, 2003; Nolin et al., 2010) can be advantageous as they do not require continuous hydrologic and meteorological measurements; however are restricted by a limited number of chemically distinct end members representing different sources of watershed discharge.

In areas where long-term glaciological measurement programs have been established, measurements of ice ablation can be compared with observed downstream runoff. Ablated glacier mass can be measured through networks of ablation stakes or estimated through changes in surface elevations from geodetic and remotely sensed data (Shuttle Radar Topography Mission, SRTM; Advanced Spaceborne Thermal Emission and Reflection Radiometer, ASTER). Limitations of these approaches lie in the ability to interpolate point measurements, coarse temporal sampling (aerial imagery), and the coarse spatial resolution and limited vertical accuracy of remotely sensed products. Additionally, assumptions of losses of water between the glacier source and measured discharge location are required.

Hydrologic models provide a framework for evaluating the proportional contribution of glacier melt water to watershed discharge and have the potential to fill knowledge gaps in observational data through simulation of glacio-hydrologic processes. Additionally, models are used to infer the sensitivity of the system to changing climatic conditions. In many cases, existing hydrologic models with a history of snowmelt related applications have been updated to include a representation of glaciological processes (e.g., HBV; DHSVM; WATFLOOD; SRM; TOPKAPI among others). These models span a range of complexity in spatial discretization, ranging from model structures that divide watersheds into lumped areas with similar physical characteristics (e.g., hydrologic response units) to models that fully distribute all parameters on a rectilinear grid. Additionally, modeling methods include a range of complexity in simulating snow and ice accumulation and ablation processes. These range from models that relate air temperature to melt rates (temperature index models) to algorithms that explicitly simulate mass and energy fluxes on snow and ice surfaces (surface energy balance, SEB). With respect to glacier extent, many models update glacier area through offline auxiliary information (e.g., historical estimates of glacier area, future projections of glacier area from a glacier model) or represent changes in glacier area through empirical volume-area scaling methods, while few

have integrated a more explicit representation of glacier dynamics (e.g., Immerzeel et al., 2012; Naz et al., 2014).

This dissertation draws upon recent developments in coupled glacio-hydrologic modeling. It uses modeling that is supplemented with and constrained by available glaciological and hydrological observational datasets. Naz et al. (2014) describes the integration of a spatially distributed glacier dynamics model (Clarke et al., 2015) into the Distributed Hydrology Soil Vegetation Model (DHSVM, Wigmosta et al., 1994). The modified DHSVM allows the continuous explicit simulation of accumulation and ablation of snow and ice, dynamic ice flow, and all watershed hydrologic processes (e.g., evapotranspiration, subsurface flow, surface runoff, channel routing and discharge) in a fully distributed framework (Fig. 1).

Using the methodology first described in Naz et al. (2014), and updated through efforts described in this dissertation, the role of glaciers and the differential response of coupled glacio-hydrologic processes are described for tropical watersheds in the South American Andes and temperate maritime and continental watersheds of western North America.

1.2. Structure of the Dissertation

This dissertation investigates the spatial and temporally varying role of glaciers in river basin hydrology using a numerical modeling approach. Chapters 2-4 are self-contained papers, each with its own abstract, conclusions, and references. Chapter 2 is under review for publication in the journal *Water Resources Research*. Chapter 3 is under review for publication in the journal *Hydrological Processes*. Chapter 4 is in preparation to be submitted for publication.

References

Barnett, T.P., J.C. Adam, and D.P. Lettenmaier. Potential impacts of a warming climate on water availability in snow-dominated regions. Nature 438.7066 (2005): 303-309.

Chapin, F. S., Walker, L. R., Fastie, C. L., & Sharman, L. C. (1994). Mechanisms of primary succession following deglaciation at Glacier Bay, Alaska. Ecological Monographs, 149-175.

Clarke, G. K., A.H. Jarosch, F. S. Anslow, V. Radić, and B. Menounos. 2015. Projected deglaciation of western Canada in the twenty-first century. Nature Geoscience, 8, 372-377, doi:10.1038/ngeo2407.

Fountain, A. G., & Tangborn, W. V. (1985). The effect of glaciers on streamflow variations. Water Resources Research, 21(4), 579-586.

Gardner, A. S., Moholdt, G., Cogley, J. G., Wouters, B., Arendt, A. A., Wahr, J., Berthier, E., Hock, R., Pfeffer, W. T., Kaser, G., Ligtenberg, S. R. M., Bolch, T., Sharp, M. J., Hagen, J. O., van den Broeke, M. R., and Paul, F.: A reconciled estimate of glacier contributions to sea level rise: 2003 to 2009, Science, 340, 852–857, doi:10.1126/science.1234532, 2013.

Gascoin, S., Kinnard, C., Ponce, R., Macdonell, S., Lhermitte, S., & Rabatel, A. (2011). Glacier contribution to streamflow in two headwaters of the Huasco River, Dry Andes of Chile. The Cryosphere, (5), 1099-1113.

Immerzeel, W. W., Van Beek, L. P. H., Konz, M., Shrestha, A. B., & Bierkens, M. F. P. (2012). Hydrological response to climate change in a glacierized catchment in the Himalayas. Climatic change, 110(3-4), 721-736.

Kaser, G., Cogley, J. G., Dyurgerov, M. B., Meier, M. F., & Ohmura, A. (2006). Mass balance of glaciers and ice caps: Consensus estimates for 1961–2004. *Geophysical Research Letters*, 33(19).

La Frenierre, J., & Mark, B. G. (2014). A review of methods for estimating the contribution of glacial meltwater to total watershed discharge. *Progress in Physical Geography*, 0309133313516161.

Mark, B. G., & Seltzer, G. O. (2003). Tropical glacier meltwater contribution to stream discharge: a case study in the Cordillera Blanca, Peru. Journal of Glaciology, 49(165), 271-281.

Moore, R. D., Fleming, S. W., Menounos, B., Wheate, R., Fountain, A., Stahl, K., & Jakob, M. (2009). Glacier change in western North America: influences on hydrology, geomorphic hazards and water quality. *Hydrological Processes*, 23(1), 42-61.

Naz, B. S., Frans, C. D., Clarke, G. K. C., Burns, P., & Lettenmaier, D. P. (2014). Modeling the effect of glacier recession on streamflow response using a coupled glacio-hydrological model. Hydrology & Earth System Sciences, 10(4).

Nolin AW, Phillippe J, Jefferson A, Lewis SL (2010) Present-day and future contributions of glacier runoff to summertime flows in a Pacific Northwest watershed: implications for water resources. Water Resources Research 46:W12509

Radić, V., & Hock, R. (2011). Regionally differentiated contribution of mountain glaciers and ice caps to future sea-level rise. *Nature Geoscience*, 4(2), 91-94.

Stahl, K., & Moore, R. D. (2006). Influence of watershed glacier coverage on summer streamflow in British Columbia, Canada. Water Resources Research, 42(6).

Wigmosta, M. S., Vail, L. W., & Lettenmaier, D. P. (1994). A distributed hydrology-vegetation model for complex terrain. *Water Resources Research*, 30(6), 1665-1679.

CHAPTER 2: PREDICTING GLACIO-HYDROLOGIC CHANGE IN THE HEADWATERS OF THE ZONGO RIVER, CORDILLERA REAL, BOLIVIA[1]

Abstract

In many partially glacierized watersheds glacier recession driven by a warming climate could lead to complex patterns of streamflow response over time, often marked with rapid increases followed by sharp declines, depending on initial glacier ice cover and the rate of climate change. Capturing such "phases" of hydrologic response is critical in regions where communities rely on glacier meltwater, particularly during low flows. In this paper, we investigate glacio-hydrologic response in the headwaters of the Zongo River, Bolivia, under climate change using a distributed glacio-hydrological model over the period of 1987-2100. Model predictions are evaluated through comparisons with satellite-derived glacier extent estimates, glacier surface velocity, in-situ glacier mass balance, surface energy flux, and stream discharge measurements. Historically (1987-2010), on average glacier melt is predicted to account for 27% of annual runoff, and 61% of dry season (JJA) runoff as the relative glacier cover reduced from 35% to 21% of the watershed. In the future, annual and dry season discharge is projected to decrease by 4%, and 27% by midcentury, and 25%, and 57% by the end of the century, respectively, following the loss of 81% of the ice in the watershed. Modeled runoff patterns evolve through the interplay of positive and negative trends in glacier melt and increased evapotranspiration as the climate warms. Sensitivity analyses demonstrate that the selection of model surface energy balance parameters greatly influences the trajectory of hydrological change projected during the first half of the 21st century. These model results underscore the importance of coupled glacio-hydrology modeling.

[1] This chapter has been submitted and is under review for journal publication:

Frans, C., E. Istanbulluoglu, D.P. Lettenmaier, B. Naz, G. Clarke, T. Condom, P. Burns, and A. Nolin (under review), Hydrologic response to glacier recession in the Cordillera Real, Bolivia, *Water Resources Research.*

2.1 Introduction

Recession of alpine glaciers has been observed across much of the globe in recent decades [*Kaser et al.*, 2006; *Gardner et al.*, 2013; *IPCC*, 2014]. Glacier recession is projected to continue throughout the 21st century in response to continued climate warming [*Radić and Hock*, 2011] resulting in decreased seasonal water storage for many populated areas located downstream from these dynamic cryospheric systems [*Barnett et al*., 2005]. Some of the largest decreases in glacier mass have been observed in the tropical glaciers of the South American Andes, which have been receding rapidly (-0.76 m w.e. yr^{-1}) since the late 1970s in response to increasing air temperature [*Rabatel et al*., 2013].

Predictions from Global Climate Models (GCMs) indicate that the observed warming will continue, and will be amplified at higher altitudes in the lower troposphere in the Andean cordilleras of Ecuador, Peru, Bolivia and Northern Chile [*Bradley et al*., 2006]. The glaciers of the tropical Andes are closely linked to the water resources of the region due to their proximity to highly populated areas and the ability of glacier melt water to buffer highly seasonal precipitation patterns [*Vuille et al.*, 2008]. Meltwater from the glaciers in the Andes plays an important role in socio-economic infrastructure of the region. It provides municipal and industrial water supply, irrigation water, hydropower, and supports ecosystem services [*Chevallier et al*., 2011; *Mark and Seltzer*, 2003; *Cauvy-Fraunié et al*., 2013; *Vergara et al*., 2007].

Glacier melt is manifested by a unique signature in catchment runoff response. The melting of snow and ice modulates seasonal availability of water by redistributing wet season precipitation into runoff during the dry season. In contrast to seasonal snow, glaciers often produce anomalously large runoff during dry and warm years [*Fountain and Tangborn*, 1985]. For this reason, as the climate warms, runoff is expected to increase initially as a result of increased rates of ablation per unit area (typically for several decades, depending on the particulars of the glacier and climate), however the glacier's area will eventually reduce to a point where runoff will decline thereafter [e.g., *Huss et al.*, 2008; *Lambrecht and Mayer*, 2009; *Moore et al.*, 2009; Baraer et al., 2012].

Understanding the distinct phases of the response of partially glacierized watersheds to glacier ice loss, and estimating the current phases of transitioning watersheds remains an important challenge in regions where glacial melt supplies anthropogenic and ecologic systems

downstream. Glaciological methods, including field measurements, remote sensing and modeling, have been applied to describe the relative role of glaciers in these changing systems [*La Frenierre and Mark*, 2014]. Previous studies analyzing the contribution of glaciers to water resources in the Andes have utilized multi-temporal estimates of glacier area derived from satellite and aerial imagery [e.g., *Soruco et al.*, 2009; *Burns and Nolin*, 2014] that describe glacier change relative to total watershed drainage area. Remote sensing can be an effective tool for monitoring glacier change over annual [e.g., *Rabatel et al*., 2012] or decadal [e.g., *Soruco et al.*, 2009] timescales, although used in isolation, it reveals little about the relative and changing contributions of glacier melt to watershed hydrology because it provides only estimates of glacier spatial extent and volume. These estimates reflect changes at coarse temporal scales and do not account for the interaction and the relative role of melt water with the non-glacierized watershed between the glaciers and downstream locations. Alternatively, statistical trend analyses of time series of discharge for individual watersheds have been applied to identify trends and phases of hydrologic response to glacier recession [e.g., *Baraer et al*., 2012; *Stahl and Moore*, 2006; *Casassa et al*., 2009]. However, many partially glacierized watersheds lack observations of discharge of suitable length, which is detrimental, because glacier recession and its hydrologic response often occur over long periods of time. Moreover, time series of discharge observations alone do not allow identification of the mechanisms that control changing inter-annual and decadal variations in discharge from transitional partially glacierized river basins.

Efforts have been made to model the coupled glacio-hydrologic behavior of partially glacierized high Andes watersheds using relatively simple hydrologic models that use spatially "lumped" and empirical representations of watershed processes [e.g., *Pouyaud et al.*, 2005; *Juen et al*., 2007; *Suarez et al.*, 2008; *Baraer et al*., 2012; *Condom et al*., 2012; *Chevallier et al*., 2011; *Soruco et al*., 2015]. Some modeling studies have used volume-area scaling relationships to simulate changes in glacier extent with changes in glacier mass [*Baraer et al*., 2012; *Condom et al*., 2012]. However, the accuracy of this method is debated because scaling parameters evolve over time under transient glacier change [*Radić et al*., 2007; *Adhikari and Marshall*, 2012], vary spatially [*Huss and Farinotti*, 2012], and do not represent characteristics of individual glaciers (e.g., local topographic controls on surface geometry). Most glacio-hydrologic studies in the Andes have not explicitly considered the role of glacier dynamic ice flow in the simulation of glacier area. While neglecting the influences of glacier dynamics on glacier area may be

justifiable for near term predictions of glacier runoff production, it is essential for accurately predicting the effects of evolving glacier area over long periods of time for the prediction of watershed hydrology [*Huss et al*., 2008; *Immerzeel et al*., 2012; *Naz et al*., 2014; *Uhlmann et al.*, 2012a,b].

Understanding and predicting the multi-faceted nature of glacier response (area, volume, discharge) and its coupling with watershed hydrology under climate variability and change is crucial in regions with rapidly melting glaciers. In this paper we present a holistic approach to investigate implications of climate change on glacierized watersheds by integrating glaciological field observations, remote sensing observations of changing glacier extent, and distributed glacio-hydrological modeling guided and constrained by these observations. We use our approach to infer long term hydrologic change in the headwaters of the Zongo River located near La Paz, Bolivia in the South American Andes. The main objectives of this study are (1) to investigate and quantify the glacio-hydrologic response to historic climatic conditions in a watershed where glacier melt has had a strong influence on discharge; (2) to evaluate and predict how this glacio-hydrologic system will change under future climate conditions; and (3) demonstrate the influence of parameter selection and calibration on model projections using an advanced glacio-hydrology simulation model.

2.2 Study Site

The headwaters of the Zongo River (16 °S, 68 °W) are located in the Cordillera Real, 30 km north of La Paz (the capital city of Bolivia) and El Alto, a large and rapidly expanding urban area (Fig 1). The 14 km^2 drainage area is defined by the crest of the Cordillera Real along the southwestern perimeter of the catchment (which divides the Altiplano to the west from Amazon basin to the east) and manmade conveyance channels on the northeastern slopes that divert runoff to a reservoir located near the middle of the catchment (Fig. 1). The study domain includes the entire drainage area above the Zongo Reservoir. This extends the domain beyond previous hydrological studies in the area that focused modeling and observational analyses on the 3 km^2 drainage area above the Tubo discharge measurement location (Fig. 1) below the terminus of Zongo glacier [e.g., *Ribstein et al*., 1994; *Francou et al*., 1995; *Wagnon et al*., 1999; *Sicart et al*., 2011]. Elevations within the basin range from 4,700 m a.s.l. to 6,088 m at the summit of Huayna Potosi. In the watershed glacier cover decreased from 35% in 1987 to 21% in

2010 (estimates derived from Landsat imagery, Section 2.4.4). The catchment is characterized by bare rock and thin soils. Where vegetation is present, it consists of sparse grasses (25%) and shrubs (17%). The catchment is the upper reach of a hydroelectric project consisting of 10 downstream power generation facilities in series along the Zongo River. These facilities have a total capacity of 174.6 MW, and provide much of the electricity for the La Paz area [*Caballero et al*., 2004]. Runoff is stored in the reservoir (Fig. 1) and is released during the dry season.

The watershed is located in the outer tropics, with a climate characterized by distinct seasonal variability in atmospheric moisture. Documenting this climate, precipitation and temperature have been measured at the Plataforma and Mevis station locations (Fig. 1), respectively, for an extended period of time. During austral summer, November to March, wet and relatively warm (2.5 °C on average, calculated from half-hourly observations at the Mevis station, 4750 m 1995-2010) conditions prevail while dry and slightly cooler (1.2 ° C on average) periods persist during austral winter, June to September. The seasonal variation of daily average temperature is relatively small (<8 deg C, *Sicart et al*., [2011]) while precipitation and atmospheric moisture follow a strong seasonal pattern. Mean annual precipitation observed at the Plataforma observation location (4,750 m) for 1971-2003 is 805 mm, 77 percent of which occurred between November and March.

Frequent cloud cover during the summer, when the extraterrestrial solar radiation flux is at its maximum, attenuates the seasonal variability in shortwave radiation at the land surface in this region. Nonetheless, clear conditions during the wet season (summer) at this latitude (high sun elevation) and altitude (low optical depth) of the study site lead to very high downward shortwave radiation (mean daily values in the summer are ~80 $W m^{-2}$ less than extraterrestrial irradiance according to *Sicart et al*., [2005]). Downward longwave radiation follows the seasonality of humidity and cloud cover, with a maximum during the summer and minimum during the winter. Clear sky emissivity is low at this high altitude, which promotes net losses of longwave radiation at the surface of snow and ice, providing significant control over surface energy dynamics during winter [*Sicart et al.*, 2005].

During the wet season, precipitation is largely associated with advection of moist air from the eastern interior continent linked with the South American monsoon [*Garreaud et al.*, 2009]. Wet season precipitation varies inter-annually with sea surface temperature (SST) of the equatorial Pacific Ocean. At times of high sea surface temperatures offshore (El Niño), advection

of moisture from the east is suppressed through increased westerly atmospheric flow, leading to below average wet season precipitation [*Vuille et al.*, 2000]. During El Niño anomalies, glacier mass balance is most frequently negative, as precipitation in the form of snow largely controls not only the mass, but the energy budget of the glaciers as fresh snow increases the reflection of incoming solar radiation [*Sicart et al*., 2011]. During La Niña years the glacier mass balance is typically near equilibrium or slightly positive [*Francou et al*., 2003]. Glacier ablation occurs throughout the year. Peak glacier ablation occurs during the transitional period leading into the wet season in the austral summer, after which fresh snowfall covers a large fraction of the glacier surface. During the wet season watershed discharge is dominated by rainfall, transient snow melt [*Lejeune et al*., 2007], and to a lesser extent, glacier melt at the lowest elevations on the glaciers. Glacier ablation is most critical to discharge during the dry season when precipitation reaches a minimum [e.g., *Ribstein et al*., 1995; *Wagnon et al*., 1999; *Sicart et al.*, 2011].

2.3 Approach

2.3.1 Glacio-Hydrological Model

To simulate the glacial and hydrologic processes across the watershed we used the Distributed Hydrology Soil Vegetation Model (DHSVM, *Wigmosta et al*., 1994), coupled with a glacier dynamics model [*Clarke et al*., 2015] as described by *Naz et al.*, [2014]. A brief description of the components of the models and their coupling is provided herein, with model components and linkages shown in Figure 2. For a complete description of the model, the reader is referred to *Naz et al.* [2014]. DHSVM is a fully distributed physically based hydrology model. It has been widely applied in the mountainous Western United States [e.g., *Storck et al*., 1998; *Elsner et al*., 2010; *Cristea et al*., 2013] as well as other regions throughout the world [e.g., *Cuo et al*., 2006; *Zhao et al*., 2009]. The surface energy balance (SEB) snow model in DHSVM consists of two snow layers [*Andreadis et al*., 2009]. In grid cells where glaciers exist, (determined by the prescribed initial condition, advancing flow of ice, or snow densification to ice), a layer of ice is included below the lower snow layer. Melting of the surface of the glacier ice layer is simulated when the snow layers have melted completely, and excess energy is available for melt as calculated through the SEB algorithms. Snow accumulation and ablation in non-glacierized grid cells is simulated using the 2 layer SEB model.

The simulation of surface accumulation and ablation processes described above is coupled with the simulation of dynamic flow of glacier ice. Glacier surface mass balance is modeled at hourly time-steps through snow accumulation and ablation, glacier ice ablation, and snow densification to ice. At the end of each month, the net change in the mass of the ice as a result of vertical fluxes of accumulation and ablation is calculated at every glacierized grid cell to develop a "mass balance" field ($\dot{b}$ meters water equivalent, m w.e.), used to force the glacier dynamics submodel of DHSVM. Dynamic cell to cell ice flow is then simulated based on a vertically integrated shallow ice approximation of the continuum mechanics equations governing ice deformation and sliding [e.g., *Mahaffy*, 1976; *Plummer and Phillips*, 2003] as formulated in *Clarke et al.* [2015] as a diffusion equation:

$$\frac{\partial S}{dt} = \nabla_{xy}\left(D\nabla_{xy}S\right) + \frac{\rho_{ice}\dot{b}}{\rho_w} \qquad (1)$$

The change in surface elevation from the flow of ice (∂S) is driven by ice surface slope ($\nabla_{xy}S$), momentum diffusivity (*D*), and $\dot{b}$ simulated over the preceding month. Diffusivity is a nonlinear function of ice thickness $\left(H\right)$ and surface slope ($\nabla_{xy}S$):

$$D(H,S_{xy}) = \frac{2A(\rho_{ice}g)^n\left|\nabla_{xy}S\right|^{n-1}}{n+2}H^{n+2} + C(\rho_{ice}g)^m\left|\nabla S_{x,y}\right|^{m-1}H^m \quad (2)$$

The first term of (2) represents Glen's flow law for ice creep, with parameters $A = 7.5738\text{x}10^{-17}$ $\text{Pa}^{-3}yr^{-1}$ and $n = 3$ [*Glen*, 1955]. The second term of (2) represents basal sliding with *m* = 3, the sliding law exponent, and *C* being the sliding law coefficient. It is likely that basal sliding contributes to ice movement to some extent. However given the uncertainties in selecting a value for the C parameter for all glaciers in the domain, in this study basal sliding was not modeled (i.e., C=0). For shrinking glaciers the processes that drive the sliding component of flow are likely to diminish over time [*Clarke et al.*, 2015]. However, in section 2.5.4 we do provide a sensitivity analysis of model results using a model configuration that includes basal sliding. Accounting for simulated ice flow through creep, the thickness and extent of glacier ice layers are updated at a monthly time step, while the SEB and distributed watershed hydrologic processes (e.g., evapotranspiration, surface/subsurface flow, channel routing, snow accumulation and ablation, etc.) are continuously simulated at an hourly simulation time step.

2.3.2 Initializing Glacier Extent and Thickness

Uncertainties in the extent and thicknesses of glacier ice used in glacio-hydrologic model applications could lead to highly uncertain model projections of hydrologic change and runoff in a warming climate [*Huss et al.*, 2014]. To estimate the glacier extent and distribution of ice thickness accurately at the beginning of the historical simulation period we used a four step spin-up procedure. In step 1, we calculated a mean annual surface mass balance field ($\bar{b}$) that is spatially distributed across the model domain to use as model forcing. This field was computed by running the hourly SEB snow/ice model of DHSVM from 1987-2010 using meteorological data described in section 2.4.2. Hourly fluxes were summed to estimate net annual change of glacier mass in each modeled year. Taking the mean of annual estimates, a mean annual net change of the ice layer ($\bar{b}$) at each grid cell is calculated. Glacier ice was assumed to always be available to melt at every grid cell location when no snow was present so that the mass balance field was spatially continuous throughout the model domain. In step 2, the glacier dynamics model was run offline (decoupled from the hydrology model) with no initial glacier thickness on the landscape, driven with constant $\bar{b}$ until a steady-state glacier ice distribution is reached. Forcing the glacier dynamics model with $\bar{b}$ calculated from recent meteorological data produces steady state ice masses that are much smaller than are observed in historical extent estimates because the ice masses present in recent decades are largely the result of past colder climate conditions. In step 3, we perturbed the mass balance forcing ($\bar{b}$) calculated in step 1 so that the extent of modeled steady state ice masses closely matches the earliest historical ice extent estimate. Up to 0.85 m w.e. was added to $\bar{b}$ to obtain a match with the observed estimate. Glacier extent derived from a 1987 Landsat image is taken as the earliest ice extent estimate**.**

Following step 3, we obtained mechanistically stable ice masses that closely matched historical glacier area estimates. However, these ice masses reflect a steady state condition, which is unrealistic for the actual state of the glaciers of this region in the mid-1980s [*Rabatel et al.*, 2013]. To represent a thinner, more realistic transient distribution of ice mass with which to initialize the hydrology model for historical simulations, a fourth step in the spin-up process was required. Accordingly, in step 4 we ran the full SEB model with the steady state ice masses from step 3, that match the boundaries of the earliest ice extent, with the hourly historical meteorological forcing data for 5 years to thin the glacier thicknesses to a representative transient

state. We used an iterative procedure to determine the number of years to use in this "thinning" simulation. We found 5 years as a sufficiently long duration for the thinning run, after which the model consistently predicted glacier recession, glacier discharge and streamflow (e.g., Figure 5, see section 2.5.1).

2.3.3 Model Calibration and Evaluation

We calibrated the model using a multi-objective complex evolution global optimization method (MOCOM-UA, *Yapo et al*. [1998]) over the historical time period where observational data are available in space and time. In model calibration our objective was to maximize the Nash-Sutcliffe Efficiency (NSE) calculated for monthly mean streamflow and log transformed streamflow, and minimize the root mean square error (RMSE) of annual net mass balance of the Zongo glacier to find optimal parameter values in calibration. To provide ranges for realistic calibration parameters, we conducted initial trial and error parameter sensitivity analyses using parameter values in the published literature. Through calibration we identified critical, spatially uniform, model parameters that improve model predictions. Parameters adjusted during model calibration included temperature lapse rate, precipitation lapse rate, maximum snow albedo, aerodynamic roughness length over snow, and glacier ice albedo. Precipitation and temperature lapse rates, snow albedo, and glacier albedo have been measured at a limited number of locations in the study area. However directly using field-estimated local parameter values did not consistently improve model predictions with respect to streamflow and glacier spatial and temporal evolution. Therefore to capture representative parameter values at the watershed-scale, sampling parameters from their physically realistic ranges as guided by field observations and literature values deemed appropriate in this study. This approach would also partially compensate for any biases in the forcing data. The ranges of the parameter values evaluated and the optimal values obtained from model calibration are listed in Table 1.

2.4 Data

2.4.1 Geospatial Data

Our modeling approach requires spatial characterization of elevation, soil depth and texture, vegetation, meteorological forcing, and the initial distribution of glacier ice described in Section 2.3.2. We applied DHSVM at a grid resolution of 50 m. Digital elevation model (DEM)

data were acquired from the Advanced Spaceborne Thermal Emission and Reflection Radiometer (ASTER) Global Digital Elevation Model Version 2 (GDEM V2) elevation product (NASA). In areas where artificial canals cross the watershed (Fig. 1) the DEM elevations were modified by decreasing elevations in the canals so that surface runoff is intercepted and conveyed to the reservoir. We estimated glacier bed topography (the elevation of the land surface under the glaciers) by running a bed stress model that calculates basal shear stress as a linear optimization problem and uses a DEM (surface topography including current glacier ice), modeled mass balance fields, and observed ice thinning rates as model input [*Clarke et al*., 2013].

We estimated soil depths across the basin empirically from topography, based on elevation, local slope and contributing area [*Westrick*, 1999]. This algorithm gives thin soils on steep slopes and ridge tops and thicker soils on gentle slopes and in depressions, within a defined range of 0.2 – 4.25 m based largely on conjecture. Soil classification data available for remote areas (e.g., Harmonized World Soil Database) are often of a spatial resolution that is too coarse for watershed scale hydrological modeling. Hence, soil texture classes were also estimated based on local slope and contributing area, with finer soils (fluvial-glacial deposits) specified in areas of low relief and high contributing areas and coarser soils (talus, lateral moraines) and bedrock specified where slopes are steep. The soil type under glaciers was specified as bedrock. This slope-derived distribution of soil texture is consistent with those described and mapped in *Caballero et al.* [2002] at a coarser spatial representation of a larger area. Vegetation was specified following an inventory of digital land cover data (Centro Digital de Recursos Naturales de Bolivia, CDRNB, http://essm.tamu.edu/bolivia/), and manually adjusted where it was not consistent with Google Earth imagery.

2.4.2 Historical Meteorological Data

The historical period we selected for model calibration and analysis is 1987-2010, based on the availability of high quality satellite imagery suitable for glacier area delineation. DHSVM's required meteorological forcings include surface air temperature, relative humidity, wind speed, downward shortwave and longwave radiation, and precipitation. An hourly model time step was preferred to account for the high diurnal variability in the surface energy dynamics. The Institute of Research for Development (IRD, France, GREATICE project) and

Compañia Boliviana de Energía Eléctrica (COBEE, a private hydroelectric utility company) have maintained intermittent and ongoing meteorological measurement stations in the basin for several decades. However, continuous hourly measurements of all of the required input variables with limited periods of missing data are only publicly available from hydrological year 2004 to 2009 at the Off-Glacier station (Fig. 1) (http://www-lgge.ujf-grenoble.fr/ServiceObs/). This limited period is not sufficient for historical model calibration, validation, and analysis of hydrological change.

To run the model for the historical period a longer hourly time series of meteorological forcing data was generated through bias correction of reanalysis meteorological data, Modern Era Retrospective-Analysis for Research and Applications (MERRA, NASA). MERRA data are available from 1979 through present. We removed systematic biases from the MERRA reanalysis products using the available observed data at the Off-Glacier station and the methods described in *Berg et al*. [2003], which were extended to finer time scales to account for diurnal biases. Raw MERRA data had large biases in magnitudes and did not realistically capture diurnal patterns when compared to the observations at the Off-Glacier station. This is largely due to the coarse spatial resolution (1/2 x 2/3°) of the MERRA output. Therefore to remove systematic diurnal and seasonal biases in the reanalysis data, we used the observed station and reanalysis data for 2004-2009 (dates with missing data removed from both sources), and computed ratios for shortwave radiation, relative humidity, wind speed, as well as absolute differences in air temperature, using the monthly mean of each hour of the day for each month of the year, and implemented corrections with the following equations. For example,

$$SW_{BC} = \frac{\overline{SW}(\text{obs})_{hr,mth}}{\overline{SW}(merra)_{hr,mth}} \times SW(merra) \qquad (3)$$

$$Ta_{BC} = \left(\overline{Ta}(obs)_{hr,mth} - \overline{Ta}(merra)_{hr,mth}\right) + Ta(merra) \qquad (4)$$

equation 3 gives the ratio-based bias correction (*BC*) of shortwave radiation (*SW*), whereas equation 4 gives the absolute difference bias correction of 2-meter air temperature (*Ta*). Comparisons of the uncorrected MERRA and observational data are reported in the Appendix, section 2A-1. Downward longwave radiation was calculated from the bias corrected relative humidity, air temperature, and shortwave radiation time series and calculated top of atmosphere solar irradiance following *Sicart et al.* [2010]. Additional stations (Fig. 1) that measured single

meteorological variables, Mevis (temperature) and Plataforma (precipitation) were used to evaluate raw and bias corrected meteorological data.

The MERRA surface precipitation monthly total accumulations compared well with observations at the Platforma station (NSE = 0.69) and at the Off-Glacier location (NSE=0.76), and hence, were not adjusted for bias. Annual differences between observations and MERRA data were relatively small, 10% on average. However, as identified by *Soruco et al*. [2009] using locally observed data, precipitation undercatch is a significant problem in this catchment. Therefore, following the findings of *Soruco et al*. [2009] who estimated gauge undercatch the MERRA precipitation data were increased by 37% to account for precipitation gauge undercatch.

We confirmed the bias-corrected MERRA data against temperature observations at the Mevis station (4750 m). For this purpose we used a lapse rate of -5.7 $^{\circ}C\,km^{-1}$, calculated by comparing the observational records at the Mevis and Off-Glacier stations, and used this to interpolate the time series to the lower elevation of the Mevis station (4750 m). The bias corrected time series of air temperature showed agreement (NSE = 0.58) with this longer record of observation (1995-2010, periods of missing observed data removed).

The bias-corrected data are representative of a single point in the watershed, the location of the local meteorological station from which the observations were taken (Off-Glacier, Fig. 1). We assumed downward longwave radiation, relative humidity, and wind speed to be spatially homogenous across the basin, while bias-corrected shortwave radiation, temperature and precipitation were estimated for each grid cell with reference to the Off-Glacier station location. To distribute temperature and precipitation across the watershed from this point we used precipitation and temperature lapse rates calibrated to obtain consistent modeled data with glacier mass and discharge observations (Table 1). Precipitation was partitioned into rain and snow using local temperature and threshold values for the maximum temperature which snowfall can occur (0.5 $^{\circ}$ C) and the minimum temperature at which rainfall can occur (-0.5 $^{\circ}$C). The bias-corrected shortwave radiation data were produced relative to a horizontal surface. In DHSVM this value is distributed for each grid element to incorporate the effects of slope, aspect, and shading.

2.4.3 Future Meteorological Forcing Data

Projections of the future climate 2011-2100, were generated by statistically downscaling GCM outputs using the Advanced Weather Generator (AWE-GEN), of *Ivanov et al.* [2007] following methods outlined in *Fatichi et al.* [2011]. Stochastic weather generators have been successfully applied in previous coupled glacier-hydrologic modeling applications (e.g., *Stahl et al*. [2008]; *Uhlmann et al*. [2012b]; *Pellicciotti et al*. [2014]) and have the benefit of reproducing the local behavior of multiple atmospheric surface variables at sub-daily time intervals. Additionally, use of the weather generator allowed us to update statistical properties through time (according to GCM predictions) and in so doing, represent a transient climate, which is required to evolve the glacier ice masses continuously. Furthermore, this approach permits the evaluation of multiple statistically plausible realizations of future meteorological forcing data rather than relying on a single deterministic projection. Based on the availability of daily projections of temperature and precipitation through the 21st century, we identified and downscaled statistically outputs from 11 GCMs (BCC-CSM1, ACCESS1, CanESM2, CCSM4, CNCRM, CSIRO-Mk3.6, GFDL-CM3, INMCM4, MIROC5, MRIGCM, NORESM1) from the CMIP5 RCP4.5 emissions pathway scenario (ensemble r1i1p1). This scenario was selected to represent moderate warming over the 21st century. The air temperature field from each GCM was taken at the 500 hPa tropospheric altitude as an index to changes at the elevation of the watershed as opposed to the 2m air temperature which reflects a much lower altitude due to the coarse spatial resolution of the GCMs.

We outline the steps in the downscaling process here but for more detail, the reader is referred to *Fatichi et al*. [2011]. First, statistical parameters used as inputs to the weather generator were calculated from the bias corrected historical reanalysis meteorological time series at the Off-Glacier site (Section 2.4.2). Next, the statistical precipitation and temperature parameters for each GCM's output were calculated for historical and future time periods at the same site. These parameters include mean, variance, skewness, frequency of zero precipitation, and the coefficients of variation at multiple temporal aggregation intervals. We calculated factors of change (ratio or absolute difference between future and historical period) in the statistical parameters for each GCM. The actual values of the parameters were not directly used; only their relative changes in time with respect to their historical values were used. Next, utilizing the factors of change of all GCMs, we used the Bayesian approach of *Tebaldi et al.* [2005] to determine probability density functions (PDFs) of the factors of change for each

statistical parameter. Using these PDFs, the median (mostly likely) factor of change for each statistical parameter was then used to change the historical weather generator parameters through time reflecting the projected future transient climate. Hence, information from the group of GCM's was integrated to calculate a single most likely factor of change for each statistical parameter that varies in time. The weather generator parameters were updated every decade to allow for the representation of inter-annual persistence in the simulation of precipitation. Updating the parameters at this coarse time interval, as opposed to annually, lead to decadal step changes in the future meteorological time series. This coarse interval was selected to prioritize the representation of inter-annual persistence of precipitation. For example, two sequential dry years would be more detrimental to glacier mass than the same two dry years separated by a normal or wet year.

We produced 30 realizations of future hourly meteorological time series with the weather generator, representing the most likely factors of change in precipitation and temperature statistical properties and uncertainty related to the stochastic nature of weather and climate. The other meteorological variables required by the hydrologic model (relative humidity, wind speed, short and long wave radiation) were not downscaled from GCM outputs; rather future changes in these variables were represented through their correlations with and dependence on temperature and precipitation in the weather generator algorithms. We considered a more complex approach based on Monte Carlo analysis to sample from the factor of change PDFs of individual statistical parameters [e.g., *Fatichi et al*., 2013], but decided against this as it requires an assumption of independence among the statistical parameters (e.g., a change in a parameter in one month is independent of the change in others; a change in a parameter is independent among temporal aggregation intervals), and greatly increases the computational burden. While we provide a range of the most probable projections for future watershed processes under a single emissions pathway scenario (RCP4.5), we acknowledge that a much broader range of uncertainty exists in future projections and future work should incorporate ongoing advances in climate modeling, downscaling, multiple emission pathways, and a comparison of multiple hydrologic/glacier modeling approaches, among others, to represent a wider range of uncertainty.

2.4.4 Model Evaluation Data

Historic remote and *in-situ* measurements of hydroclimatic states and fluxes are critical for model calibration and evaluation. In this study we used glacier mass balance estimated using several methods, glacier surface velocity, glacier discharge, surface energy balance measurements, and satellite-based glacier extent. IRD's glacier monitoring program has made point glacier mass balance measurements on Zongo glacier since the early 1990s. The mass balance data are derived from measurements of a network of stakes in the ablation zone and snow pits in the accumulation zone. These data are available through the Glacioclim database (http://www-lgge.ujf-grenoble.fr/ServiceObs/). *Soruco et al.* [2009] report time series of cumulative net mass balance of the Zongo glacier estimated from hydrological measurements (discharge and precipitation), glaciological (glacier mass measurements of IRD), and geodetic methods (photogrammetry) which were digitized in this study for model confirmation. Discharge data from a location near the terminus of the Zongo glacier (Tubo, Fig. 1) and surface energy measurements were made available by IRD and have been utilized in previous publications [e.g., *Sicart et al*., 2005; *Sicart et al*., 2011].

Observed glacier extent data are required to evaluate the model's skill in reconstructing rates of recession. We utilized satellite-based estimates of glacier area derived from atmospherically corrected Landsat Thematic Mapper scenes using a Normalized Snow Difference Index (NDSI) threshold following the methods of *Burns and Nolin* [2014]. Images were taken at the end of the dry season and during relatively dry years to avoid mapping snow outside of glacier areas. 6 Landsat Thematic Mapper scenes were processed and used to analyze glacier recession (8/2/1987, 9/30/1991, 6/21/1995, 8/3/1999, 8/3/2005, and 8/17/2010). The use of Landsat data was preferred over field measurements of glacier boundaries (which in most years are limited to the lower boundary of Zongo glacier) because the Landsat data is spatially continuous across the entire watershed. The 5 most recent Landsat-derived ice extent estimates were compared with field measurements of the lower boundary of Zongo glacier. The Landsat derived data are within +/- 50-150 m distance of locally measured terminus positions.

2.5 Results and Discussion

2.5.1 Model Evaluation

DHSVM is a physically-based model and requires minimal calibration as necessary. Because this study focuses on snow and glacier ice processes, snow roughness length, and snow

and ice albedo were calibrated. In addition, to improve model forcing we also selected precipitation and temperature lapse rates through calibration. Here we present optimal parameter values found during calibration (Section 2.3.3) and compare those with values measured at the study location. The optimal values reported in Table 1 are in agreement with previous work and those derived from local measurements. The optimal precipitation lapse rate of 15 $\%km^{-1}$ is within the range derived from weather station observations and high elevation snow pits, 10-40 $\%\,km^{-1}$. The temperature lapse rate (-8.4 $°C\,km^{-1}$) is stronger than the mean temperature lapse rate of -5.7 $°C\,km^{-1}$ calculated between the Mevis station (4750 m) and the Off-Glacier station (5050 m) where a mean monthly range of -7.5 - -4.2 $°C\,km^{-1}$ is observed. The optimal value may be more representative of the distribution of temperature at the watershed scale (elevation ranges 4,700-6,088m) than rates calculated from observations at lower elevations or may be compensating for biases in the forcing data. DHSVM decays snow albedo from a maximum value as a function of time after snow fall [*Laramie and Schaake*, 1972].The maximum snow albedo we found with calibration is 0.83, consistent with observed values for fresh snow in the area where convective precipitation results in more granular graupel-like snowfall that decreases maximum albedo [*Lejeune et al*., 2007]. The optimal glacier albedo, 0.39 is slightly greater than that reported by *Sicart et al.* [2011], 0.35. In reality this value is likely to have high spatial variability, whereas high values are observed near the equilibrium line altitude and low values observed near the terminus. An exact match with observational based parameters is not expected as the calibrated parameters will reflect some compensation for any biases in the forcing data, biases in observational data used in calibration, and model construct.

Prior to drawing conclusions as to the role of glaciers in the hydrologic context of the watershed, we evaluated the model's performance in reproducing historical time series of the hydrological and glaciological variables that have been measured in-situ. Modeled and observed (reconstructed using hydrological measurements) mean annual net mass balance for the 1987-2006 period were -0.69 and -0.77 (m w.e.), respectively. To confirm the spatial predictions of the model against observations we compared the modeled annual mass balance, reported as the spatial mean within 100-meter elevation intervals, with the mean of point measurements for each corresponding elevation range (Fig. 3a). For comparison, only elevation intervals with actual measurements (not interpolated measurements) are provided. The model generally reproduced

the non-linear altitudinal gradient in annual mass balance (NSE = 0.75), with some negative biases at lower elevations (Fig 3a).

Differences in the match with the glaciological point measurements are expected as previous studies have demonstrated that the point measurements alone cannot explain net mass balance changes observed using hydrological [*Sicart et al*., 2005] or geodetic methods [*Soruco et al*., 2009]. As compared with the other methods of estimating net mass balance of Zongo glacier, net mass balance using interpolated point glaciological measurements underestimates mass losses. *Sicart et al*. [2005] hypothesize that mass losses in steep areas without measurements are higher than those estimated from interpolated measurements because the presence of seracs increases the surface area exposed to melt. Because the source of bias in the glaciological measurements is not entirely clear, the model was not calibrated further as some overestimation of ablation (as compared to glaciological measurements) is required to capture net mass changes of Zongo glacier and discharge observed below the terminus.

Figure 3b shows the cumulative net mass balance of Zongo glacier modeled and reconstructed from hydrological observations and glaciological observations adjusted with geodetic data reported by *Soruco et al.* [2009]. Overall, the model was able to capture the historical trajectory of cumulative net mass changes of the Zongo glacier (Fig. 3b). However, the variability of modeled annual mass balance (σ = 0.53 m) is less than observed using the hydrological approach (σ = 0.74 m). This is partly attributed to the reanalysis monthly precipitation time series having lower variance (σ = 0.05 m) than the observations at the Plataforma location (σ = 0.065 m, Supplemental Fig. 5).

As a final step in comparing in-situ glaciological measurements on Zongo glacier to predictions of the model, we compared glacier ice surface velocities (Fig. 3c). An accurate representation of the velocities in the model indicates that the glacier dynamics algorithms used to evolve glacier area are representative of the actual physical processes. We compared the distribution of measured surface velocities (displacement of stake positions using GPS measurements) with those of the model for three 100 m elevation intervals on the lower reaches of Zongo glacier for the period 1991-2010 (Fig. 3c). The modeled surface velocities were calculated by increasing the modeled depth averaged ice velocity by a factor of 1.25 [*Cuffey and Patterson*, 2010]. The differences between median velocities measured and modeled for the intervals of 5000-5099 m and 5100-5200 m are small, -1.2 and 2.6 $\mathrm{m\ yr^{-1}}$. There is greater

variance in the model estimates as they include every 50m grid cell in the elevation interval each year, where the measurements are limited to 5-21 measurements across the entire glacier each year. Surface velocities are under predicted in the lowest elevation interval where the modeled median velocity is 9.8 $\mathrm{m\ yr^{-1}}$ less than observed. The total number of observations in this band over the time period is low, 16, while the modeled sample consists of 641 individual annual velocities that may better represent the spatial mean. Additionally, some discrepancies may be introduced by the approximation of ice flow (section 2.3.1).

In addition to evaluating the simulated changes in mass, we compared the modeled glacier area with estimates derived from satellite imagery over the historical period. Figure 4 shows the predicted ice thickness (ice water equivalent, IWE, m w.e.) and extent and satellite derived glacier extent at the start of the historical period (1987 panel a), in 1999 (panel b), and at the end of the historical period (2010, panel c). The general pattern of areal retreat is reproduced by the model across the watershed. Nonetheless, there are some inconsistencies in the simulated and satellite-derived extents. The ice mass near the southwest perimeter retreated significantly in the satellite-derived data, but not in the model (see Figure 4c indicated with an arrow). Also, the upper lateral boundaries of Zongo glacier do not shrink as they do in the Landsat derived data. Several aspects of the modeling approach could explain these shortcomings. The model lacks a representation of reflected and emitted longwave radiation from surrounding terrain that could be a significant source of heat to the margins of valley glaciers [*Sicart et al*. 2011] and could increase the rate of retreat. Another model limitation that could lead to mismatch in the glacier boundaries is that the SEB parameters are spatially uniform. In steep mountain regions where erosion may be active, changes in snow and ice surface albedo may result from sediment deposition, which is not incorporated in the current model. Lastly, the method of initializing the glacier ice distribution (Section 2.3.2) introduces some uncertainty. The actual state of the glaciers in the mid-1980s was a product of a long period of climate fluctuations which was not explicitly used to spin up the glacier masses due to limited knowledge of long-term climate forcing.

More complex models of ice flow can be used to predict glacier evolution. However, in this implementation we chose to use a simplified glacier flow model suitable for watershed to regional scale predictions [*Clarke et al*., 2015]. *Réveillet et al.* [2015] implemented a highly sophisticated full Stokes model to simulate ice flow of Zongo glacier. Our modeled historical ice

thickness distribution (Fig. 4) compares well with the boundaries, and the general spatial patterns predicted in figure 3 of *Réveillet et al.* [2015]. For example maximum modeled ice thickness in 1997 is 132 m for this study, corresponding to 120 m in the same area of the glacier for *Réveillet et al.* [2015]. The lower value 12 m difference in the thickest part of the glacier may be a product of basal sliding used in the Stokes method.

A time series of discharge measured below the terminus of the Zongo glacier at the Tubo site (Fig. 1) was used to evaluate the simulated discharge volume. At this measurement point the upslope contributing area covered by glacier ice varied between 75% in 1987 and 55% in 2010. Therefore model predictions at this point largely demonstrate the model's performance in predicting flows driven by snowmelt, glacier melt, and rain produced runoff. Fig. 5 shows the monthly mean modeled and observed time series of discharge for hydrological years 1992 through 2009. Average annual flow ($\mu_{obs} = 150$ l/s) and flow variation ($\sigma = 99$ l/s) match well ($\mu_{\mathrm{mod}}/\mu_{obs}$ = 0.98; $\sigma_{\mathrm{mod}}/\sigma_{obs}$ = 0.93). Besides these statistical comparisons, the NSE of 30-day mean discharge and natural log of discharge (which is more sensitive to low flows) are calculated as 0.65 and 0.77, respectively. The model was able to capture the seasonal and inter-annual variability of discharge; however its skill was less at shorter timescales (sub-monthly). Several elements of the model application contribute to this shortcoming. First, short-term model error is likely dominated by the inaccuracy of the meteorological forcing data. The historical data were derived from reanalysis products with a coarse spatial resolution (1/2 x 2/3 °) that were bias corrected using local data (Section 2.3.4). Therefore, while systematic seasonal and diurnal biases are removed, local hydrologic behavior attributed to "event" time scales (days to weeks) are not likely to be reproduced accurately. This likely is the largest source of error. Also, while storage/release and refreezing of melt water is explicitly represented in the modeled snow layers, the model does not represent englacial and subglacial routing of melt water through the glacier ice layer [*Naz et al*., 2014]. A small proglacial lake between the glacier terminus and gauge location developed as the glacier retreated. This lake likely has some influence on storage and routing of discharge. The lack of these processes in the model limits the accuracy of the timing of simulated discharge at short time intervals, but does not affect the accuracy of the seasonal and long term projected runoff, which are generally well simulated.

We also compared the modeled mean monthly land surface energy fluxes with local measurements [*Sicart et al*., 2005] conducted during the hydrological year of 2000 at an

elevation of 5050 meters on the Zongo glacier. 1:1 plots comparing monthly fluxes and a bar plot with modeled and observed net shortwave radiation (SW, incoming minus reflected), net longwave radiation (LW, downward minus emitted), sensible heat (SH) and latent heat (LE) exchanges are shown in Figure 6. A positive (negative) flux represents net energy gain (loss) at the glacier surface. While there are uncertainties in the measurement of these variables [*Helgason and Pomeroy*, 2012; *Lundquist et al*., 2015], as well as complications in the comparison of measurements at a point with fluxes simulated over the model's 50 m grid cell, the simulated and measured seasonality of energy exchanges are in agreement (Fig. 6e). However, large biases are apparent in late summer (MAM) shortwave radiation, which is heavily dependent on cloud cover (represented in model forcing) and albedo (represented in snow model algorithms and parameterization), and has the greatest non-seasonal variability. This positive bias in SW can be linked to over-predicted discharge at the end of the wet season in some years (e.g., 2000, 2006; Fig. 5). The highest bias is in the losses of latent heat (sublimation) during the winter months which may lead to positive biases in energy simulated at the snow/ice surface during these months. This bias in the exchange of latent heat is likely linked to a simplified formulation for the correction for atmospheric stability utilized in the model [*Andreadis et al.,*2009], inaccuracies in wind speed and relative humidity used as model forcings, and the lack of a representation of seasonally varying aerodynamic roughness length over snow/ice [*Wagnon et al.*, 1999], which is reduced to a constant in the model, and uncertainty in the measurement of daily sublimation with rudimentary lysimeters [*Wagnon et al.*, 1999; *Sicart et al.*, 2005].

This bias in net shortwave radiation and latent heat can be reduced by calibrating the model against the point-scale fluxes measured in the field. We conducted point scale calibrations where the decay of snow albedo was modified and a representation of seasonal katabatic cooling of air temperature over glacier surfaces was included. To represent the latter, near surface air temperature on the glacier was decreased (with respect to the interpolated value from the off glacier station) based on a comparison of on and off glacier measurements of temperature at locations with the same elevation (5050 m, Fig 1). The seasonal variability of the differences between on and off glacier mean monthly temperature ranges from 0 in January, when there is no clear difference observed, to 2.41 ℃ in June where near surface air temperature is colder on the glacier. This model configuration decreased MAM net shortwave radiation by 11% and increased sublimation (negative latent heat flux) by 70%, reducing model biases to some extent.

While fine-tuning of the model provided improved predictions at the point scale, when the model was run at the watershed scale with point-calibrated parameter values, model skill for predicting glacier extent, mass balance, and discharge lessened. Because the goal of this paper is to examine watershed-scale predictions, it was deemed relevant to use model runs with watershed-scale calibration.

2.5.2 Historical Model Application

We ran the model using the historical bias-corrected NASA-MERRA data from 1987-2010 to examine and quantify the glacio-hydrologic response to historical climate. The definition of glacier melt has varied in the literature [see *La Frenierre and Mark*, 2014] while some define the glacier contribution as all the water leaving the glacier footprint, including snowmelt and rain falling on the glacier [e.g., *Mark and Seltzer*, 2003; *Gascoin et al*., 2011], others include only the melting of glacier ice [e.g., *Stahl et al*., 2008; *Favier et al*., 2009; *Ragettli and Pellicciotti*, 2012; *Immerzeel et al*., 2013]. The choice of definition is largely constrained by the method of analysis. Whereas some modeling approaches can more easily separate water sourced from snow and ice, many field measurement approaches cannot easily differentiate the two. We use the latter definition, as in many high alpine watersheds snowmelt will continue to be an important component of the water balance for some time after glaciers have receded.

To describe the role of glaciers in watershed discharge we analyzed the modeled discharge entering the reservoir, which collects runoff from the entire catchment through the canal system (Fig. 1). Measurements of all the discharge entering the reservoir are not available for use in this study for model confirmation. Therefore, we rely on the model confirmation reported in Figure 5 to justify the use of this model for predictions at the catchment scale. Historically (1987-2010), on average the modeled glacier melt represents 27% of annual discharge in the watershed (Fig. 7a). This contribution is enhanced during the dry season (winter, JJA), 61% (on average), when seasonal precipitation is at a minimum. The quantity and relative contribution of glacier melt is reduced in wet years (e.g., WY 2008, Fig. 7b) when fresh snow cover provides an albedo feedback that increases the reflection of shortwave radiation at the surface and reduces melt. Glacier melt discharge increases substantially in dry years (e.g., WY 1998, Fig. 7c). For example, during the El Niño event of 1998, when warm and dry conditions persisted during the wet season (summer, DJF), the glacier melt contribution was 34%

during January, compared to a long-term (1987-2010) average of 13% for the same month. During January, fresh snowfall usually results in minimum melting at the glacier surface and accumulation at high elevations. In El Niño years discharge was further enhanced by the melting of accumulated snow at higher elevations in the watershed as reflected in the catchment mean monthly hydrograph (Fig. 7c). During these years discharge can exceed precipitation through high amounts of glacier melt and melting of "carry over" snow stored at high elevations.

2.5.3 Hydrologic Response to Glacier Recession through the 21st Century

We conducted simulations forced with 30 realizations of the future climate (as described in section 2.3.4). These realizations reflect inter-annual variability in temperature and, on average, predict a warming of approximately 3°C by the end of the century (Fig. 8 a,b), consistent with previously reported estimates for the region from GCM outputs [*Bradley et al*., 2006; *Vuille et al*., 2008]. While annual precipitation is highly variable, the average over all of the future realizations indicates an 8% decrease in annual precipitation by the end of the century (Fig 8c), mostly attributed to reduced precipitation during the transitional period prior leading into the wet season (Fig 8d). This result is consistent with predictions of wet season precipitation projected by regressing future GCM zonal flow patterns, (generally accepted to be accurately simulated by GCMs; see *Christensen et al*., [2007]; and *Luce et al*., [2013]) with precipitation station observation locations [*Minvielle and Garreaud,* 2011] and end of century projections of precipitation using a higher resolution regional climate model [*Urrutia and Vuille,* 2009]. Nonetheless, it should be emphasized that there is considerable uncertainty in predictions of future precipitation using GCMs [*Buytaert et al*., 2010].

To examine the response to the future climate at the watershed scale, we evaluated the progression of glacier mass and area. For future projections we report the mean and range (in parentheses) of the ensemble of 30 future stochastic climate realizations. With respect to the initial state in 1987, the glacier area and volume are projected to decline 50(48-53)% and 61(60-66)% by 2050 and 73(71-77)% and 81(79-84)% by end of century, respectively. Figure 9 shows the mean predicted distribution of glacier ice in the watershed for years 2040, 2060, 2080, and 2100. While the glaciers do not completely disappear, their termini retreat to higher elevations. On average the terminus of the Zongo glacier is projected to retreat 1.9 km to an elevation of

~5300 m in 2100. This is a sharp contrast to beginning of the historical period when the glacier extended to 4850 m.

To determine how the evolving change in glacier area will affect discharge seasonality, we composited mean monthly flows of total runoff and glacier melt and their % change with respect to the historical period into two periods, the near future (2030-2050) and late century (2080-2100) plotted in Figure 10. The ranges of future data reflect the variability of climate represented through the multiple stochastic realizations of future meteorological forcing. In the near future, discharge entering the reservoir is expected to decrease during dry months, with the largest decreases occurring in August, 30 (21-39)% less than the 1987-2010 mean. Mid-century, wet season discharge is predicted to increase. As temperatures rise, high elevation areas that historically accumulated snow (which would eventually densify to glacier ice) contribute more to runoff through increased transient snowmelt and rainfall at the expense of mass accumulation. At the end of century, watershed discharge is projected to continue to decline throughout the year, with dry season (JJA) flows declining by 57% on average and the glacier melt contribution becoming negligible (Fig. 10b,d). Annual runoff is predicted to change -4(-15- 2)% and -24(-33- -18)% for the mid and late century time periods. These declines are linked to declining contributions of glacier melt associated with loss of area; however decreases in precipitation leading into the wet season and increased evapotranspiration also play a significant role. Late century, increased evapotranspiration and decreased precipitation largely offset runoff gains from high elevation areas that transitioned from zones of snow accumulation to snowmelt and rain dominated zones earlier in the century.

To identify the temporal patterns in the continuous hydrologic response to glacier change, we tracked the progression of total watershed runoff and glacier melt annually and during the dry season (JJA) between 1987 and 2100 in Figure 11 (a,b). Both annual and dry season runoff showed a pattern of increase until around 2010 and are predicted to decrease sometime within the following decade. Dry season runoff declines steadily until the second half of the century when the glacier contribution tapers to a minimum (Fig. 11b). The mean of the coefficient of variation (CV) of dry season flow for all future climate realizations (calculated using a moving 30 year window) steadily increases from 0.23 over the historical period to 0.49 at the end of century. This increased variability is linked to (1) decreasing contribution from glacier melt in sustaining low flows; and (2) precipitation events during the dry season (albeit small in

magnitude and less frequent) occurring as rain rather than snowfall over larger areas of the watershed. On average the change in CV of annual flows is small, increasing from 0.1 to 0.13 over the course of the 21st century. Likewise, CV of annual precipitation shows no clear temporal pattern (range of 0.14-0.15 throughout the period). Historically, the largest annual flows were attributed with dry and warm years (El Nino) where snow and ice stored in the watershed had a large contribution to runoff. These high annual flows decrease in time as the amount of ice and snow stored in the watershed is reduced.

As described above, changes in glacier melt have a strong influence on temporal patterns of watershed discharge. Concurrent with these changes, the relative contributions of snowmelt and rain and losses through evapotranspiration will evolve with the changes in climate. The progression of these fluxes at the annual time scale, and composited seasonally for the historical period, midcentury, and late century is shown in Figure 12. The fluxes entering the watershed (snowmelt, rain, glacier melt) do not include the effects of any losses through watershed processes (e.g., evapotranspiration, soil moisture storage). In contrast, runoff plotted in Figure 10a,b and 11 shows the glacier melt component of stream discharge generated in the watershed which includes the effects of these losses by routing the mass through the watershed. Unlike the trajectory of changes in glacier melt, changes in rain, snowmelt and evapotranspiration show patterns of change (Fig. 12a) that closely reflect increasing air temperature (Fig. 8a). In addition to reductions in runoff input from declining glaciers with climate change, the growing amount of evapotranspiration from November to the end of March leads to significant losses of annual runoff. As air temperature gradually warms above the freezing point (at the 5050 m reference location) evapotranspiration losses increase, by as much as 86% (from 140 to 264mm) by the end of century. This demonstrates the importance of the response of the non-glacierized portions of the watershed for predicting future runoff patterns in a warming climate.

Aside from the influence of snow cover on glacier melt and mass evolution, the transition of snowmelt to rain-derived discharge does not have a large influence on seasonal redistribution of water. In contrast to temperate mountainous watersheds, in high altitude tropical watersheds snow cover outside of glacier areas and at lower elevations on glaciers is often transient, melting within days of falling. This prevents the development of a snowpack and leads to small time lags between snowfall and runoff events [*Lejeune et al.*, 2007]. For this reason, a transition from

snowmelt to rain-derived discharge plays a lesser role in major seasonal changes in discharge patterns.

2.5.4 The role of glacier dynamics and parameter selection in model projections

In many mountainous watersheds, observational datasets are unavailable or are of short duration which makes model parameter selection and model calibration difficult. This leads modelers to select parameters based on values reported in the literature or use parameters from other regions. To examine the sensitivity of the glacio-hydrology model to model configuration and parameter selection, we compared the results from calibrated parameters presented above with alternate configurations (i.e., no glacier flow and with creep and basal sliding in the glacier model) and ranges of SEB and climate parameters that are plausible for this location. To facilitate this comparison we compared modeled glacier area (Fig. 13 a-g) and dry season (winter, JJA) runoff (h-n) from 1987-2100. JJA runoff was selected as it is most sensitive to changes in glacier area. It is presented as a 10-year centered running mean for clarity. A single realization of the future climate is used for the projected time period. This analysis reflects model sensitivity, not parameter uncertainty. In most cases the evaluated parameters were not be able to reproduce historical hydroclimatic patterns as accurately as the calibrated parameters.

We first analyzed the role of glacier dynamics. The model uses a vertically integrated shallow ice approximation which simulates creep, but we have neglected the influence of basal sliding due to uncertainties in its parameterization for all glaciers in the watershed (Section 2.3.1). We compared this assumption with a model configuration that does not include ice flow (no lateral movement of ice, Static) and one that includes basal sliding in addition to movement through creep (Creep + Sliding). Excluding ice flow leads to more rapid retreat (Fig. 13a) as ice at lower elevations is not replenished by ice flow from higher elevations. This in turn leads to less of an increase in JJA runoff early in the 21st century (Fig. 13h). When dynamics are represented, a much larger peak in runoff is observed because ice flow allows the ice bodies to sustain for a longer duration at lower elevations with warmer air temperatures. Late in the 21st century the static case has more glacier area and JJA runoff because mass accumulated at higher elevations earlier in the time period was not redistributed to lower elevations. In the configuration that considered basal sliding, the sliding law coefficient (C, equation 2) was set to $2.0\text{x}10^{-11}\text{Pa}^{-2}\text{yr}^{-1}$, the upper limit in the range presented by *Clarke et al.* [2015]. The inclusion of

this configuration of basal sliding resulted in negligible differences in modeled glacier area (Fig. 13a). This formulation increased mean surface velocities below 5200 m 0.3-1.8 m yr^{-1} during the historical period. Based on this analysis and the agreement with surface velocities when basal sliding is neglected (Fig. 3c) it is likely that the role of basal sliding is low during this period of retreat.

Next, we explored SEB and climate parameters that have significant influence on rates of ablation (Fig. 13 b-f, i-m). We evaluated the projected response using different values of glacier albedo, maximum snow albedo, aerodynamic roughness length over snow and ice, and the precipitation and temperature lapse rates. For each case only the parameter being analyzed is altered, all other parameters remained at their calibrated values and the ice flow configuration utilized the creep only case. In most cases, differences between selected parameters were most pronounced for JJA runoff in the early part of the 21st century (Fig. 13 h, j-k, m-n). Later in the century glacier ice is limited to high elevation areas and does not contribute a significant amount of melt during the winter months.

While the other parameters largely controlled the magnitude of dry season discharge response, maximum snow albedo greatly changes the rate of retreat (Fig. 13c) which leads to temporal shifts in the response of JJA runoff, while the magnitude and shape of response remains intact. Decreasing maximum albedo to 0.8 (calibrated = 0.83) results in peak dry season runoff response occurring approximately a decade earlier. Increasing this value to 0.9 delays retreat until 2004 shifting peak runoff response to a decade later. Increasing aerodynamic roughness length to 5 mm (calibrated = 0.7 mm) promotes sensible and latent heat exchanges at the glacier surface, leading to increased recession and initial increased runoff. Applying a single value to both snow and ice may be problematic [Brock et al. 2006]. Selecting realistic ranges for each surface individually would likely narrow this response range. The temperature lapse rate determines the elevation of the zero degree isotherm. Increasing this value amplifies the sensitivity of higher elevation areas to rising temperatures leading to more rapid recession. These findings are consistent with those of *Ragettli and Pellicciotti* [2012] who found temperature lapse rate and an empirical solar radiation parameter to be the most sensitive in a glacio-hydrological model application in central Chile.

Wind speed was bias corrected using local observations at the Off-Glacier station where there is a complete dataset with all of the required variables (Section 2.4.2) and treated as a

spatially homogenous field throughout the watershed. Wind speed is likely to vary across the landscape and it is uncertain whether the station we used for bias correction is representative of an average value for the entire basin. For example, during the period of 2004-2009, the mean wind speed at this location (2.86 m sec^{-1}) was 18% higher than that observed at the On-Glacier measurement location (2.42 m sec^{-1}, Fig. 1). To test potential uncertainties associated with this assumption we increased and decreased wind speed by 25%. Decreasing wind speed decreased glacier melt and recession, while increasing wind speed had the opposite effect. This leads to approximately 7 year difference in the timing of peak response and a 16% difference in peak magnitude within the range evaluated. These responses depended on the calibrated roughness length value. The optimal value of roughness length (0.7 mm) is on the lower end of the range of measurements reported by *Brock et al.,* [2006]. This may reflect compensatory effects for a positive bias in wind speed with respect to a field that would be more representative of the entire watershed.

2.6 Conclusions

In partially glacierized watersheds climate change can yield highly complex glacio-hydrologic responses over time. Understanding and predicting the different factors that control such behavior is important in regions where the aquatic environment and anthropogenic systems rely on glacier melt water. In this study we improve the understanding of the complex response of a partially glacierized watershed within the context of the headwaters of the Zongo River in Andean cordilleras of Bolivia. Driven by retrospective and future climate forcing our glacio-hydrologic model analysis provide the following general results:

a) Considering glacier ice dynamics in a distributed hydrology model is essential for predicting the climate change impacts in partially glacierized watersheds.
b) The skewed shape of runoff response with time is controlled by the interplay between temporally varying positive and negative trends in glacier ice melt, and the positive trend of evapotranspiration under a warming climate.
c) Increased evapotranspiration from non-glacierized areas of the basin will have an increasing influence on water availability with rising temperatures and is an essential component to consider in long-term projections.

d) The buffering effect of glacier melt on low flows will diminish in time, increasing variability during the dry season. Identifying increases in flow variability as flows decline is critical for water management purposes.
e) Calibration and selection of Surface Energy Balance (SEB) and climate model parameters plays a significant role in model projections of glacier area and runoff patterns. Long-term projections are highly sensitive to selection of maximum snow albedo, surface roughness, and temperature lapse rate.

This study demonstrates the potential of applying advanced process based simulation models for prediction of future water availability in partially glacierized river basins. Parameter sensitivity analyses provide a cautionary example of the potential for a high degree of uncertainty in future projections when applying such complex models in areas that lack local data to properly constrain model parameter selection and model calibration. Ongoing and future advances in the remote observation of processes in these high alpine environments (e.g., sensing from satellite and unmanned aerial vehicles) will aid in application and testing complex glacio-hydrological models.

Acknowledgement:

The Modern Era Retrospective-analysis for Research and Applications (MERRA) reanalysis meteorological data can be downloaded from the Goddard Earth Sciences Data and Information Services Center (GES-DISC, http://disc.sci.gsfc.nasa.gov). Most of the glaciological and meteorological data measured in the watershed that were utilized in this study can be downloaded from the Glacioclim database (http://www-lgge.ujf-grenoble.fr/ServiceObs/). Non-public glaciological and meteorological data can be obtained with agreement from the Institute of Research for Development (IRD). The CMIP5 general circulation model output can be downloaded from the World Climate Research Program (WCRP, http://cmip-pcmdi.llnl.gov/cmip5/). The Landsat Thematic Mapper scenes can be downloaded from the United States Geological Survey (USGS, http://earthexplorer.usgs.gov/). All glacio-hydrological model data presented in this manuscript are available by request through the corresponding author (chrisf2@uw.edu). Surface energy balance observations were provided by Jean Emmanuel Sicart (jean-emmanuel.sicart@ird.fr). This research was supported by the NASA Interdisciplinary Research in Earth Science Program - Grant NNX10AP90G.

References

Adhikari, S. and S. Marshall (2012), Glacier volume-area relation for high-order mechanics and transient glacier states, Geophys. Res. Lett., 39, L16 505, doi:10.1029/2012GL052712.

Andreadis, K. M., P. Storck, and D. P. Lettenmaier (2009), Modeling snow accumulation and ablation processes in forested environments, Water Resour. Res., 45, W05429, 1–13, doi:10.1029/2008WR007042.

Baraer, M., B. G. Mark, J. M. McKenzie, T. Condom, J. Bury, K. Huh, C. Portocarrero, J. Gómez, and S. Rathay (2012), Glacier recession and water resources in Peru's Cordillera Blanca, J. of Glaciol. 58, 207, 134-150.

Barnett, T. P., J. C. Adam, and D. P. Lettenmaier (2005), Potential impacts of a warming climate on water availability in snow-dominated regions, Nature, 438(7066), 303-309.

Berg, A. A., J.S. Famiglietti, J.P. Walker, and P.R. Houser (2003), Impact of bias correction to reanalysis products on simulations of North American soil moisture and hydrological fluxes, J. of Geophys. Res-Atmos. (1984–2012), 108(D16).

Bradley, R. S., M. Vuille, H. F. Diaz, and W. Vergara (2006), Threats to water supplies in the tropical Andes, Science, 312(5781), 1755-1756.

Brock, B. W., I. C. Willis, and M. J. Sharp (2006), Measurement and parameterization of aerodynamic roughness length variations at Haut Glacier d'Arolla, Switzerland, J. of Glaciol., 52(177), 281-297.

Burns, P. and A. Nolin (2014), Using atmospherically-corrected Landsat imagery to measure glacier area change in the Cordillera Blanca, Peru from 1987 to 2010, Remote Sens. of Environ., 140, 165-178.

Buytaert, W., M. Vuille, A. Dewulf, R. Urrutia, A. Karmalkar, and R. Celleri (2010), Uncertainties in climate change projections and regional downscaling in the tropical Andes: implications for water resources management, Hydrol. Earth Syst. Sc., 14(7).

Caballero, Y., V. Jomelli, P. Chevallier, and P. Ribstein (2002), Hydrological characteristics of slope deposits in high tropical mountains (Cordillera Real, Bolivia), Catena, 47(2), 101-116.

Caballero, Y., P. Chevallier, R. Gallaire, and R. Pillco (2004), Flow modelling in a high mountain valley equipped with hydropower plants: Rio Zongo Valley, Cordillera Real, Bolivia. Hydrol. Process, 18(5), 939-957.

Casassa, G., P. López, B. Pouyaud, and F. Escobar (2009), Detection of changes in glacial run-off in alpine basins: examples from North America, the Alps, central Asia and the Andes. Hydrol. Process., 23(1), 31-41.

Cauvy-Fraunié, S., P. Andino, R. Espinosa, R. Calvez, F. Anthelme, D. Jacobsen, and O. Dangles, (2013), Glacial flood pulse effects on benthic fauna in equatorial high-Andean streams, Hydrol. Process., doi: 10.1002/hyp.9866.

Chevallier, P., B. Pouyaud, W. Suarez, and T. Condom (2011), Climate change threats to environment in the tropical Andes: glaciers and water resources, Reg. Environ. Change, 11(1), 179-187.

Christensen, J.H., B. Hewitson, A. Busuioc, A. Chen, X. Gao, I. Held, R. Jones, R.K.

Kolli, W.-T. Kwon, R. Laprise, V. Magaña Rueda, L. Mearns, C.G. Menéndez, J.

Räisänen, A. Rinke, A. Sarr and P. Whetton (2007), Regional Climate Projections. In:

Climate Change 2007: The Physical Science Basis. Contribution of Working Group I to

the Fourth Assessment Report of the Intergovernmental Panel on Climate Change

[Solomon, S., D. Qin, M. Manning, Z. Chen, M. Marquis, K.B. Averyt, M. Tignor and

H.L. Miller (eds.)]. Cambridge University Press, Cambridge, United Kingdom and New

York, NY, USA.

Clarke, G. K., F. Anslow, A. Jarosch, V. Radic, B. Menounos, T. Bolch, and E. Berthier (2013), Ice volume and subglacial topography for western Canadian glaciers from mass balance fields, thinning rates, and a bed stress model, Journal of Climate, 26(12), 4282-4303.

Clarke, G. K., A.H. Jarosch, F. S. Anslow, V. Radić, and B. Menounos (2015), Projected deglaciation of western Canada in the twenty-first century. Nature Geosci., 8, 372-377, doi:10.1038/ngeo2407.

Condom, T., M. Escobar, D. Purkey, J. C. Pouget, W. Suarez, C. Ramos, J. Apaestegui, A. Tacsi, and J. Gomez (2012), Simulating the implications of glaciers' retreat for water management: a case study in the Rio Santa basin, Peru, Water Int., 37, no. 4 (2012): 442-459.

Cristea, N. C., J. D. Lundquist, S. P. Loheide, C. S. Lowry, and C. E. Moore (2013), Modeling how vegetation cover affects climate change impacts on streamflow timing and magnitude in the snowmelt-dominated upper Tuolumne Basin, Sierra Nevada, Hydrol. Process., doi: 10.1002/hyp.9909.

Cuffey, K. M. and W.S.B. Paterson (2010), The physics of glaciers, 4th edn. Butterworth-Heinemann, Oxford.

Cuo, L., T. W. Giambelluca, A. D. Ziegler, and M. Nullet (2006), Use of the distributed hydrology soil vegetation model to study road effects on hydrological processes in Pang Khum Experimental Watershed, northern Thailand. Forest Ecol. and Manag, 224(1), 81-94.

Elsner, M. M., L. Cuo, N. Voisin, J.S. Deems, A.F. Hamlet, J.A. Vano, and D. P. Lettenmaier, (2010), Implications of 21st century climate change for the hydrology of Washington State. Clim. Chang., 102(1-2), 225-260.

Fatichi, S., V. Y. Ivanov, and E. Caporali (2011), Simulation of future climate scenarios with a weather generator. Advan. in Water Resour., 34(4), 448-467.

Fatichi, S., V. Y. Ivanov, and E. Caporali (2013), Assessment of a stochastic downscaling methodology in generating an ensemble of hourly future climate time series. Clim. Dynam., 40(7-8), 1841-1861.

Favier, V., M. Falvey, A. Rabatel, E. Praderio, and D. López (2009), Interpreting discrepancies between discharge and precipitation in high-altitude area of Chile's Norte Chico region (26–32°S), Water Resour. Res., 45, W02424, doi:10.1029/2008WR006802.

Fountain, A. G., and W. V. Tangborn (1985), The effect of glaciers on streamflow variations, Water Resour. Res., 21, 579–586.

Francou, B., P. Ribstein, R. Saravia, and E. Tiriau (1995), Monthly balance and water discharge of an inter-tropical glacier: Zongo Glacier, Cordillera Real, Bolivia, 16 S. J. of Glaciol., 41(137), 61-67.

Francou, B., M. Vuille, P. Wagnon, J. Mendoza, and J. E. Sicart (2003), Tropical climate change recorded by a glacier in the central Andes during the last decades of the twentieth century: Chacaltaya, Bolivia, 16 S., J. of Geophys. Res-Atmos (1984–2012), 108(D5).

Gardner, A. S., et al. (2013), A reconciled estimate of glacier contributions to sea level rise: 2003 to 2009, Science 340, 6134, 852-857.

Garreaud, R. D., M. Vuille, R. Compagnucci, and J. Marengo (2009), Present-day south american climate, Palaeogeogr., Palaeoclimatol., Palaeoecol., 281(3), 180-195.

Gascoin, S., C. Kinnard, R. Ponce, S. Macdonell, S. Lhermitte, and A. Rabatel (2011), Glacier contribution to streamflow in two headwaters of the Huasco River, Dry Andes of Chile, The Cryosphere, (5), 1099-1113.

Glen, J. W., The creep of polycrystalline ice, Proc. R. Soc. London, Ser. A, 228, 519–538, 1955.

Helgason, W., and Pomeroy, J. (2012), Problems closing the energy balance over a homogeneous snow cover during midwinter, J. of Hydromet., 13(2), 557-572.

Huss, M., D. Farinotti, A. Bauder, and M. Funk (2008), Modelling runoff from highly glacierized alpine drainage basins in a changing climate. Hydrol. Process, 22(19), 3888-3902.

Huss, M. and D. Farinotti (2012), Distributed ice thickness and volume of all glaciers around the globe, J. Geophys. Res., 117, F04010, doi:10.1029/2012JF002523, 2012.

Huss, M., M. Zemp, P. C. Joerg, and N. Salzmann (2014), High uncertainty in 21st century runoff projections from glacierized basins, J. of Hydrol. 510 (2014): 35-48.

Immerzeel, W. W., L. P. H., Van Beek, M. Konz, A. B. Shrestha, and M. F. P. Bierkens, (2012), Hydrological response to climate change in a glacierized catchment in the Himalayas, Climatic Change, 110(3-4), 721-736.

Immerzeel, W. W., F. Pellicciotti, and M. F. P. Bierkens (2013), Rising river flows throughout the twenty-first century in two Himalayan glacierized watersheds. Nature Geoscience, 6(9), 742-745.

IPCC (2014): Climate Change 2014: Impacts, Adaptation, and Vulnerability. Part A: Global and Sectoral Aspects. Contribution of Working Group II to the Fifth Assessment Report of the Intergovernmental Panel on Climate Change [Field, C.B., V.R. Barros, D.J. Dokken, K.J. Mach,

M.D. Mastrandrea, T.E. Bilir, M. Chatterjee, K.L. Ebi, Y.O. Estrada, R.C. Genova, B. Girma, E.S. Kissel, A.N. Levy, S. MacCracken, P.R. Mastrandrea, and L.L. White (eds.)]. Cambridge University Press, Cambridge, United Kingdom and New York, NY, USA, 1132 pp.

Ivanov, V.Y., R.L. Bras, and D.C. Curtis (2007), A Weather Generator for Hydrological, Ecological, and Agricultural Applications, Water Resour. Res., 43, W10406, doi: 10.1029/ 2006WR005364.

Jarosch, A. H., C. G. Schoof, and F. S. Anslow (2013), Restoring mass conservation to shallow ice flow models over complex terrain, Cryosphere, 7(1), 229-240.

Juen, I., G. Kaser, and C. Georges (2007), Modelling observed and future runoff from a glacierized tropical catchment (Cordillera Blanca, Perú), Global Planet. Change, 59(1), 37-48.

Kaser, G., J. G. Cogley, M. B. Dyurgerov, M. F. Meier, and A. Ohmura (2006), Mass balance of glaciers and ice caps: consensus estimates for 1961–2004, Geophys. Res. Let., 33(19).

La Frenierre, J., and B. G. Mark (2014), A review of methods for estimating the contribution of glacial meltwater to total watershed discharge, Prog. in Phys. Geogr., 38(2), 173-200.

Lambrecht, A., and C. Mayer (2009), Temporal variability of the non-steady contribution from glaciers to water discharge in western Austria, J. Hydrol., 376, 353–361.

Lejeune, Y., L. Bouilloud, P. Etchevers, P. Wagnon, P. Chevallier, J. E. Sicart, J. E., E. Martin, and F. Habets (2007), Melting of snow cover in a tropical mountain environment in Bolivia: Processes and modeling, J. of Hydrometeor., 8(4), 922-937.

Luce, C. H., J. T. Abatzoglou, and Z. A. Holden (2013), The Missing Mountain Water: Slower Westerlies Decrease Orographic Enhancement in the Pacific Northwest USA, Science, 342(6164), 1360-1364.

Lundquist, J. D., N.E. Wayand, A. Massmann, A., M.P. Clark, F. Lott, and N.C. Cristea (2015), Diagnosis of insidious data disasters, Water Resour. Res. (in press)

Mahaffy, M. W. (1976), A three-dimensional numerical model of ice sheets: Tests on the Barnes Ice Cap, Northwest Territories, J. of Geophys. Res., 81(6), 1059-1066.

Mark, B. G., and G. O. Seltzer (2003), Tropical glacier meltwater contribution to stream discharge: a case study in the Cordillera Blanca, Peru, J. of Glaciol., 49(165), 271-281.

Minvielle, M., R. D. Garreaud (2011), Projecting Rainfall Changes over the South American Altiplano, J. Climate, 24, 4577–4583. doi: http://dx.doi.org/10.1175/JCLI-D-11-00051.1

Moore, R. D., S. W. Fleming, B. Menounos, R. Wheate, A. Fountain, K. Stahl, K. Holm, and M. Jakob (2009), Glacier change in western North America: influences on hydrology, geomorphic hazards and water quality, Hydrol. Process. 23, 1 42-61.

Moriasi, D. N., J. G. Arnold, M. W. Van Liew, R. L. Bingner, R. D. Harmel, and T. L. Veith (2007), Model evaluation guidelines for systematic quantification of accuracy in watershed simulations. Trans. ASABE, 50(3), 885-900.

Naz, B. S., C. D. Frans, G. K. C. Clarke, P. Burns, and D. P. Lettenmaier (2014), Modeling the effect of glacier recession on streamflow response using a coupled glacio-hydrological model, Hydrol. Earth Syst. Sci., 18, 787-802, doi:10.5194/hess-18-787-2014.

Pellicciotti, F., M. Carenzo, R. Bordoy, and M. Stoffel (2014), Changes in glaciers in the Swiss Alps and impact on basin hydrology: Current state of the art and future research, Sci. Total Environ., 493, 1152-1170.

Plummer, M. A., and F. M. Phillips (2003), A 2-D numerical model of snow/ice energy balance and ice flow for paleoclimatic interpretation of glacial geomorphic features, Quaternary Sci. Rev., 22(14), 1389-1406.

Pouyaud, B., M. Zapata, J. Yerren, J. Gomez, G. Rosas, W. Suarez, and P. Ribstein (2005), On the future of the water resources from glacier melting in the Cordillera Blanca, Peru, Hydrolog. Sci. J., 50(6), 999–1022.

Rabatel, A., A. Bermejo, E. Loarte, A. Soruco, J. Gomez, G. Leonardini, and J.E. Sicart (2012), Can the snowline be used as an indicator of the equilibrium line and mass balance for glaciers in the outer tropics?, J. of Glaciol., 58(212), 1027-1036.

Rabatel, A., et al. (2013), Current state of glaciers in the tropical Andes: A multi-century perspective on glacier evolution and climate change, Cryosphere, 7, 81–102, doi:10.5194/tc-7-81-2013.

Radić, V., R. Hock and J. Oerlemans (2007), Volume-area scaling vs flowline modelling in glacier volume projections, Ann. Glaciol., 46, 234–240, 2007.

Radić, V., and R. Hock (2011), Regionally differentiated contribution of mountain glaciers and ice caps to future sea-level rise, Nature Geosci., 4(2), 91-94.

Ragettli, S., and F. Pellicciotti (2012), Calibration of a physically based, spatially distributed hydrological model in a glacierized basin: On the use of knowledge from glaciometeorological processes to constrain model parameters, Water Resour. Res., 48, W03509, doi:10.1029/2011WR010559.

Réveillet, M., A. Rabatel, F. Gillet-Chaulet, and A. Soruco. (2015), Simulations of changes to Glaciar Zongo, Bolivia (16 S), over the 21st century using a 3-D full-Stokes model and CMIP5 climate projections, Ann. of Glaciol., 56(70), 89.

Ribstein, P., E. Tiriau, B. Francou, and R. Saravia (1995), Tropical climate and glacier hydrology: a case study in Bolivia, J. of Hydrol., 165(1), 221-234.

Sicart, J. E., P. Wagnon, and P. Ribstein (2005), Atmospheric controls of the heat balance of Zongo Glacier (16 S, Bolivia), J. of Geophys. Res- Atmos. (1984–2012), 110(D12).

Sicart, J. E., R. Hock, P. Ribstein, and J. P. Chazarin (2010), Sky long-wave radiation on tropical Andean glaciers: Parameterization and sensitivity to atmospheric variables, J. Glaciol., 56(199), 854–860, doi:10.3189/002214310794457182.

Sicart, J. E., R. Hock, P. Ribstein, M. Litt, and E. Ramirez (2011), Analysis of seasonal variations in mass balance and meltwater discharge of the tropical Zongo Glacier by application of a distributed energy balance model, J. of Geophys. Res- Atmos. (1984–2012), 116(D13).

Soruco, A., C. Vincent, B. Francou, P. Ribstein, T. Berger, J. E. Sicart, and Y. Lejeune (2009), Mass balance of Glaciar Zongo, Bolivia, between 1956 and 2006, using glaciological, hydrological and geodetic methods, Ann. Glaciol., 50(50), 1-8.

Soruco, A., C. Vincent, A. Rabatel, B. Francou, E. Thibert, J.E. Sicart, and T. Condom (2015), Contribution of glacier runoff to water resources of La Paz city, Bolivia (16 S), Ann. of Glaciol., 56(70), 147.

Stahl, K., R. D. Moore, J. M. Shea, D. Hutchinson, and A. J. Cannon (2008), Coupled modelling of glacier and streamflow response to future climate scenarios, Water Resour. Res. 44, 2: W02422.

Stahl, K., and R. D. Moore (2006), Influence of watershed glacier coverage on summer streamflow in British Columbia, Canada, Water Resour. Res., 42, W06201, doi:10.1029/2006WR005022.

Storck, P., L. Bowling, P. Wetherbee, and D. P. Lettenmaier (1998), Application of a GIS-based distributed hydrology model for prediction of forest harvest effects on peak stream flow in the Pacific Northwest. Hydrological Processes, 12(6), 889-904.

Suarez, W., P. Chevallier, B. Pouyaud, and P. Lopez (2008), Modelling the water balance in the glacierized Parón Lake basin (White Cordillera, Peru), Hydrolog. Sci. J. 53(1), 266-277.

Tebaldi, C., R. L. Smith, D. Nychka, and L. Mearns (2005), Quantifying uncertainty in projections of regional climate change: A Bayesian approach to the analysis of multimodel ensembles, J. Climate, 18(10).

Uhlmann, B., F. Jordan, and M. Beniston (2012a), Modelling runoff in a Swiss glacierized catchment—part I: methodology and application in the Findelen basin under a long-lasting stable climate. Int. J. Climatol., 33(5), 1293-1300.

Uhlmann, B., F. Jordan, and M. Beniston (2012b), Modelling runoff in a Swiss glacierized catchment—Part II: daily discharge and glacier evolution in the Findelen basin in a progressively warmer climate. International Journal of Climatology, 33(5), 1301-1307.

Urrutia, R., and M. Vuille (2009), Climate Change projections for the tropical Andes using

a regional climate model: Temperature and precipitation simulations for the end of the

21st century. J. Geophys. Res., 114, D02108, doi:10.1029/2008JD011021.

Vergara, W., A. Deeb, A. Valencia, R. Bradley, B. Francou, A. Zarzar, A. Grünwaldt, and Se. Haeussling (2007), Economic impacts of rapid glacier retreat in the Andes, Eos, Transactions American Geophysical Union 88, 25: 261-264.

Vuille, M., B. Francou, P. Wagnon, I. Juen, G. Kaser, B. G. Mark, and R. S. Bradley (2008), Climate change and tropical Andean glaciers: Past, present and future, Earth-Sci. Rev., 89(3), 79-96.

Vuille, M., R. S. Bradley, and F. Keimig (2000), Interannual climate variability in the Central Andes and its relation to tropical Pacific and Atlantic forcing, J. Geophys. Res., 105, 12,447–12,460.

Wagnon, P., P. Ribstein, G. Kaser, and P. Berton (1999), Energy balance and runoff seasonality of a Bolivian glacier, Global Planet Change, 22,1: 49-58.

Westrick, K. 1999. Soil depth calculation ‘‘aml’’ [online]. Available from www.hydro.washington.edu/Lettenmaier/Models/DHSVM/index.shtml [accessed February 2014].

Wigmosta, M. S., L. W. Vail, and D. P. Lettenmaier (1994), A distributed hydrology-vegetation model for complex terrain, Water Resour. Res., 30, 1665–1679.

Wigmosta, M.S., B. Nijssen, P. Storck, and D.P. Lettenmaier, 2002: The Distributed Hydrology Soil Vegetation Model, In Mathematical Models of Small Watershed Hydrology and Applications, V.P. Singh, D.K. Frevert, eds., Water Resource Publications, Littleton, CO., p. 7-42.

Yapo, P. O., H. V. Gupta, S. Sorooshian, Multi-objective global optimization for hydrologic models, J. Hydrol., 204, 83–97, 1998.

Zhao, Q., Liu, Z., Ye, B., Qin, Y., Wei, Z., and Fang, S. (2009), A snowmelt runoff forecasting model coupling WRF and DHSVM, Hydrol. Earth Sys. Sci., 13(10), 1897-1906.

Tables

Table 1. Range of parameters sampled and optimal parameter values used in simulations.

Model Parameter	**Range Analyzed**	**Optimal**
Snow Roughness Length (mm)	0.5-5	0.7
Precip. Elevation Gradient (%/km)	0-100	15
Temperature Lapse Rate (°C/m)	-0.009 - -0.003	-0.0084
Maximum Snow Albedo	0.8-0.9	0.83
Glacier Ice Albedo	0.3-0.4	0.39

Figures

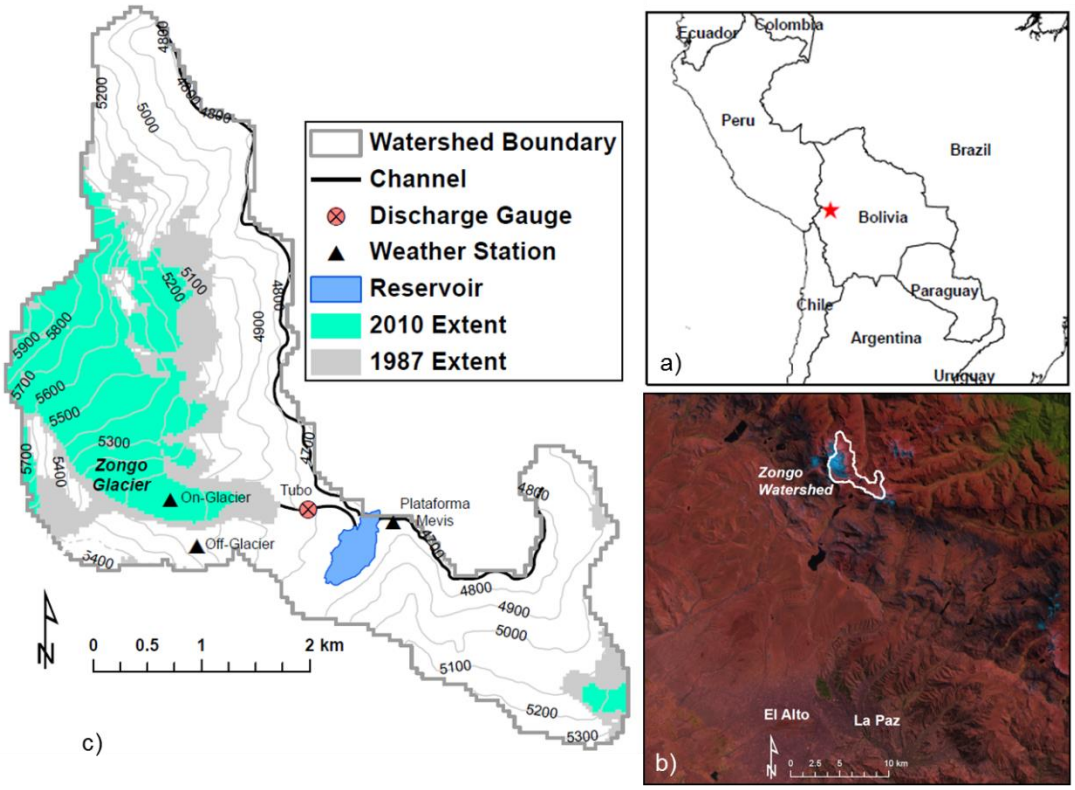

Figure 1: Zongo headwaters study site in Bolivia: (a) regional map, red star indicates the location of the study site; (b) false color satellite image including La Paz and El Alto; (c) watershed map showing equal elevation lines (m), glacier historical extent from Landsat-TM imagery, and in-situ observation locations.

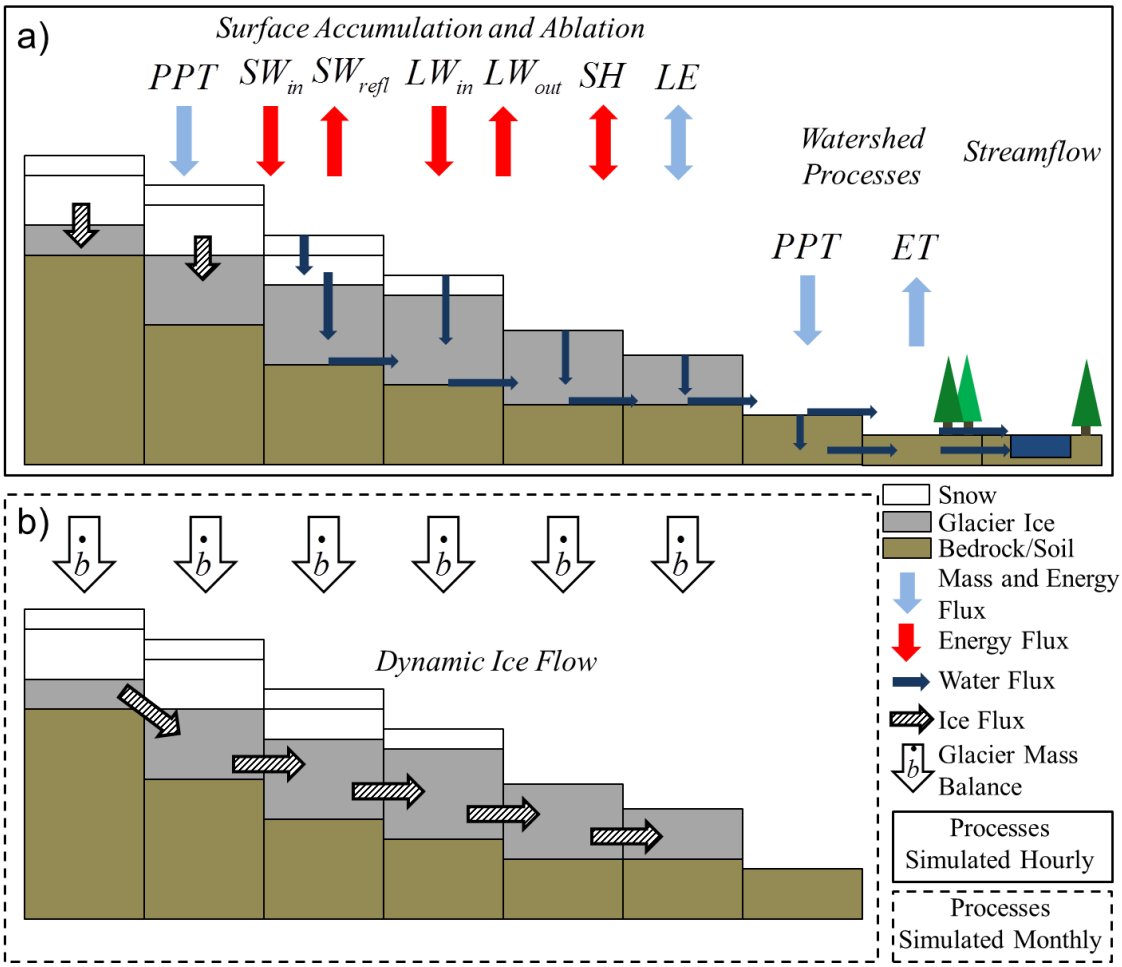

Figure 2: Schematic showing the first order processes simulated by the coupled glacier-hydrology model. (a) Land surface and hydrology component of the coupled model illustrating the fluxes of mass and energy between the atmosphere and land surface implemented on snow, glacier ice, and soil/vegetation surfaces. Arrows indicate precipitation, PPT; incoming shortwave radiation, SW_{in}; reflected shortwave radiation, SW_{refl}; downwelling longwave radiation, LW_{in}; emitted longwave radiation, LW_{out}; sensible heat, SH; latent heat, LE; and evapotranspiration, ET. (b) Illustration of the glacier dynamics component of the model that simulates lateral dynamic ice flow driven by gravity as ice accumulates with positive ice mass balance ($\dot{b}$).

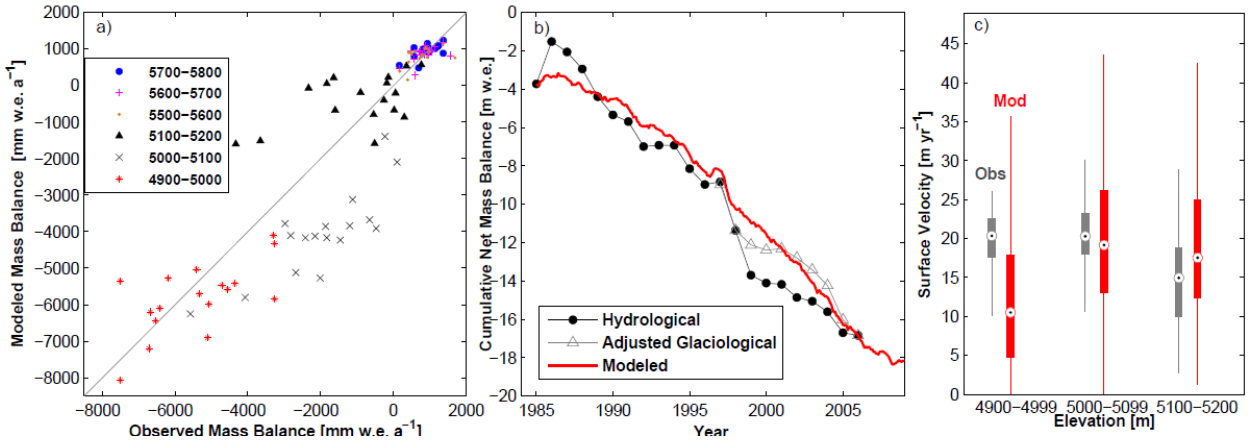

Figure 3: (a) Modeled and annual mass balance plotted for each 100 m elevation interval on Zongo Glacier (1992-2010). (b) Modeled (red), and observed cumulative net mass balance estimated from hydrological measurements (black) and adjusted glaciological measurements (gray). Observations were digitized from *Soruco et al.* [2009]. (c) Box plots showing the distribution of observed and modeled surface velocity in three elevation intervals on the lower reaches of Zongo Glacier. Measured elevation band averaged mass balance and surface velocity data were taken from the Glacioclim database (http://www-lgge.ujf-grenoble.fr/ServiceObs/).

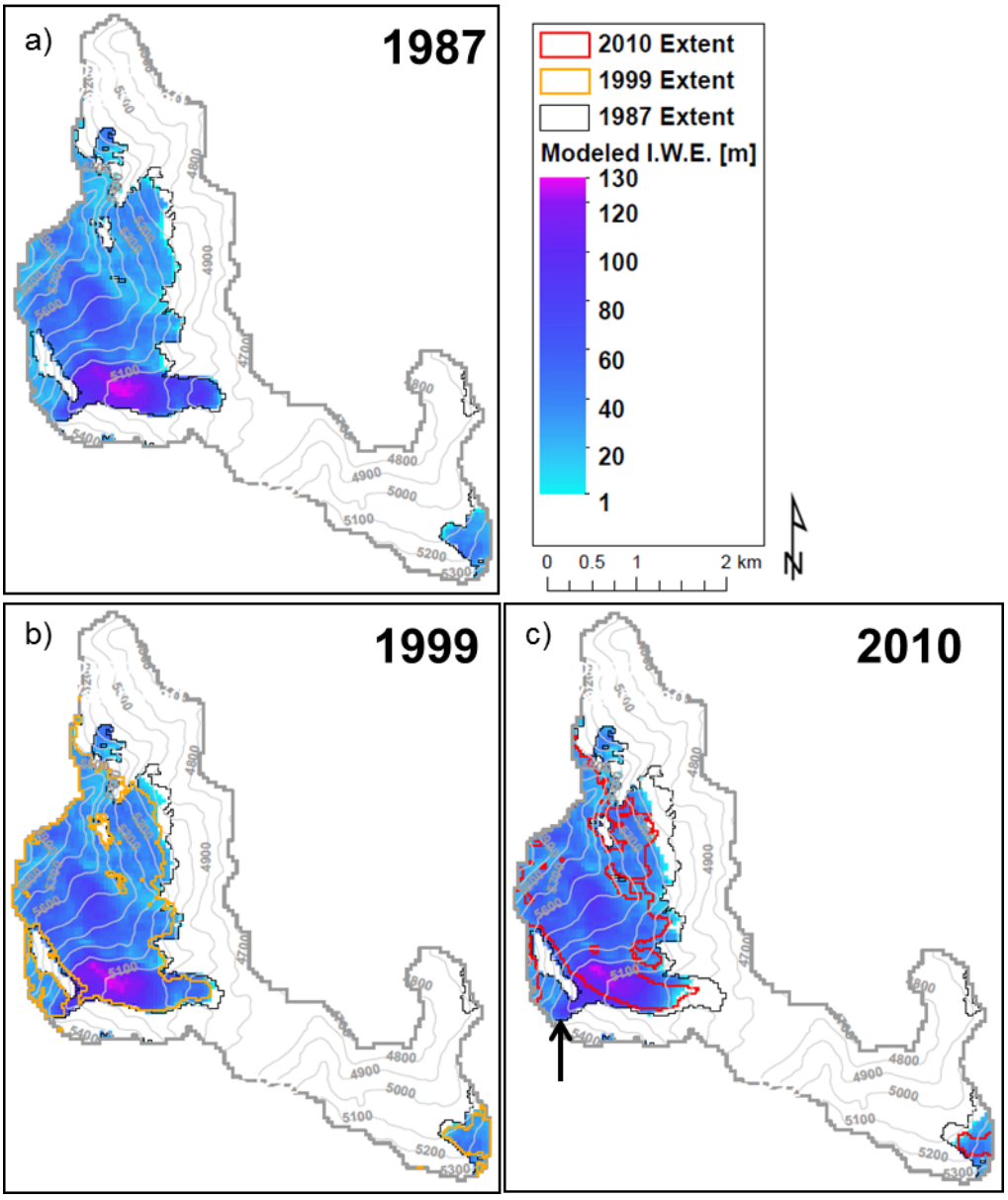

Figure 4: Modeled ice water equivalent (IWE) for (a) 1987, (b) 1999, and (c) 2010. Satellite derived estimates of glacier area are shown with the thin solid black (1987), yellow line (1999), and red line (2010). The arrow indicates an area of significant mismatch between modeled and observed extent.

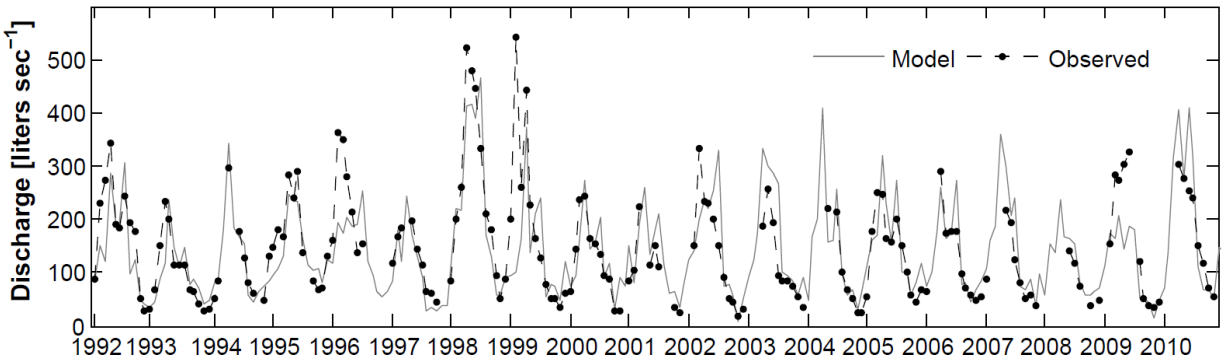

Figure 5: Simulated and observed monthly mean discharge at the measurement location below the terminus of Zongo glacier. Discharge measurements that contain periods of missing data were removed from the calculation of mean discharge values. Year ticks signify Sept. 1 of the labeled hydrological year.

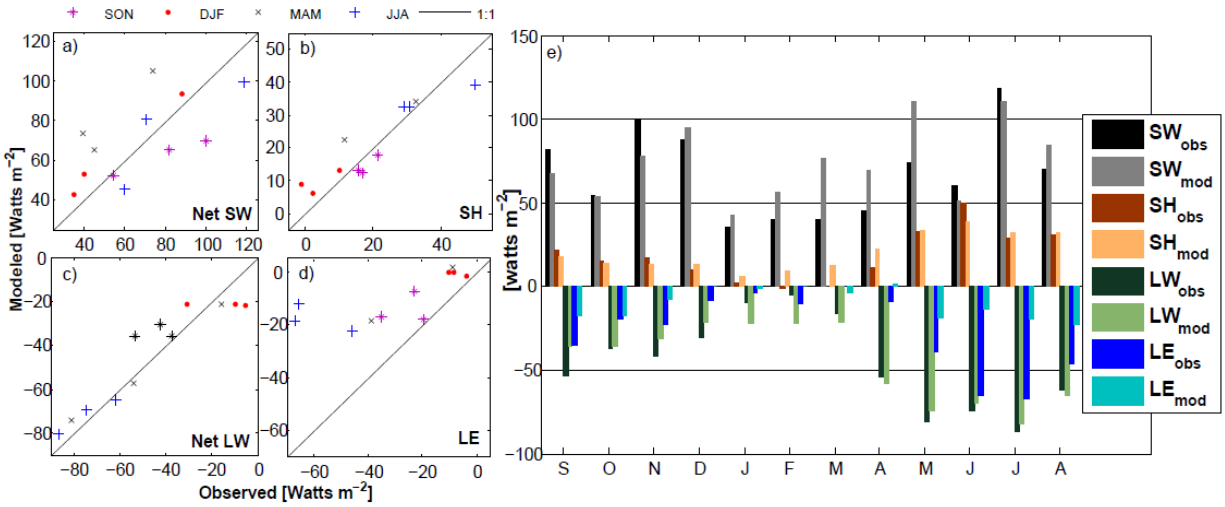

Figure 6: Modeled (mod) and observed (obs) surface energy fluxes at 5050 m a.s.l. on Zongo glacier for the hydrological year 1999/2000: (a-d) 1:1 plots showing model performance; (e) plotted as monthly time series to show seasonal dynamics. Observations are taken from *Sicart et al*., [2005]. Turbulent fluxes were not measured during March.

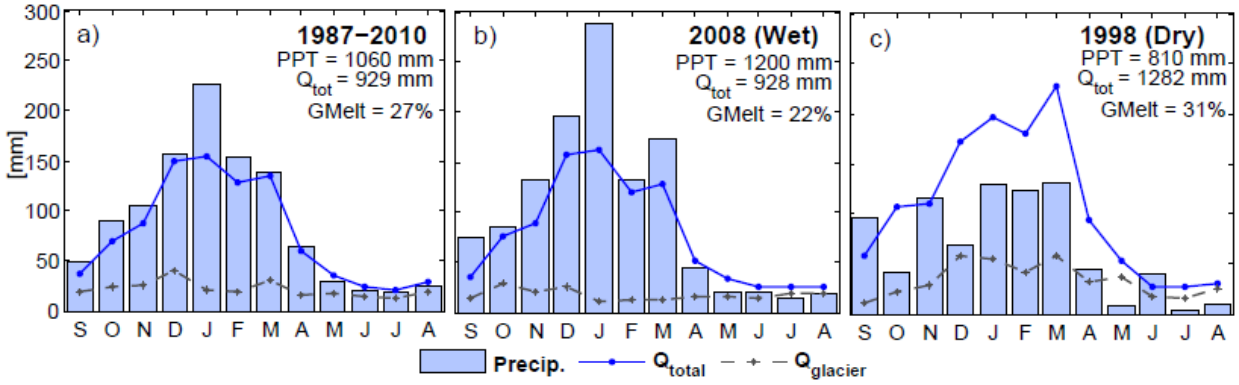

Figure 7: Monthly mean precipitation (bars), modeled total discharge (blue, solid line) entering the reservoir, and glacier melt (gray, dashed line) plotted for: (a) the historical period (1987-2010); (b) a wet year (2007-2008); and (c) a dry year (1997-1998). In the inset annual

precipitation (PPT), runoff (Q_{tot}), and percent of glacier melt contribution (%GMelt) are reported.

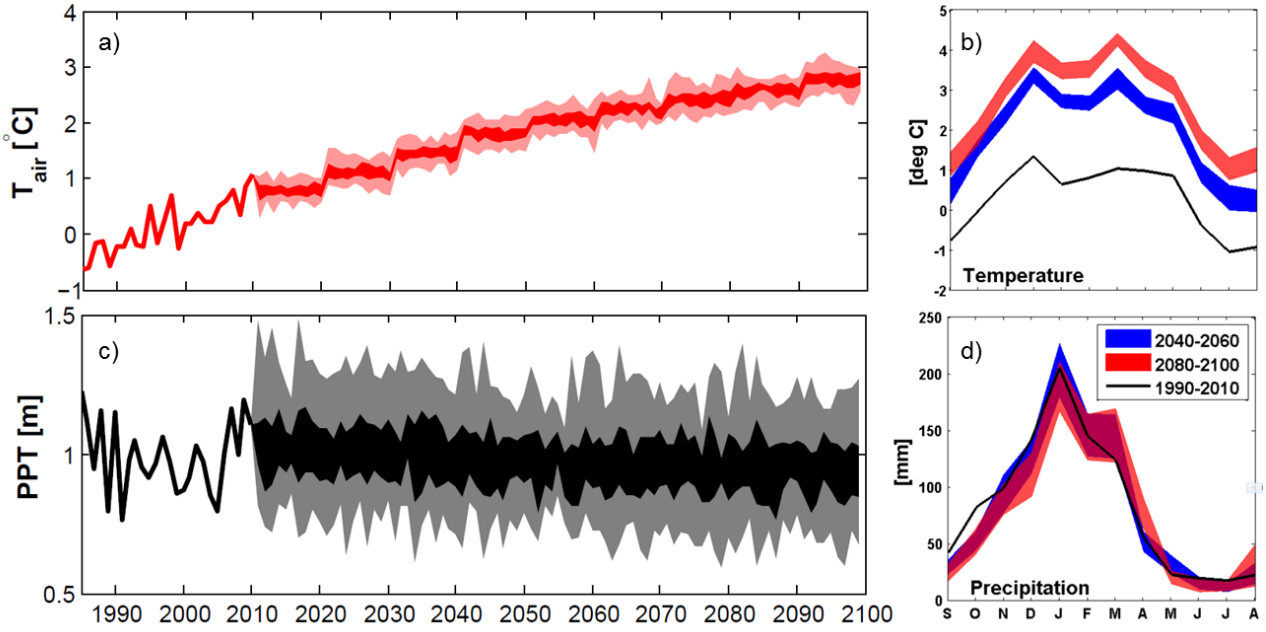

Figure 8: (a) Historical and projected annual mean air temperature and (c) annual precipitation. The full range of values reflect variability represented through statistical downscaling, while the darker regions represent the interquartile range of the projections. The seasonality of (b) air temperature and (d) precipitation is shown for the historic time period (1990-2010, black line), the near future (2040-2060, blue), and the far future (2080-2100, red). The ranges represented for the time periods reflect the ranges in mean monthly values of the future realizations. The data reflect the elevation of the meteorological station used in the analysis (5050 m a.s.l.).

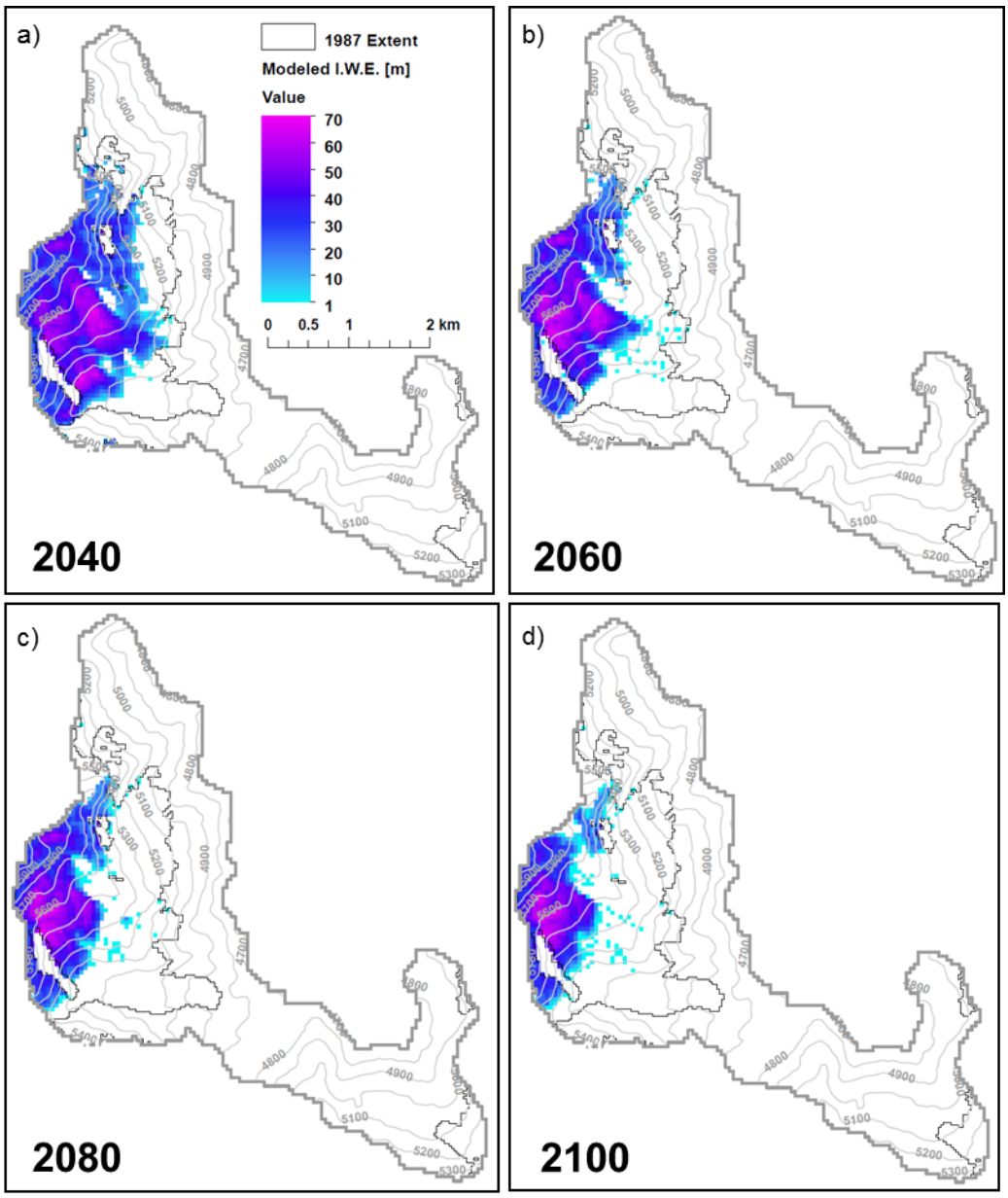

Figure 9: Projected glacier area and thickness at the end of WY 2040, 2060, 2080, and 2100. Satellite derived glacier extent estimates for 1987 are shown with a black outline.

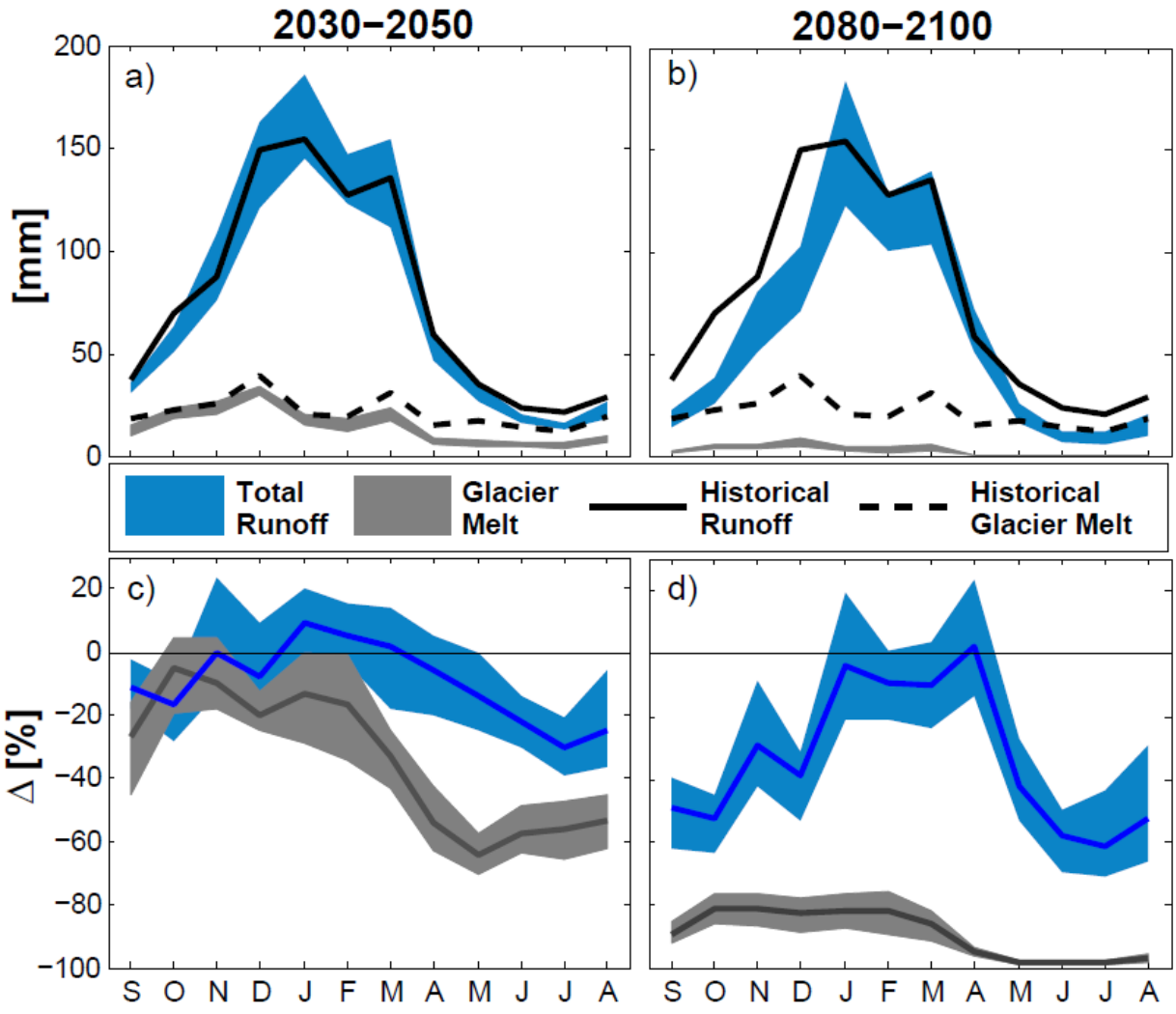

Figure 10: Mean monthly runoff (sourced from rain, snowmelt, and glacier melt) entering the reservoir predicted for (a) the near future (2030-2050) and (b) far future (2080-2100). Percent change relative to 1987-2010 in total runoff and glacier melt for the (c) near and (d) far future. Mean values of percent change (with respect to historical) between scenarios are indicated by the dark solid lines.

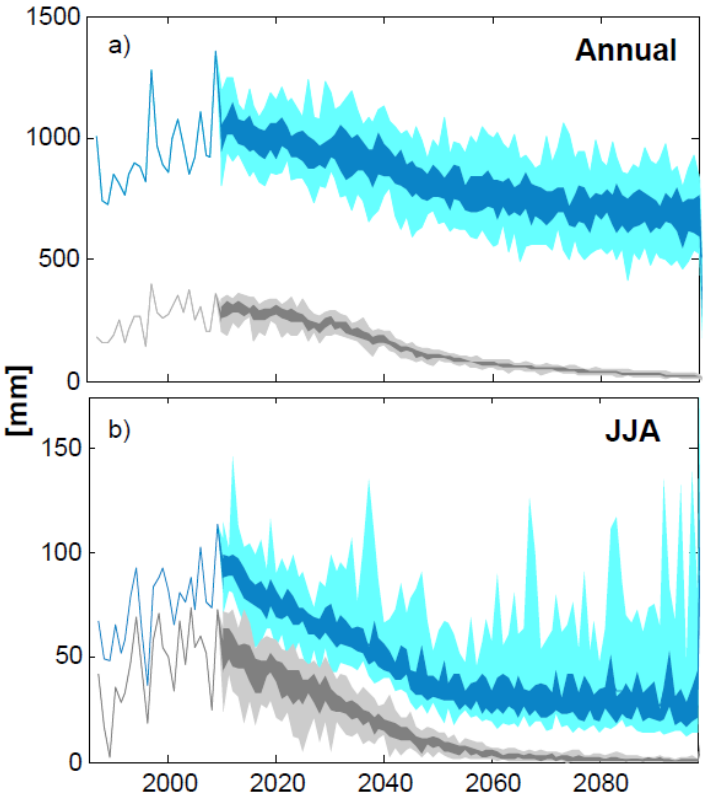

Figure 11: (a) Annual and (b) dry season (JJA) total runoff (rain + snowmelt + glacier melt, blue) and glacier melt (gray) for the entire watershed. Lighter colors indicate the full range of future projections using multiple stochastic realizations of the transient future climate and dark colors denote the interquartile range of the projections.

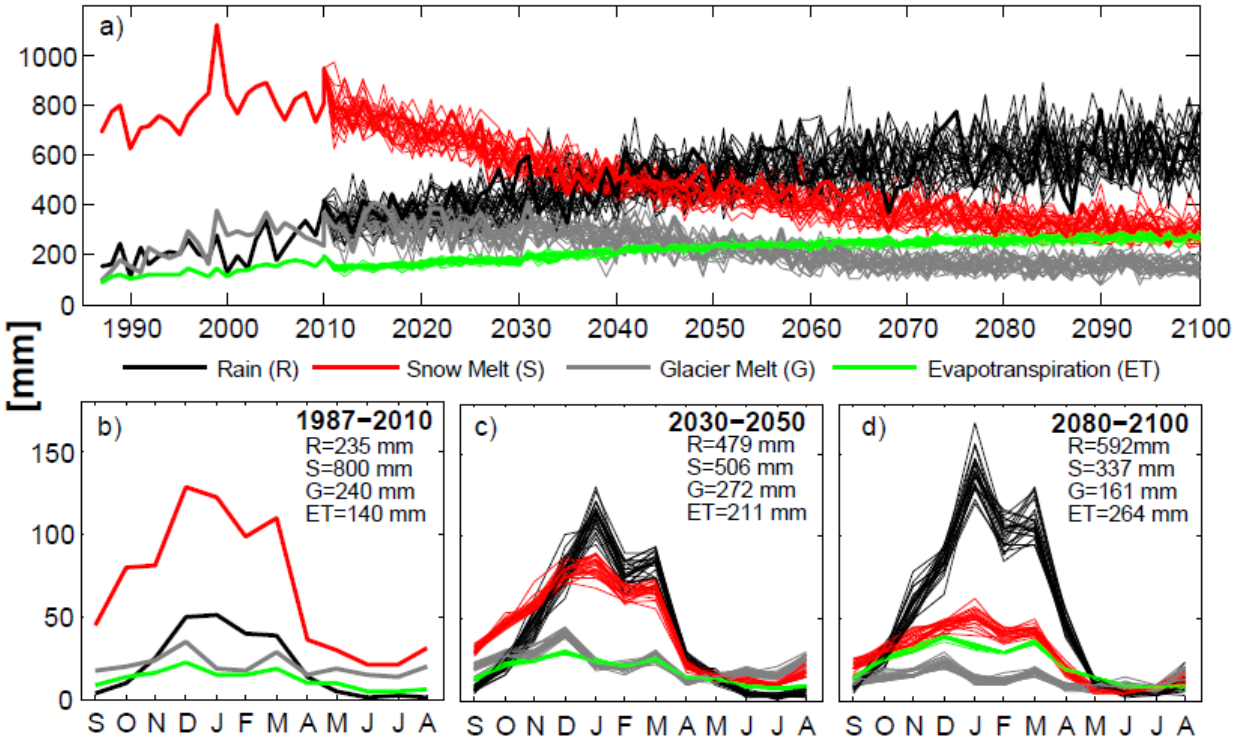

Figure 12: Historical and projected annual (a) and seasonal (b-d) fluxes of rain, snow melt, glacier melt and evapotranspiration (ET) in the watershed.

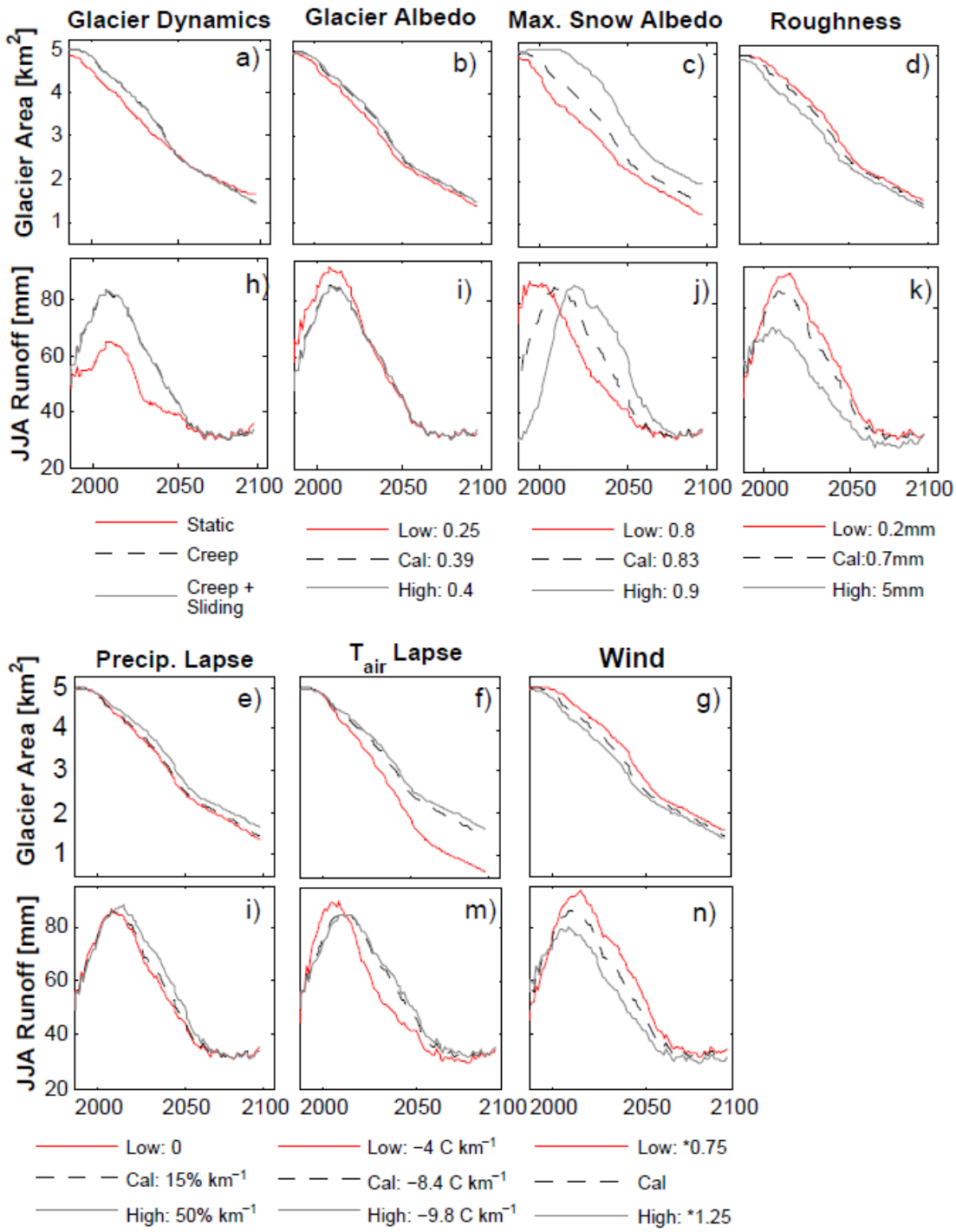

Figure 13: Sensitivity of (a-g) glacier area and (h-n) JJA runoff to different model configurations and parameter selection for a single future climate realization. The optimal parameter value (Cal) was found through multi-objective calibration while the low and high values represent physically plausible end members for the region. A wind multiplier was not used in calibration however a range was tested for this analysis. The results reflect the 10-year centered mean of simulations using a single climate forcing realization.

Appendix 2A

2A-1. Reanalysis Data Bias Correction

We provide comparisons of raw MERRA reanalysis meteorological variables with those that were locally measured at the Off-Glacier (5050 m, Appendix 2A Figures 2.A1-5). From these comparisons we derived ratios (RH, SW, wind) and absolute differences (temperature) for each hour of the day, for each month of the year to use in bias correction of the longer time series of reanalysis data. Bias correction was not applied to precipitation as the statistical probability distributions at the Plataforma locations are similar (Figure 2.A5) and monthly accumulations were in approximate agreement (NSE=0.76). The largest differences are observed in precipitation events with low accumulation and the highest accumulation. The reanalysis data contains more frequent small precipitation events, and precipitation amounts that are lower than the observable amount (0.2 mm) with field instrumentation.

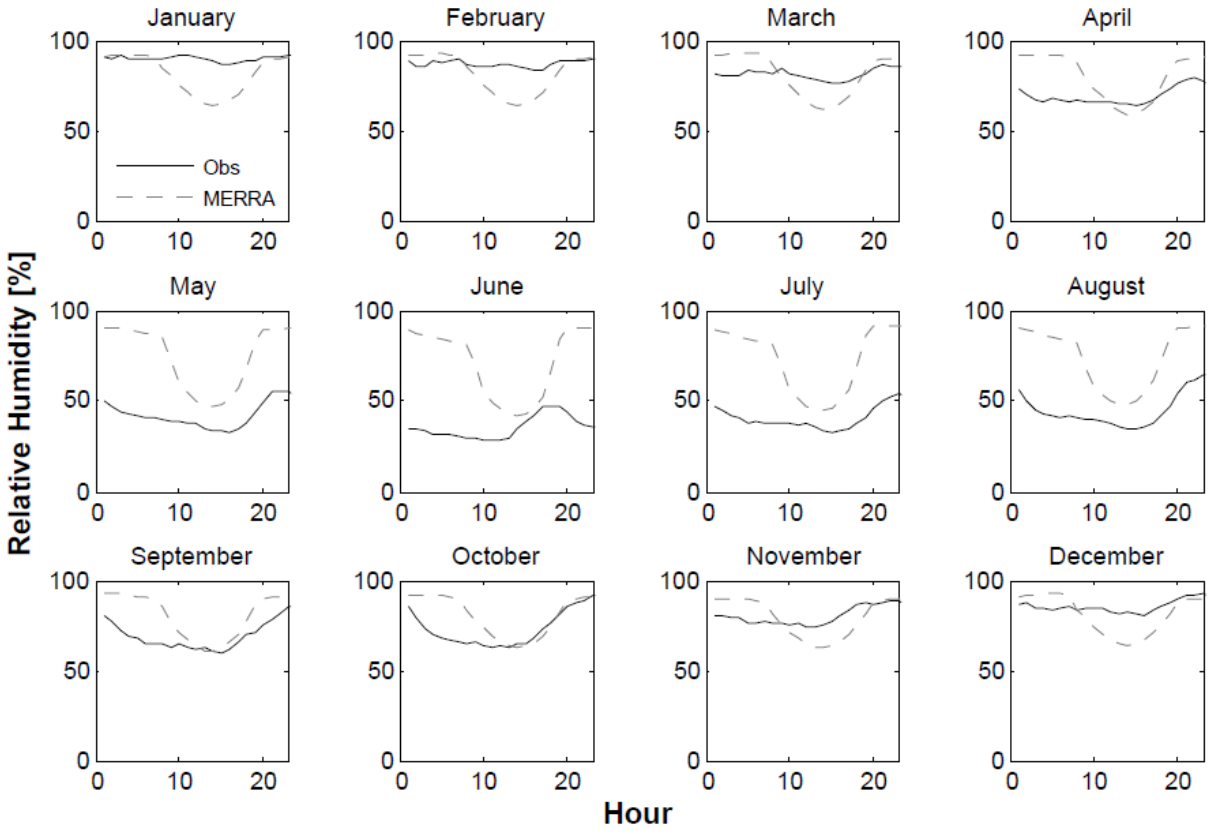

Figure 2.A1. Comparison of MERRA and locally measured (Hors-Glacier) hourly relative humidity.

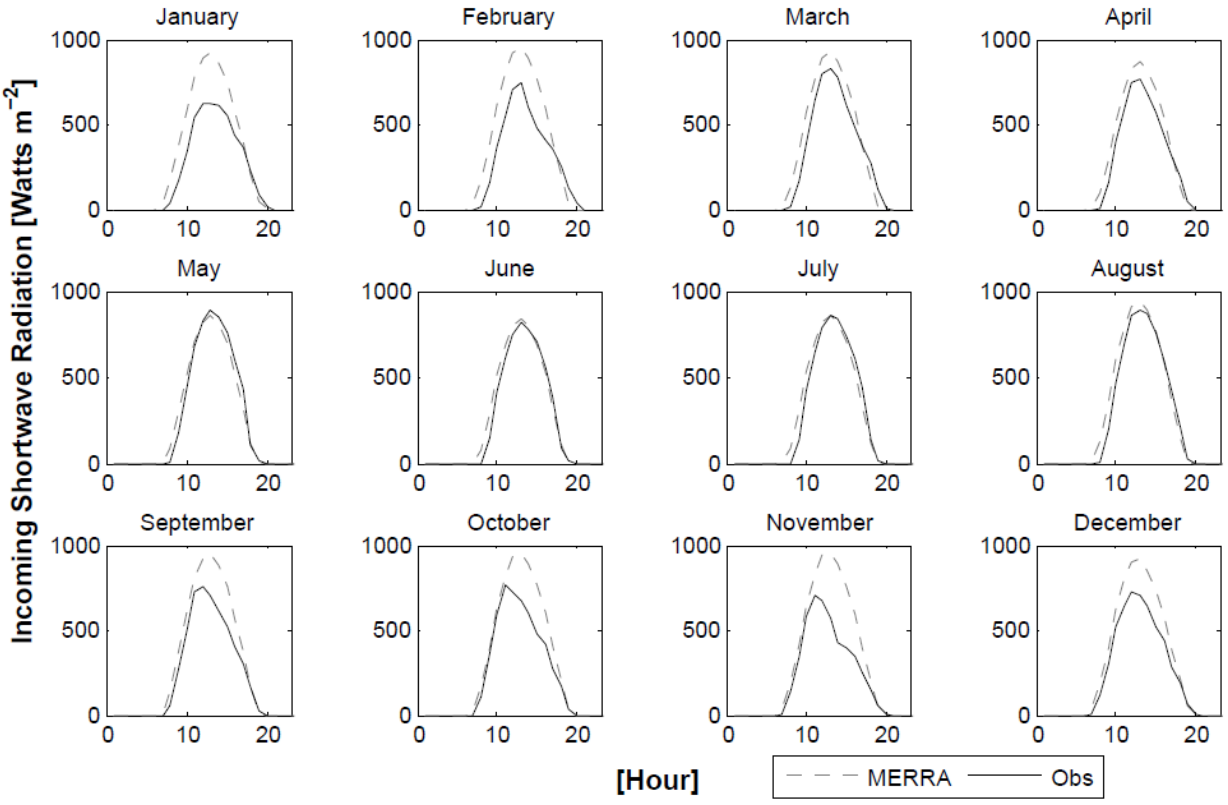

Figure 2.A2. Comparison of MERRA and locally measured (Hors-Glacier) hourly shortwave radiation.

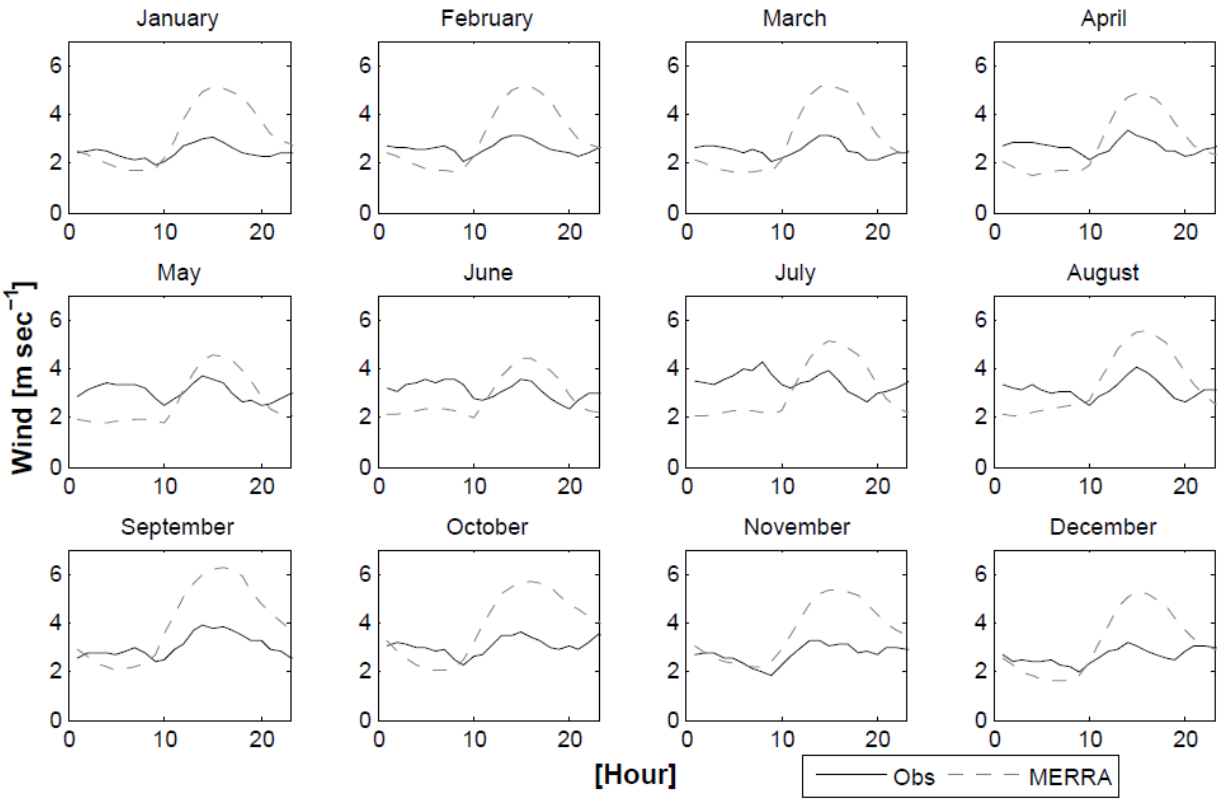

Figure 2.A3. Comparison of MERRA and locally measured (Hors-Glacier) hourly wind speed.

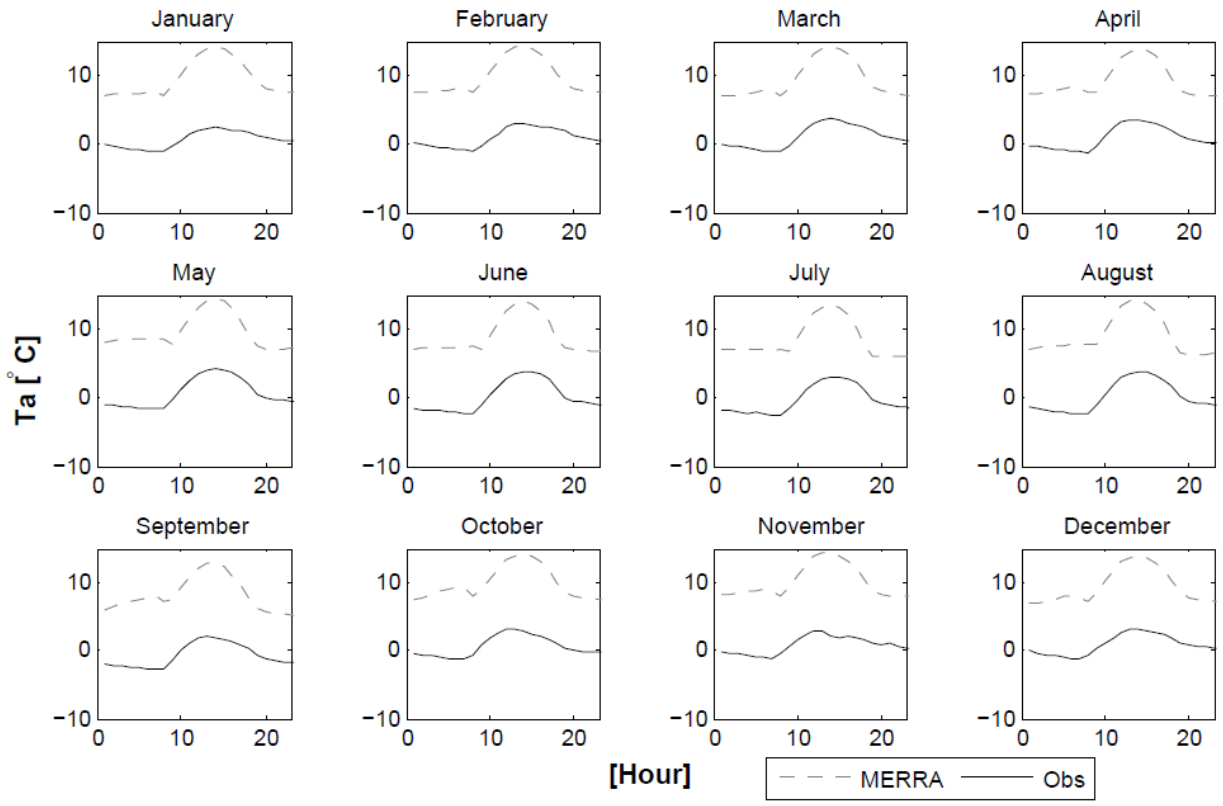

Figure 2.A4: Comparison of MERRA and locally measured (Hors-Glacier) hourly near surface air temperature.

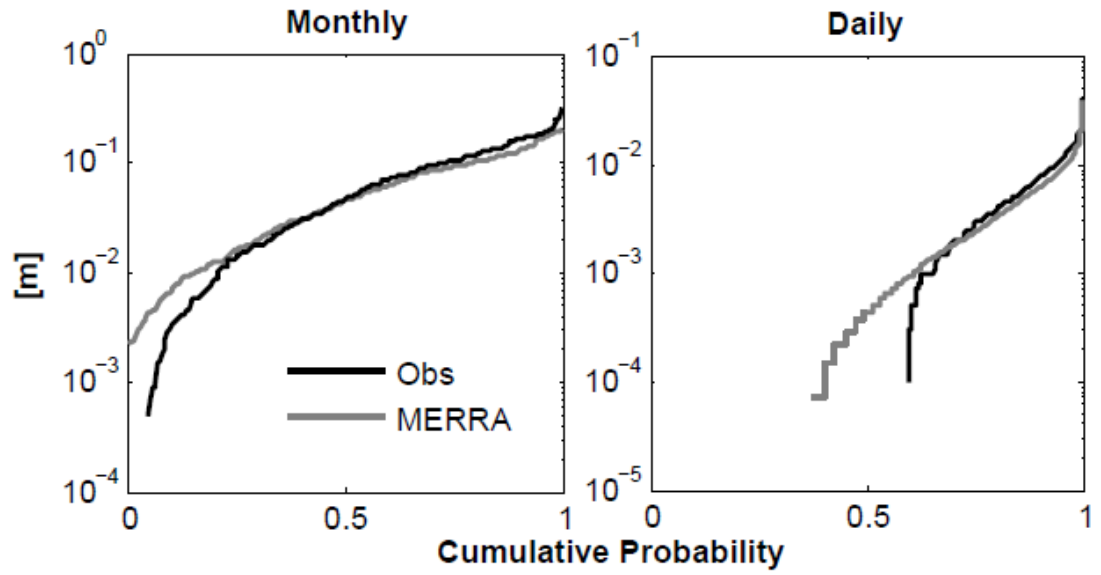

Figure 2.A5: Comparison of MERRA and locally measured precipitation (Plataforma) for monthly and daily temporal aggregation intervals for hydrological years 1992-2010.

CHAPTER 3: IMPLICATIONS OF DECADAL TO CENTURY SCALE GLACIO-HYDROLOGICAL CHANGE FOR WATER RESOURCES OF THE HOOD RIVER BASIN, OR U.S.A.[2]

Abstract

In glacier fed rivers melting of glacier ice sustains streamflow during the driest times of the year, especially during drought years. Anthropogenic and ecologic systems that rely on this glacial buffering of low flows are vulnerable to glacier recession as temperatures rise. We demonstrate the evolution of glacier melt in watershed hydrology over the course of 184 years through the application of a coupled hydrological and glacier dynamics model in the Hood River Basin in Northwest Oregon, U.S.A. Melt water originating from glaciers on the northern flanks of Mount Hood is a vital source of irrigation water for crops in the basin; diversions for agricultural water supply are located in close proximity to the glaciated headwaters. Continuous simulations of glaciological processes (mass accumulation and ablation; lateral flow of ice; heat conduction through supra-glacial debris) which are directly linked with seasonal snow dynamics as well as other key hydrologic processes (evapotranspiration; subsurface flow) show that historically, the contribution of glacier melt to basin water supply was up to 79% at upland water management locations. Supraglacial debris cover modulates the rate of glacier recession and progression of dry season flow at upland stream locations with debris covered glaciers. Model results indicate that dry season (July-Sept.) discharge sourced from glacier melt started to decline early in the 21st century following glacier recession that started early in the 20th century. Changes in climate over the course of the current century will lead to 14-63% (18-78%) losses in dry season discharge volumes across the basin for IPCC emission pathway RCP4.5 (RCP8.5). The largest losses are predicted at upland drainage locations of water diversions that were dominated historically by glacier melt and seasonal snowmelt. We demonstrate that the contribution of glacier melt not only varies greatly in space, but also in time. It displays a strong decadal scale

[2] This chapter has been submitted and is under review for publication:
Frans, C., E. Istanbulluoglu, D.P. Lettenmaier, G. Clarke, T. Bohn, and M. Stumbaugh (under review), Risks to glacier fed water resources: hydrological change in the Hood River Basin, OR U.S.A. 1916-2099 Hydrological Processes.

fluctuation that is super-imposed on the effects of a long-term climatic warming trend. This decadal variability results in reversals in trends in glacier melt which underscores the importance of long time series of glacio-hydrologic analyses for evaluating the hydrological response to glacier recession.

3.1 Introduction

Mountain glaciers provide an important source of water in climates with highly seasonal precipitation patterns as snow and ice masses in partially glacierized watersheds redistribute wet season precipitation to streamflow at times of the year where there are few other sources of water entering streams (Meier, 1969; Fountain and Tangborn, 1985; Barnett et al., 2005). During dry and warm years when seasonal snow accumulation is reduced, the contribution of glaciers to low flows is further amplified as a larger area of glacier surfaces is exposed to melt for longer durations of the year (Fleming and Clarke, 2005) . As the climate warms, this natural buffering of low flows provided by glaciers is expected to increase initially; however reductions in glacier area will eventually overcome enhanced rates of melting from warmer temperatures (Hock et al., 2005; Moore et al., 2009; Baraer et al., 2012). Hence, recession of these glacier ice masses poses a significant risk to downstream water users and ecological systems.

The timescales at which increased ablation from climate warming augments streamflow and the rate of declines after a peak in augmentation are not well understood. Observational records of discharge downstream from glaciers are often not long enough to identify these peaks. Furthermore, these phases of response to a positive trend in temperature may become less distinct over short time intervals as they can be superimposed on streamflow patterns linked to natural decadal climate variability (e.g., Beebee and Manga, 2004).

Previous research has directed efforts toward diagnosing the contribution of glacier melt to streamflow in western North America (Nolin et al., 2010; Pelto, 2011; Pelto, 2008; Moore and Demuth, 2001; Stahl and Moore, 2006; Stahl et al. 2008; Jost et al. 2012). Many of these studies analyzed short periods of observation (Nolin et al., 2010), were conducted in small drainages at locations close to the glacier termini positions (Moore and Demuth, 2001; Nolin et al., 2010), did not differentiate seasonal snowmelt and glacier ice melt (Stahl and Moore, 2006; Nolin et al., 2010), or used water balance methods that simplify or do not consider the non-glacierized portions of watershed (Pelto, 2008; 2011). More recently model applications that simulate both hydrologic processes and glacier mass have been used to describe the glacier melt contribution to streamflow (e.g., Jost et al., 2012; Stahl et al., 2008; Naz et al., 2014; Immerzeel et al., 2012; Ragettli and Pellicciotti, 2012). When constrained by and evaluated with local observations,

models allow analyses of processes at spatial and temporal scales that cannot be accomplished with local observations alone. Furthermore, models can be used to test hypotheses of how a partially glacierized system may respond as the climate continues to warm.

In glacierized watersheds where streamflow is utilized for agriculture and domestic uses and where aquatic habitats rely on glacier-driven low flows the following three questions are critical for resource managers: (1) what is the seasonal contribution of glaciers to streamflow along a stream network fed by glaciers? (2) how do glaciers respond to climate variability and climate warming? and (3) what is the relationship between glacier melt and streamflow response over time? These questions are important in the Hood River basin of northwestern Oregon (Fig. 1) whose headwaters are in the glaciers of Mt. Hood. We examine the contribution of glacier melt to streamflow in the Hood River basin at a range of spatial scales for 184 years using a spatially distributed hydrology model coupled with a glacier dynamics model as described in (Naz et al., 2014). To account for the influence of debris on ablation from the glacier surfaces a debris surface energy balance model (DSEB) is incorporated based on the work of Reid and Brock (2010). In what follows we first describe the study site in greater detail, and follow with a brief description of the modeling framework. We follow with results of our historic reconstructions, and projections of the response of the coupled glacier and hydrologic system through the end of the 21st century.

3.2 Study Site

The Hood River heads on the northern flanks of Mount Hood, a glaciated stratovolcano that reaches an elevation of 3429 m a.s.l. (North American Vertical Datum of 1988 (NAVD 88)). The Hood River drainage basin (~880 km^2) includes 89 km^2 of mostly irrigated agricultural land, largely consisting of perennial crops (apple and pear orchards and grape vineyards) that have high water demand during summer months. Stream discharge in the basin is managed through flow diversion structures and 2 small storage reservoirs (5.1 Gl capacity) that provide agricultural water supply to meet seasonal irrigation demands. Irrigation diversions occur from April 15 through September 30, peaking in July or August. In some reaches consumptive diversion during the irrigation season is estimated to be 40% of natural flow (Coccoli, 2002). Reliable irrigation water supply for fruit trees and vines is more critical than for annual herbaceous crops as a deficit of water can not only lead to reduced yields in the current year, but

can also reduce yields in subsequent years or result in death of the plants (Steduto et al., 2012). Furthermore, water deficits can be detrimental beyond the period of peak evapotranspiration as the fruit continues to develop prior to late summer and autumn harvest (Steduto et al., 2012). In addition to irrigation, water in the basin is used for hydropower, potable water supply for a population of 40,000, protection of aquatic species, and recreation.

Many of the agricultural water supply diversion structures are located on streams at high elevations in close proximity to partially glacierized headwater catchments. Glaciers in these upland catchments have retreated up to 60% over the past century (Lillquist and Walker, 2006; Jackson and Fountain, 2007). The fraction of glacier cover in the basin above its outlet at the Columbia River is modest (<1%), however it is as large as 20% in smaller headwater drainages that are located above water diversion locations. The change in area of individual glaciers over the historical period has been highly variable. The two largest glaciers in the Hood River drainage, Eliot and Coe (Fig. 1), have experienced the smallest amounts of areal change which is largely attributed to supra-glacier debris (colluvium) cover on their ablation areas, northerly exposure, and the elevation range of the accumulation areas (Jackson and Fountain, 2007). Debris cover complicates surface energy dynamics and ablation rates of underlying glacier ice as thin layers of debris lower the local albedo and enhance ablation, while continuous thicker layers of debris act as an insulator and retard ablation (Clark et al., 1994; Conway and Rasmussen, 2000; Mihalcea et al., 2006). While these historical patterns of glacier retreat over the 20th century on Mount Hood have been well documented, the consequences of these changes on streamflow are not known. Moreover, the contribution of glacier melt to streamflow and water resource management across the basin is not fully understood.

3.3 Methodology

3.3.1 Hydrological Model

The distributed hydrology soil vegetation model, DHSVM (Wigmosta et al., 1994), served as the modeling foundation for the simulations of hydrological processes across the heterogeneous landscape. DHSVM has been widely applied in mountainous watersheds across the globe, with numerous applications in the Pacific Northwest (e.g., Elsner et al., 2010; Cuo et al., 2011; Jost et al., 2009; Casola et al., 2009). The model provides a physically based representation of snowmelt and evapotranspiration and an analytical representation of the routing

of surface and subsurface flow based on the distribution of watershed characteristics (topography, vegetation, soil, climate) and physical and analytical parameters over the discretized model domain (Kampf and Burges, 2007). For applications in mountainous areas with complex topography, the more salient components of the model include a surface energy balance (SEB) multilayer snow and ice melt and accumulation model (Andreadis et al., 2009; Naz et al., 2014). To simulate spatial changes in glacier mass and area, a representation of glacier dynamics (Jarosch et al., 2013; Clarke et al., 2015) is integrated into the hydrological modeling framework (Naz et al., 2014).

The ablation areas of the Eliot and Coe glaciers (Fig. 1), the two largest glaciers in the basin, are partially covered with a layer of colluvial debris. To account for the influence of debris on ablation rates we have integrated algorithms based on the debris covered glacier SEB model of Reid and Brock (2010) that solves the following energy balance equations vertically with fine scale vertical node spacing. The debris surface temperature (T_s) is iteratively calculated to balance the energy fluxes at the atmosphere-debris interface considering the temperature of the atmosphere (T_a) (at 2 m) and underlying debris (T_d),

$$SW_{net} + LW_{in} + LW_{out}(T_s) + H(T_s, T_a) + LE(T_s, T_a) + G(T_s, T_d) + P(T_s, T_a) = 0 \qquad (1)$$

where SW_{net} is net shortwave radiation, LW_{in} is incoming longwave radiation, LW_{out} is outgoing longwave radiation, H is sensible heat flux, LE is the latent exchange, G is the flux of heat to subsurface debris layers, and P is the energy advected from liquid precipitation. Equation 1 is linked with the internal temperature profile within the debris layer ($T_d(z,t)$) through the conductive surface heat flux term (G), and is modeled by calculating conductive heat fluxes through the debris,

$$\rho c \frac{\partial T_d(z,t)}{\partial t} = \frac{\partial}{\partial z}\left(k_{debris} \frac{\partial T_d(z,t)}{\partial z} \right) \qquad (2)$$

where ρ, c, and k_{debris} are the density, specific heat capacity and the effective thermal conductivity of the debris. The total thickness of the debris is discretized into N computational nodes with vertical spacing dz. To determine ablation rates, the conductive heat flux at the lower boundary, the debris-ice interface, is calculated as,

$$G_{ice} = k_{debris} \frac{T_d(N-1) - T_f}{dz} \qquad (3)$$

where G_{ice} is the conductive heat flux to the underlying ice, $T_d(N-1)$ is the temperature of the debris at the computation node above the debris-ice interface, and T_f is the temperature of the debris-ice interface (assumed to be constant at 0° C). The algorithms as implemented are consistent with Reid and Brock (2010) with the exception of the numerical method of estimating surface temperature. Where Reid and Brock (2010) used the Newton-Raphson technique, we use the Brent method (Brent, 1973) to reduce computation time. Additionally for computational stability we discretize the debris layer into 20 vertical computational nodes for all model debris covered grid cells, regardless of total debris thickness.

3.3.2 Data

The model is forced with meteorological data at 3 hour intervals. The meteorological forcing data consist of precipitation, air temperature, relative humidity, wind speed, downwelling longwave radiation, and downward shortwave radiation. We use a gridded dataset generated using observed daily minimum and maximum temperature, accumulated precipitation, and mean wind speed that have been interpolated from NOAA Cooperative Observing Network (Co-Op) weather stations to a 1/16 degree spatial resolution (~6 km) following the methods of Hamlet and Lettenmaier, (2005). Using these methods the data are adjusted so that long term trends are consistent with those observed at stations of the NOAA Global Historical Climatology Network (GHCN-D) which are of the highest quality and have been corrected for any introduction of biases from changes in station location and instrumentation, among others. Additionally, the data are scaled to be consistent with the climatology of the Parameter-elevation Regressions on Independent Slopes Model data (PRISM, version 3) which accounts for finer spatial scale variability imposed by complex topography (Daly et al., 1994). Hamlet and Lettenmaier (2005) provide a complete description of this methodology. The Mountain Microclimate Simulation model (MTCLIM; Thornton and Running, 1999), as implemented by Bohn et al. (2013), is used to disaggregate these variables to sub-daily time intervals and to estimate the other required meteorological variables (shortwave radiation, longwave radiation, relative humidity). In DHSVM the input meteorological variables are further interpolated to the model resolution (90 meters) using elevation gradients (temperature, precipitation) and seasonal and diurnally varying scaling to represent the influence of topography on solar radiation.

Geospatial input data required by the model include elevation, vegetation classification, soil texture classification, initial glacier ice thickness, and supraglacial debris thickness. Digital elevation model (DEM) data at 30 m. spatial resolution were obtained from the United States Geological Survey (USGS; ned.usgs.gov/). Vegetation classification was specified following the National Land Cover Database (NLCD 2001; www.mrlc.gov/nlcd2001.php). Soil classification data from the Natural Resource Conservation Service (NRCS) soil database (SSURGO; http://websoilsurvey.nrcs.usda.gov/) and the Soil Resource Inventory (SRI) were used to define soil texture classifications across the basin. All data were resampled (bilinearly) to 90 meter spatial resolution for consistency. Parameters for each vegetation class (leaf area index, rooting depth, stomatal resistance) and soil texture (porosity, lateral conductivity, field capacity) were taken from previous DHSVM applications in the region and adjusted during model calibration as needed. Glacier bed topography, the elevation of the land surface beneath the glacier ice was estimated using the method of Clarke et al. (2013). Supraglacial debris thickness on Eliot glacier was interpolated to the model grid resolution from point measurements (Jackson, 2007). No measurements of debris thickness are available for Coe glacier, thus aerial imagery archived in Google Earth was used to identify debris extent and the longitudinal gradient in debris thickness observed on Eliot glacier was used to estimate the distribution of debris thickness. The thickness of the debris at each model element was assumed to be constant in time.

A multistep spin-up procedure was used to estimate the initial distribution of ice thickness early in the 20^{th} century. In this procedure the glacier dynamics model that simulates ice movement through creep (offline from the hydrological model) is forced with a temporally constant spatially distributed surface mass balance field so that the modeled steady state ice extent closely matches historical estimates. Due to the lack of knowledge of historical ice thicknesses this method assumes that if the extent simulated using glacier dynamics matches the observed extent, it provides an accurate estimate of the distribution of ice thickness at the time of observation. This assumption is tested by comparing modeled and observed rates of recession during the historical period of analysis. Furthermore, using the glacier dynamics model to spin-up the glaciers provides a distribution of ice that is mechanistically stable. Naz et al. (2014) provide a more detailed description of this methodology. Area estimates provided in Jackson and Fountain (2007) were used to delineate the historical extent.

We used output of general circulation models (GCMs) from the Coupled Model Inter-Comparison Project 5 (CMIP5, Taylor et al., 2012) to project glacier and hydrologic conditions through the end of the 21st century. Projections of 9 GCMs (Table 1) selected based on the PNW model skill rankings of Rupp et al. (2013) and available climate variables of representative concentration pathway scenarios RCP4.5 and RCP8.5 were used. Daily maximum and minimum temperature, and precipitation and wind speed from the GCM output were downscaled to 1/16 degree spatial resolution using the Multivariate Adaptive Constructed Analogs (MACA) statistical downscaling method (Abatzoglou and Brown, 2012). Generation of the sub-daily meteorological forcing data follows the methods previously outlined for the historical data.

3.4 Results

3.4.1 Model Evaluation

Glacio-hydrological model results require calibration and evaluation with historical observations of both hydrological and glaciological variables (e.g., Finger et al., 2011). We calibrated and evaluated our model by comparing simulations with observations and estimates of glacier extent, measurements of glacier ablation under debris, and discharge observations. Following comparisons of our model predictions with observations we adjusted selected calibration parameters accordingly. Key parameters that were calibrated are the precipitation elevation gradient, glacier albedo, maximum snow albedo used in temporal decay curves, and soil depth.

We compared modeled discharge with naturalized stream discharge estimated from measurements and known water management operations by the U.S. Bureau of Reclamation (www.usbr.gov/pn/programs/studies/oregon/hoodriver/index.html) at the Hood River at Tucker Bridge USGS gauging station (14120000, Fig. 1) for water years 2002-2011. The naturalized discharge was estimated by adding water diverted by irrigation districts and potable water, seasonal filling of two small reservoir systems and subtracting seasonal reservoir drawdowns and return flow from irrigation districts. This information was provided by the water users at monthly time intervals. The model results reflect naturalized unregulated flow because the model does not represent water management infrastructure and operations.

The Nash Sutcliffe Efficiencies (NSEs) for simulations of the Hood River at Tucker Bridge is 0.61 and 0.78 for daily and monthly mean discharge (2002-2011). At the USGS gauging station

on the West Fork near Dee (USGS No. 14118500, Fig. 1) the model NSE values are 0.55 and 0.81 for daily and monthly mean streamflow, respectively, for the period WY 1933-1991. Visual comparisons of mean monthly flows for these two locations are shown in Figure 2. At both locations the model over predicts winter flows, however the model performance improves during the melt and low flow season, the time of year that is critical for water resource management. The model underestimates September discharge slightly, which may be attributed to a model deficiency in simulating deep subsurface flow and uncertainty in the estimation of naturalized discharge.

3.4.2 Defining Glacier Melt Contribution to Discharge

A critical first step in assessing the role of glaciers in catchment hydrology is to define how the glacier contribution to streamflow discharge is quantified. Glacier contribution to streamflow has generally been defined either as all water leaving the glacier footprint (including direct flow from rain and snowmelt) or the melting of glacier ice only (see La Frenierre and Mark, 2014). Nolin et al. (2010) conducted a geochemical isotopic mixing analysis of the Middle Fork of the Hood River to determine the relative contribution of glaciers to stream discharge. Samples of discharge from the glacier terminus, groundwater from downstream areas outside of the glaciers, and discharge from a stream location where these two sources are mixed were used in the analysis. In their approach, all water leaving the glacier footprint is lumped as glacier melt. To facilitate comparison with these estimates, we plot the ratio of the modeled discharge leaving the footprint of the Eliot glacier to total discharge modeled downstream in Eliot Creek (Fig. 3) above the confluence with the Middle Fork (Fig. 1). The dates and locations are consistent with those sampled during WY 2007 by Nolin et al. (2010). For the sequence of the three sampling dates, the method of Nolin et al. found the glacier contribution to be 88$\pm$4, 78$\pm$3, and 76$\pm$3% at a single sampling time on the given day. For these dates the model simulated the diurnal range of glacier contribution to be 74-95, 75-92, and 58-76%. The geochemically derived estimates fall within in these ranges for the corresponding sampling dates (Fig. 3).

Modeled discharge derived only from the melting of glacier ice is also plotted (excluding snowmelt, rain); highlighting the differences between the two definitions of glacier melt contribution. During the period before Sept. 15 the mean contribution from the glacier footprint is 84% while the contribution from the melting of only glacier ice is 60%. The relative glacier

contribution from these two definitions diverges the most after mid-September when autumn rainfall and transient snowmelt increases, outweighing the contribution of glacier ice melt (Fig. 3). In the analyses we report in the remainder of this article, we take the glacier contribution to discharge as melting of glacier ice only; we do not include snowmelt and rain on the glaciers. These seasonal sources of water will still contribute to runoff generation after a glacier has receded. Limiting the definition of the glacier contribution to only include the melting of glacier ice is more appropriate to long-term water management considerations, as it does not include fluxes of water that will still be present in a non-glacierized state.

3.4.3 Historical Contribution of Glacier Melt to Discharge

Figure 4 shows modeled mean monthly hydrologic fluxes aggregated across the basin over the period 1916-2005. The largest input of water in the basin is in the form of snowmelt. This occurs during the wet season (November to March) in the form of transient snowmelt at low to mid elevations. During spring and summer (April to September) seasonal snowmelt occurs, gradually decreasing through the dry season. Rainfall occurs throughout the year with a maximum flux in Autumn (September to November) before temperatures decrease and lead to a transition to (mostly) snow in the winter. Potential evapotranspiration calculated for a short reference crop (alfalfa, PETref) and modeled evapotranspiration (ET) follow the seasonal cycle of solar radiation. Irrigation is not represented in the model; hence, actual evapotranspiration is higher than modeled. At the scale of the entire basin the flux from the melting of glacier ice is the smallest input. However, the glacier melt season (JAS) starts when rainfall is at its minimum, snowmelt is minimum, and moisture limitation is maximum (as indicated by the difference between PET and ET).

To obtain a more detailed perspective on the importance of glacier melt, we identify its relative contribution to stream discharge across the basin. Figure 5 shows the modeled mean total discharge and mean glacier melt discharge by day of year over the historical model time period 1916-2005. Also included in the figure is the maximum glacier melt discharge modeled on each day of the year over this time period. As for basin scale discharge patterns (Fig. 5a), the role of glacier melt at the outlet of the basin is modest; on average the maximum contribution of glacier melt is about 7% during September. However, during dry and warm years the contribution is as high as 24%. The contribution of glacier melt is much larger at upstream

locations, with the strongest influence at the Eliot Creek diversion location (Fig. 1) where glacier melt contributes up to 54% of daily discharge on average (1916-2005), and is as high as 79% (Fig. 5f), which occurred in Sept. 1924. Historically, dry and warm years (1924, 1977, 1987, 1991, 1994, and 2001) lead to the highest glacier melt contributions. The meteorological data is less reliable during early in the period of analysis however high contribution in 1924 is probable as the glacier state was responding to warm dry PDO after the end of the last little ice age (*Jackson and Fountain*, 2007).

3.4.4 The role of debris cover on glacier ablation and retreat

Incorporation of algorithms that represent energy dynamics of supra-glacier debris cover into our model allows us to identify the role of surface debris cover on ablation. Jackson and Fountain (2007) measured ice melt throughout a melt season on the ablation area of Eliot glacier with ablation stakes. We compared our modeled ablation at every grid cell with debris cover between 9/24/2004 and 7/28/2005 with the measurements of Jackson and Fountain (2007) (Figure 6). The model has a roughly exponential decay of ablation with increasing thickness of debris overlying the ice, consistent with the observations. The modeled ablation is more variable than the observations, probably in part because the model domain extends into areas that are often shadowed by the surrounding terrain, and are generally not represented by the observations. To ensure that the model replicated the observed pattern, the constant for the effective thermal conduction of the debris layer (k_{debris}, equations 2 and 3) was adjusted iteratively while all other constants remained fixed (Section 3.1).

To demonstrate the role of debris cover on the response of glacier area, we ran the DHSVM/glacier dynamics model combination for the historical (1916-2005) period. Figures 7a and 7b show ice thickness with and without the representation of debris and its role on the SEB at the end of 2004. In Figures 7a and 7b, the initial model extent is the glacier extent that was used as an initial condition in the model simulations, which was determined through model spinup (Section 3.2). The observation-derived glacier area estimates of Jackson and Fountain (2007) are shown for ~1904 and 2004. The figures demonstrate how the presence of debris cover on Eliot and Coe glaciers reduced the glaciers' sensitivities to warming and slowed their overall retreat. We show the relative significance of the debris-modulated rate of retreat to stream discharge by plotting the ratio of September total discharge volume (Q_{tot}) modeled at the Eliot

creek diversion location (located downstream of Eliot glacier) without debris to the simulation with debris (panel c). In the case of no debris, higher ablation rates lead to higher discharge early in the time period and faster recession (panel b) which results in more rapid declines in September discharge volumes. A threshold in glacier area is reached at about 1958 when the higher rate of ablation per unit area of the debris free condition is overcome by the reduction of area through recession. In the last decade of the period discharge is 14% lower in the no debris cover condition.

A key assumption of these model-based analyses is that the debris thickness varies in space however is constant throughout the entire time period. Local debris thickness will vary as surface colluvium melts out of the ice, is deposited from erosion of adjacent slopes, and as the surface of the ice moves. Debris thickness may increase in time with increasing temperature as melting increases. We use the thicknesses measured in 2004 throughout the entire period because historical debris thicknesses are not known. Shallower thicknesses of debris earlier in the century would have increased the rate of retreat by allowing more ablation.

3.4.5 Projected long-term glacio-hydrological change: 1916 – 2099

To analyze long term glacio-hydrological change and infer future evolution of the Hood river system, we extended our period of analysis through 2099 using time series of future meteorological data statistically downscaled from 9 general circulation models for two emissions pathway scenarios (Section 3.2). Projected seasonal changes in mean annual temperature and precipitation are plotted in Figures 8 (a-b) and seasonal changes are summarized in Table 2. This long period of analysis allows us to explore glacio-hydrological trends in response to warming temperatures. This long period of analysis helps to avoid confounding long-term trends with low frequency multi-decadal variability that complicates interpretation of shorter time series.

Figs. 8c-d show the relative changes in glacier area and volume over the simulation period. Area change is shown relative to the initial area, and in the case of the observed data point (blue; Fig. 8c), relative to observational estimates early in the 20th century. Consistent with the observation based findings of Jackson and Fountain (2007), rapid declines in area and volume (as inferred by observed thinning) occurred during warm and dry conditions early in the 20^{th} century (Fig. 8c,d). During the 1950's to 1970's temperatures cooled and were accompanied by higher precipitation (Fig. 8 a,b) which resulted in reduced rates of retreat and some advances

and increases in glacier volume. After the mid-1970s, temperatures increased and precipitation decreased leading to more loss of area and volume. These periods of warm-dry and cold-wet conditions are now attributed to phases of the Pacific Decadal Oscillation (PDO, Mantua et al. 1997) which have been shown to have a strong influence on glacier mass fluctuations (Bitz and Battisti, 1999; Moore and Demuth, 2001; Josberger et al., 2007). Over the historical period 1916-2004 the model predicted a 28% loss of glacier area which is within the range of uncertainty of the estimates of Jackson and Fountain (2007) who estimated a loss of a loss of 25 ± 10% for these glaciers (blue dot, Fig. 8; spatial changes are shown in Fig. 7). Glacier ice volume is more variable as it tracks precipitation variability, whereas glacier dynamics modulate the response of glacier area resulting in a more muted response to precipitation. Spikes in glacier area that do not correspond to spikes in glacier volume (e.g., early in the 21st century) indicate snow densification to ice outside of main glacier bodies during colder periods and do not indicate advances of large bodies of ice. Changes in volume do not always reflect changes in glacier area. This is consistent with observations of Eliot Glacier volume by Jackson and Fountain (2007) who found that increased glacier thickness did not always correspond to gains in glacier area. This highlights the advantage of using a physical representation of glacier dynamics relative to simpler volume-area scaling approaches that are often used for glacier climatic response studies.

In the future period continued loss of glacier area and volume is predicted at nearly the same rate for both emissions pathway scenarios until about 2030. The loss of area and volume slows midcentury for scenario RCP4.5 reflecting a reduced rate of increasing temperature (Fig. 8a). The rate of volume and area loss decreases at 2075 under RCP8.5 when ice only remains at the highest elevations (above 2350 m). By the end of the 21st century, glacier area is projected to decrease 69 (59-81)% under RCP4.5 and 89 (80-96)% under RCP8.5, relative to the 2004 extent.

To evaluate how these changes in glacier area influence changes in dry season discharge we deconstructed long-term modeled discharge at the Eliot Creek diversion location, the water management location with the largest glacier contribution. Figure 9 shows 10-year centered mean modeled discharge volume from 1916-2099 during the entire dry season (July-Sept.; panels a,c) and during September only (panels b,d). Total discharge is plotted and is also separated into its sources: non-glacial (snowmelt + rain) and glacier melt. At this time of year most of the non-glacier component is from snowmelt. During the historical period the prominent pattern associated with PDO phases is clear. In cool-wet periods (e.g., 1945-1955) there is high

snowmelt and low glacier melt, while in warm-dry periods (e.g., 1955-1960) there is less snowmelt and glacier melt increases. Historically, the interaction between these two discharge sources decreased variability in total discharge in response to variations in climate, demonstrating the buffering effect of glacier melt on streamflow. As the temperatures warmed after 1970 the amplitude of the snowmelt phases decreased and an overall negative trend dominates. In the future time period, decadal variability persists in the individual GCMs; however, it is not reflected in the ensemble mean because the timing of the decadal variability differs between GCM models. For July-Sept. discharge volume, sustained and slightly increasing glacier melt partially compensates losses of snowmelt; however, declines in glacier melt after 2010 further exacerbate the negative trend in total streamflow. For September flows the declining trend in glacier melt occurred earlier (1990) playing a more important role in declining water availability at this time of the year.

Fig. 10 expands this long term analysis to other locations in the basin. We plot the changes in dry season (July-Sept.) total discharge relative to the mean of dry season discharge for a reference period spanning 1916-1950. Changes in total discharge are expressed as a 10-year centered mean for clarity. Trends are negative across the basin, with the sharpest declines in the partially glacierized upland basins (Eliot and Coe Creek in the Middle Fork). In the ensemble mean for all of the locations, under RCP4.5 total discharge is predicted to decline 12-44% midcentury (2040-2060) and 14-63% late century (2080-2099). Under RCP8.5, total discharge is predicted to decline 13-49% midcentury and 18-78% late century. The largest declines in total runoff are expected in the upland drainages that experience losses in glacier area and that historically were more affected by seasonal snowmelt. The West Fork is the least sensitive basin as it had very little glacier contribution in the past and includes more low elevation area (Fig. 1) that is less sensitive to changes in snowmelt. Model streamflow projections for all locations represent natural, unregulated flow because the model does not represent water management effects. This assumption is important to consider when analyzing results for the downstream locations where upstream withdrawals and irrigation from diverted water and pumped groundwater change the water balance.

The relative glacier contribution to dry season flows expressed as a fraction of total flow is also shown in Figure 10 (green). At the headwater locations these fractions are predicted to increase until ~2040. However, at the Eliot Creek location glacier melt discharge volume is

predicted to begin to decline around 2010 (Fig. 9). This increasing relative contribution despite declining glacier melt volume is the result of more rapid reductions in non-glacial sources of runoff. Despite decreasing melt volume the relative contribution of glacier melt remains high until mid-century at these headwater locations. Furthermore, as the seasonal snowpack date of disappearance shifts earlier in the year, the relative contribution of glacier melt increases earlier during the dry season. This increases the importance of glacier melt at times closer to the period of peak evapotranspiration (mid-July; Fig. 4) and maximum irrigation withdrawals. Historically glacier melt displayed the largest contribution after this period, late August through September.

Our analyses have focused on the time of year when water demand is at its peak. The water resource infrastructure that was designed with reliance on available summer water may no longer be appropriate in a warmer climate. Given the projected decreases in water availability in the summer further analyses extended to all seasons can support the exploration of options for providing additional storage that will be needed (e.g., surface water storage, artificial aquifer recharge) and conservation measures (e.g., increased irrigation efficiency, improved surface water conveyance).

3.5 Conclusions

We have evaluated long-term changes in the contribution of glacier melt to the Hood River system using a spatially distributed hydrological model coupled with a glacier dynamics model. Our period of analysis spans 184 years from 1916 through 2099, which allows us to assess changes both in the period of almost 100 years during which observations are available, and through the remainder of the 21st Century (based on downscaled climate model projections). Our analysis shows that:

- Supra-glacier debris cover plays a significant role on ablation rates retarding the retreat of glaciers. A comparison with a modeled debris-free condition showed that the reduced recession resulted in up to 14% more September discharge volumes, by the end of the historical period.
- The fraction of Hood River streamflow that originates as glacier melt is greatest in late summer in the headwater catchments, and ranges from 54% on average (maximum 79%) in the Eliot Creek basin to a much smaller 7% (maximum 24%) at the outlet of the basin.

- An ensemble of model simulations driven with projections of future climate indicate that dry season discharge (JAS) could decrease up to 78% by the end of the current century in headwater streams that were historically snow and ice melt dominated.
- The relative contribution of glacier melt to discharge in headwater tributaries is projected to increase until ~2040 despite declining glacier melt volume, but will decline thereafter.
- Strong decadal variability in modeled glacier melt is superimposed on declines linked to a long-term warming trend. Long time series of observed and modeled data are required to describe evolving glacio-hydrological processes in regions that experience pronounced natural climate variability.

Our work highlights the relevance of dynamic process based glacio-hydrological modeling frameworks for future water management, land use, and conservation planning. The Hood River basin is one glacier fed system in the Pacific Northwest facing downstream risks posed by glacier recession with continued warming. Further modeling and observational studies are required to characterize and understand glacio-hydrological change for different river systems of varying environmental and climatic settings.

Acknowledgement:

We thank Matthew Bachmann, Howard Conway, and Andrew Fountain for their feedback after a presentation of this study and Niklas Christensen for providing naturalized stream flow data. This research was supported by the NASA Interdisciplinary Research in Earth Science Program - Grant NNX10AP90G.

References

Abatzoglou JT, Brown TJ. 2012. A comparison of statistical downscaling methods suited for wildfire applications. *International Journal of Climatology* **32**(5), 772-780. doi: 10.1002/joc.2312

Andreadis KM, Storck P, Lettenmaier D P. 2009. Modeling snow accumulation and ablation processes in forested environments. *Water Resources Research*, **45**(5).

Baraer M, Mark BG, McKenzie JM, Condom T, Bury J, Huh K, Portocarrero C, Gómez J, Rathay S. 2012. Glacier recession and water resources in Peru's Cordillera Blanca. *Journal of Glaciology* **58**, no. 207 (2012): 134-150.

Barnett TP, Adam JC, Lettenmaier DP. 2005. Potential impacts of a warming climate on water availability in snow-dominated regions. *Nature*, **438**(7066), 303-309.

Bitz CM, Battisti DS. 1999. Interannual to Decadal Variability in Climate and the Glacier Mass Balance in Washington, Western Canada, and Alaska. *Journal of Climate*, **12**(11), 3181-3196.

Bohn TJ, Livneh B, Oyler JW, Running SW, Nijssen B, Lettenmaier DP. 2013. Global evaluation of MTCLIM and related algorithms for forcing of ecological and hydrological models. *Agricultural and Forest Meteorology*, **176**, 38-49.

Brent RP. 1973. Chapter 4: An Algorithm with Guaranteed Convergence for Finding a Zero of a Function. In *Algorithms for Minimization without Derivatives*, Prentice-Hall: Englewood Cliffs, NJ, ISBN 0-13-022335-2

Casola JH, Cuo L, Livneh B, Lettenmaier DP, Stoelinga MT, Mote PW, Wallace JM. 2009. Assessing the Impacts of Global Warming on Snowpack in the Washington Cascades. *Journal of Climate*, **22**(10), 2758-2772.

Clark DH, Clark MM, Gillespie AR. 1994. Debris-covered glaciers in the Sierra Nevada, California, and their implications for snowline reconstructions. *Quaternary Research*, **41**(2), 139-153.

Clarke GKC, Anslow F, Jarosch A, Radic V, Menounos B, Bolch T, Berthier E. 2013. Ice volume and subglacial topography for western Canadian glaciers from mass balance fields, thinning rates, and a bed stress model. *Journal of Climate*, **26**(12), 4282-4303.

Clarke GKC, Jarosch A, Anslow F, Radic V, Menounos B. 2015. Projected deglaciation of Western Canada in the 21st century. *Nature Geoscience*, in press.

Coccoli H. 2002. Hood River Watershed Action Plan. Hood River Soil and Water Conservation District. June 19, 2002. Hood River, Oregon. 74 p.

Conway H, Rasmussen L.A. 2000. Summer temperature profiles within supraglacial debris on Khunibu Glacier, Nepal. In Debris-covered Glaciers: Proceedings of an International Workshop Held at the University of Washington in Seattle, Washington, USA, 13-15 September 2000 (No. 264, p. 89). IAHS.

Cuo L, Beyene TK, Voisin N, Su F, Lettenmaier DP, Alberti M, Richey JE. 2011. Effects of mid-twenty-first century climate and land cover change on the hydrology of the Puget Sound basin, Washington. *Hydrological Processes*, **25**(11), 1729-1753, doi: 10.1002/hyp.7932.

Daly C, Neilson P, Phillips DL. 1994. A statistical-topographic model for mapping climatological precipitation over mountainous terrain. *Journal of Applied Meteorology* **33**: 140–158.

Elsner MM, Cuo L, Voisin N, Deems JS, Hamlet AF, Vano JA, Mickelson K, Lee SY, Lettenmaier DP. 2010. Implications of 21st Century climate change for the hydrology of Washington State. *Climatic Change* **102**(1-2) 225-260, doi:10.1007/s10584-010-9855-0

Finger D, Pellicciotti F, Konz M, Rimkus S, Burlando P. 2011. The value of glacier mass balance, satellite snow cover images, and hourly discharge for improving the performance of a physically based distributed hydrological model. *Water Resources Research* **47**(7).

Fleming SW, Clarke GK. 2005. Attenuation of high-frequency interannual streamflow variability by watershed glacial cover. *Journal of Hydraulic Engineering*, **131**(7), 615-618.

Fountain AG, Tangborn WV. 1985. The effect of glaciers on streamflow variations. *Water Resources Research*, **21**(4), 579-586.

Hamlet AF, Lettenmaier D. P. 2005. Production of Temporally Consistent Gridded Precipitation and Temperature Fields for the Continental United States. *Journal of Hydrometeorology* **6**(3), 330-336.

Hock R, Jansson P, Braun LN. 2005. Modelling the response of mountain glacier discharge to climate warming. In Global Change and Mountain Regions (A State of Knowledge Overview)., Huber UM, Bugmann HKM, Reasoner MA (eds). Springer: Dordrecht; 243–252.

Immerzeel WW, Van Beek LP, Bierkens MF. 2010. Climate change will affect the Asian water towers. *Science* **328**(5984), 1382-1385.

Immerzeel WW, Van Beek LPH, Konz M, Shrestha AB, Bierkens MFP. 2012. Hydrological response to climate change in a glacierized catchment in the Himalayas. *Climatic change* **110**(3-4), 721-736.

Jackson KM. 2007. Spatial and morphological change of Eliot Glacier, Mount Hood, Oregon, Ph.D. dissertation, Portland State Univ., Portland, Oregon.

Jackson KM, Fountain AG. 2007. Spatial and morphological change on Eliot Glacier, Mount Hood, Oregon, USA. *Annals of Glaciology* **46**(1), 222-226.

Jarosch AH, Schoof CG, Anslow FS. 2013. Restoring mass conservation to shallow ice flow models over complex terrain. *The Cryosphere* **7**(1), 229-240.

Josberger EG, Bidlake WR, March RS, Kennedy BW. 2007. Glacier mass-balance fluctuations in the Pacific Northwest and Alaska, USA. *Annals of Glaciology* **46**(1), 291-296.

Jost G, Moore RD, Weiler M, Gluns DR, Alila Y. 2009. Use of distributed snow measurements to test and improve a snowmelt model for predicting the effect of forest clear-cutting. *Journal of Hydrology*, **376**(1), 94-106.

Jost G, Moore RD, Menounos B, Wheate R. 2012. Quantifying the contribution of glacier runoff to streamflow in the upper Columbia River Basin, Canada. *Hydrology and Earth System Sciences* **16**(3), 849-860.

Kampf, S. K., and S. J. Burges. 2007. A framework for classifying and comparing distributed hillslope and catchment hydrologic models, *Water Resources Research*, **43**, W05423, doi:10.1029/2006WR005370.

La Frenierre J, Mark BG. 2014. A review of methods for estimating the contribution of glacial meltwater to total watershed discharge. *Progress in Physical Geography* **38**(2), 173-200.

Lillquist K, Walker K. 2006. Historical glacier and climate fluctuations at Mount Hood, Oregon. *Arctic, Antarctic, and Alpine Research* **38**(3), 399-412.

Mantua NJ, Hare SR, Zhang Y, Wallace JM, Francis RC. 1997. A Pacific interdecadal climate oscillation with impacts on salmon production. *Bulletin of the American Meteorological Society* **78**(6), 1069-1079.

Meier MF. 1969. Glaciers and water supply. *Journal American Water Works Association* **61**: 8–12.

Mihalcea C, Mayer C, Diolaiuti G, Lambrecht A, Smiraglia C, Tartari G. 2006. Ice ablation and meteorological conditions on the debris-covered area of Baltoro glacier, Karakoram, Pakistan. *Annals of Glaciology* **43**(1), 292-300.

Moore RD, Demuth MN. 2001. Mass balance and streamflow variability at Place Glacier, Canada, in relation to recent climate fluctuations. *Hydrological Processes* **15**(18), 3473-3486.

Moore RD, Fleming SW, Menounos B, Wheate R, Fountain A, Stahl K, Holm K, Jakob, M. 2009. Glacier change in western North America: influences on hydrology, geomorphic hazards and water quality. *Hydrological Processes* **23**, 1: 42-61.

Moriasi DN, Arnold JG, Van Liew MW, Bingner RL, Harmel RD, Veith TL. 2007. Model evaluation guidelines for systematic quantification of accuracy in watershed simulations. *Transactions of the American Society of Agricultural and Biological Engineers* **50**(3), 885-900.

Naz BS, Frans CD, Clarke GKC, Burns P, Lettenmaier DP. 2014. Modeling the effect of glacier recession on streamflow response using a coupled glacio-hydrological model. *Hydrology and Earth System Sciences* **18**(2), 787-802.

Nolin AW, Phillippe J, Jefferson A, Lewis SL. 2010. Present-day and future contributions of glacier runoff to summertime flows in a Pacific Northwest watershed: Implications for water resources. *Water Resources Research* **46**(12).

Pelto MS. 2008. Impact of climate change on North Cascade alpine glaciers, and alpine runoff. *Northwest Science* **82**(1), 65-75.

Pelto MS. 2011. Skykomish River, Washington: Impact of ongoing glacier retreat on streamflow. *Hydrological Processes* **25**(21), 3356-3363.

Ragettli S, Pellicciotti F. 2012. Calibration of a physically based, spatially distributed hydrological model in a glacierized basin: on the use of knowledge from glaciometeorological processes to constrain model parameters. *Water Resources Research* **48**: 1–20. doi:10.1029/2011WR010559.

Reid TD, Brock BW. 2010. An energy-balance model for debris-covered glaciers including heat conduction through the debris layer. *Journal of Glaciology* **56**(199), 903-916.

Rupp DE, Abatzoglou JT, Hegewisch KC, Mote PW. 2013. Evaluation of CMIP5 20th century climate simulations for the Pacific Northwest USA. *Journal of Geophysical Research: Atmospheres*, **118**(19), 10-884.

Stahl K, Moore RD. 2006. Influence of watershed glacier coverage on summer streamflow in British Columbia, Canada. *Water Resources Research* **42**(6).

Stahl K, Moore RD, Shea JM, Hutchinson D, Cannon, AJ. 2008. Coupled modelling of glacier and streamflow response to future climate scenarios. *Water Resources Research*, **44**(2).

Steduto P, Hsiao TC, Fereres E, Raes D. 2012. Crop yield response to water. FAO irrigation and drainage paper, 66.

Taylor KE, Stouffer RJ, Meehl GA. 2012. An Overview of CMIP5 and the experiment design. *Bulletin of the American Meteorological Society* **93**(485-498) doi:10.1175/BAMS-D-11-00094.1.

Thornton PE, Running, SW. 1999. An improved algorithm for estimating incident daily solar radiation from measurements of temperature, humidity, and precipitation. *Agricultural and Forest Meteorology* **93**(4), 211-228.

Wigmosta MS, Vail LW, Lettenmaier DP. 1994. A distributed hydrology-vegetation model for complex terrain. *Water Resources Research* **30**(6), 1665-1679.

Tables

Table 1: CMIP5 general circulation model out used for projections of future climate under RCP4.5 and RCP8.5 emissions scenarios.

Model Name	Model Agency	Ensemble
bcc-cssm1-1	Beijing Climate Center, China Meteorological Administration	r1i1p1
CanESM2	Canadian Centre for Climate Modeling and Analysis	r1i1p1
CCSM4	National Center of Atmospheric Research, USA	r6i1p1
CNRM-CM5	National Centre of Meteorological Research, France	r1i1p1
CSIRO-Mk3-6-0	Commonwealth Scientific and Industrial Research Organization/Queensland Climate Change Centre of Excellence, Australia	r1i1p1
HadGEM2-CC	Met Office Hadley Center, UK	r1i1p1
IPSL-CM5A-MR	Institut Pierre Simon Laplace, France	r1i1p1
MIROC5	Atmosphere and Ocean Research Institute (The University of Tokyo), National Institute for Environmental Studies,and Japan Agency for Marine-Earth Science and Technology	r1i1p1
NorESM1-M	Norwegian Climate Center, Norway	r1i1p1

Table 2: Changes in seasonal precipitation and air temperature as projected by 9 statistically downscaled GCM outputs spatially aggregated across the basin. Changes in precipitation are shown as ratios while changes in temperature are shown as absolute values. The mean of 9 GCMs is reported while the range of the GCMs is denoted in parentheses.

Precipitation

	DJF	MAM	JJA	SON
1950-2005 (mm)	823	419	120	482
2040-2060 (RCP4.5)	1.06 (0.87-1.27)	1.02 (0.89-1.24)	0.86 (0.53-1.39)	1.01 (0.88-1.17)
2040-2060 (RCP8.5)	1.10 (0.84-1.32)	1.02 (0.77-1.23)	0.84 (0.46-1.20)	1.00 (0.83-1.27)
2080-2099 (RCP4.5)	1.09 (0.87-1.33)	0.99 (0.88-1.2)	0.86 (0.56-1.28)	1.03 (0.84-1.26)
2080-2099 (RCP8.5)	1.09 (0.89-1.27)	0.99 (0.82-1.19)	0.78 (0.42-1.19)	1.05 (0.88-1.32)

Temperature

	DJF	MAM	JJA	SON
1950-2005 (°C)	-0.2	5.4	14.7	7.8
2040-2060 (RCP4.5)	2.0 (1.2-2.9)	1.8 (1.2-2.5)	2.7 (1.6-3.9)	2.2 (1.2-3.1)
2040-2060 (RCP8.5)	2.4 (1.5-3.6)	2.1 (1.0-3.1)	3.4 (2.2-5.0)	2.9 (2.1-3.9)
2080-2099 (RCP4.5)	2.8 (1.6-3.9)	2.6 (2.1-3.3)	3.8 (2.6-5.1)	3.1 (2.2-4.3)
2080-2099 (RCP8.5)	4.6 (3.2-6.1)	4.2 (2.6-5.6)	6.7 (5.1-9.2)	5.4 (3.7-6.9)

Figures:

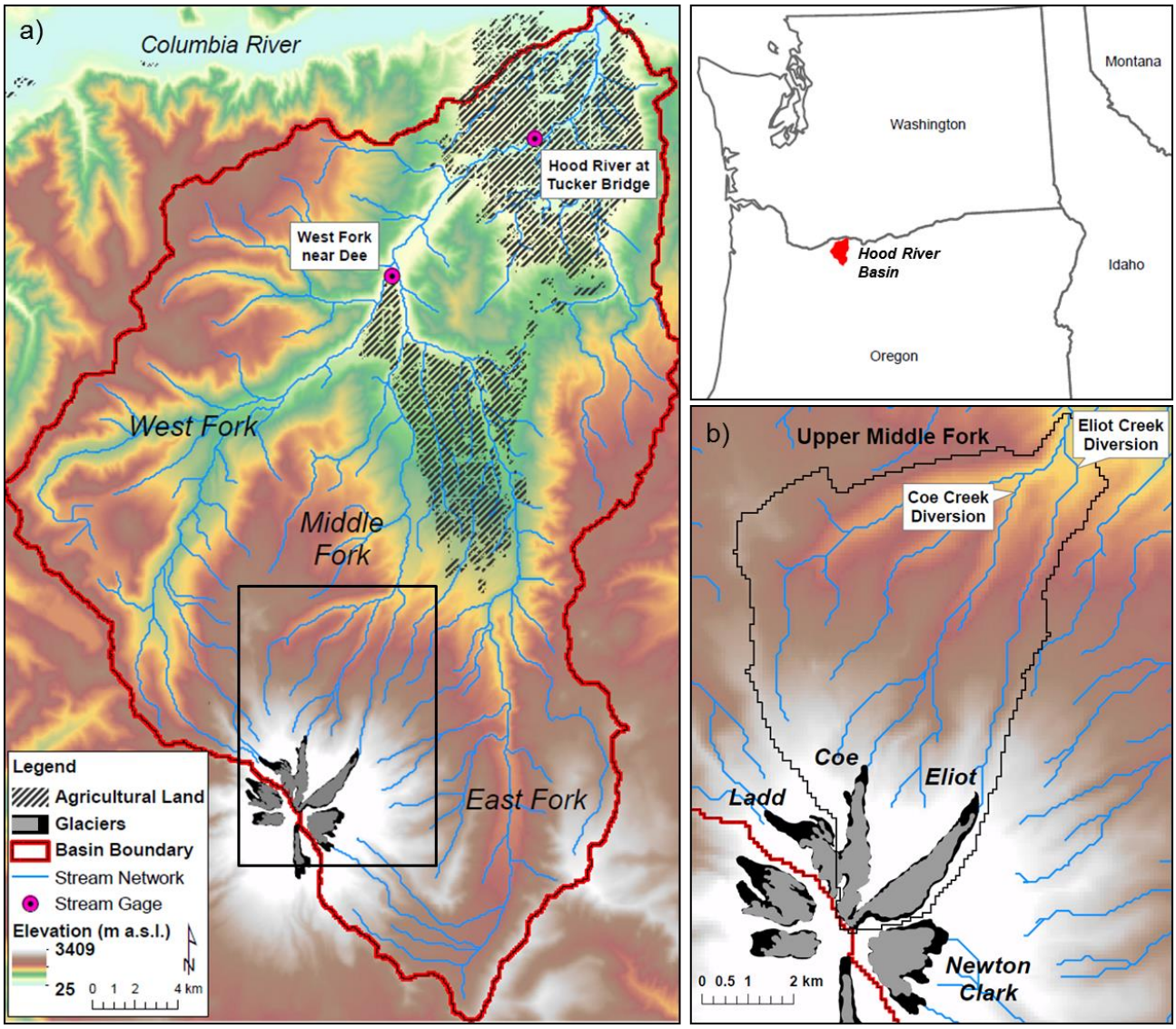

Figure 1: Location of the Hood River Basin in NW Oregon U.S.A. Glacier area estimates of ~1904 (black) and 2004 (gray) are from Jackson and Fountain (2007).

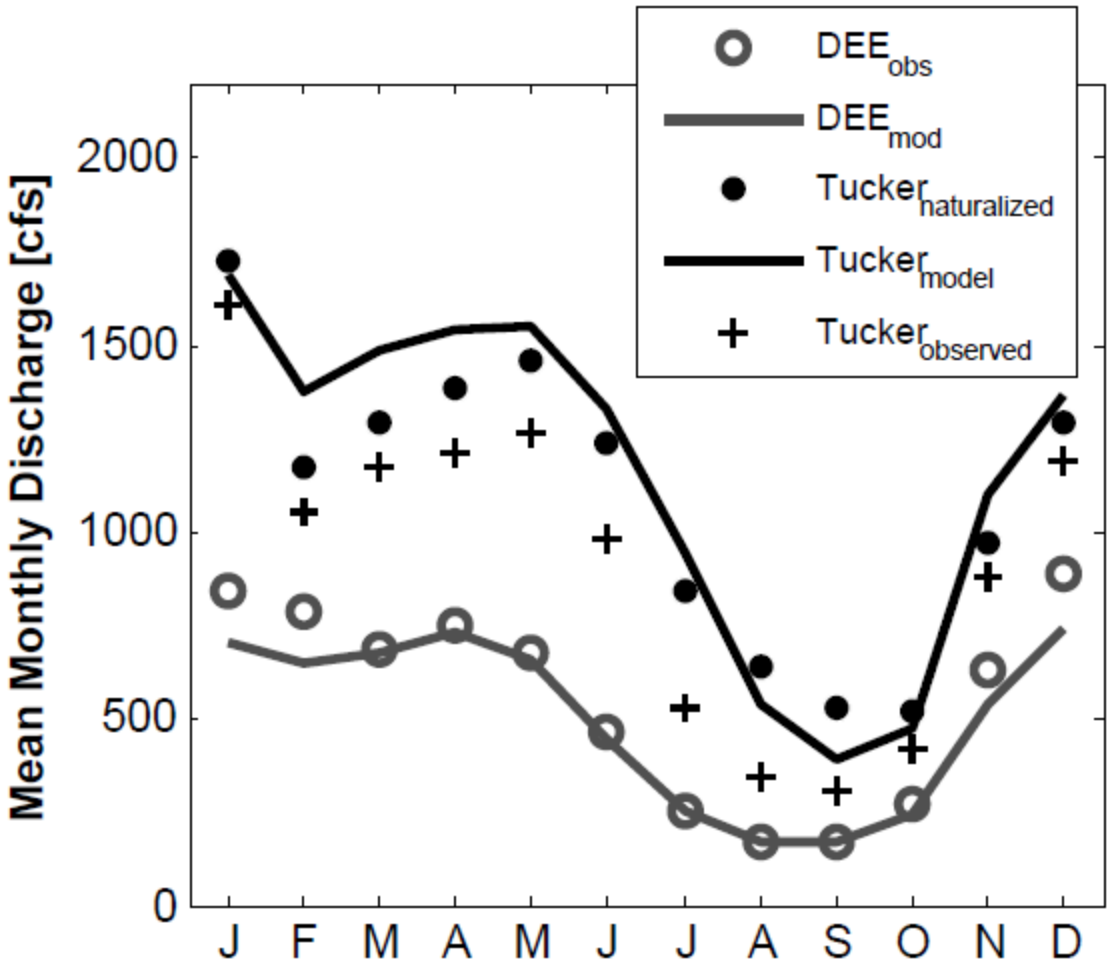

Figure 2: Comparison of mean monthly observed and simulated flows on the West Fork of the Hood River near Dee, OR (WY 1933-1991). At the Hood River at Tucker Bridge location estimates of naturalized discharge are compared with the modeled flows (WY 2002-2011) and actual observed flows (including the effects of regulation, water management).

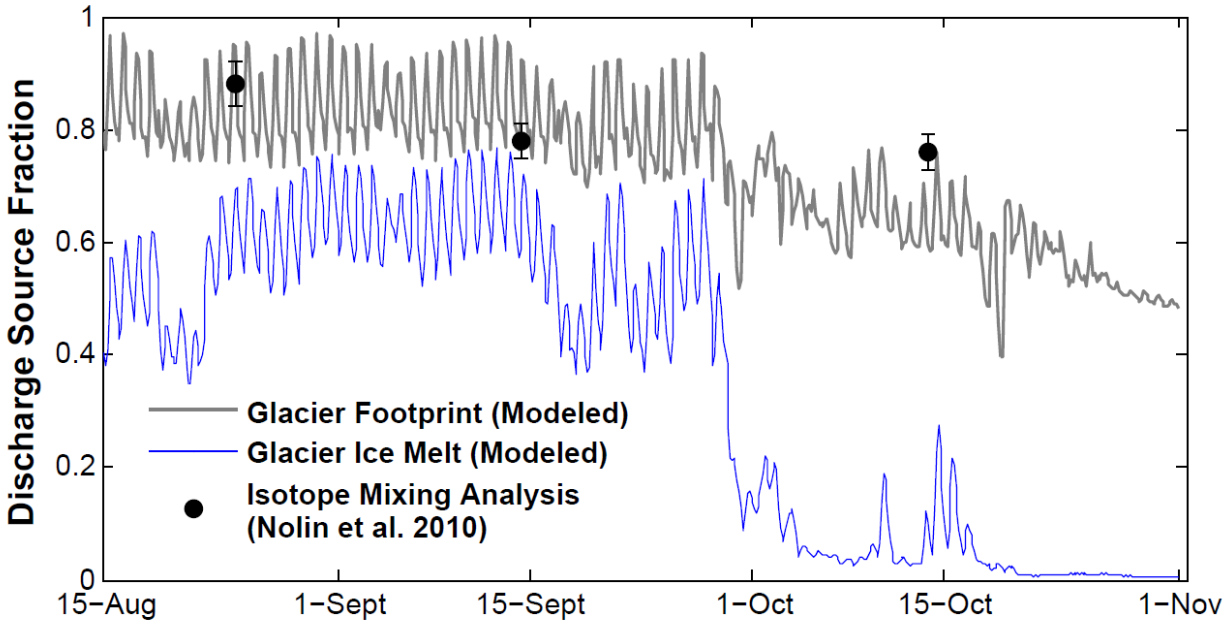

Figure 3: The modeled relative contribution of snowmelt, rain, and glacier melt from the footprint of Eliot glacier (gray) and from the melting of glacier ice only (blue) to downstream discharge of Eliot Creek above the confluence with the Middle Fork. Estimates of the contribution from the glacier footprint from oxygen isotope sampling are plotted in black on each date of sampling (Nolin et al. 2010).

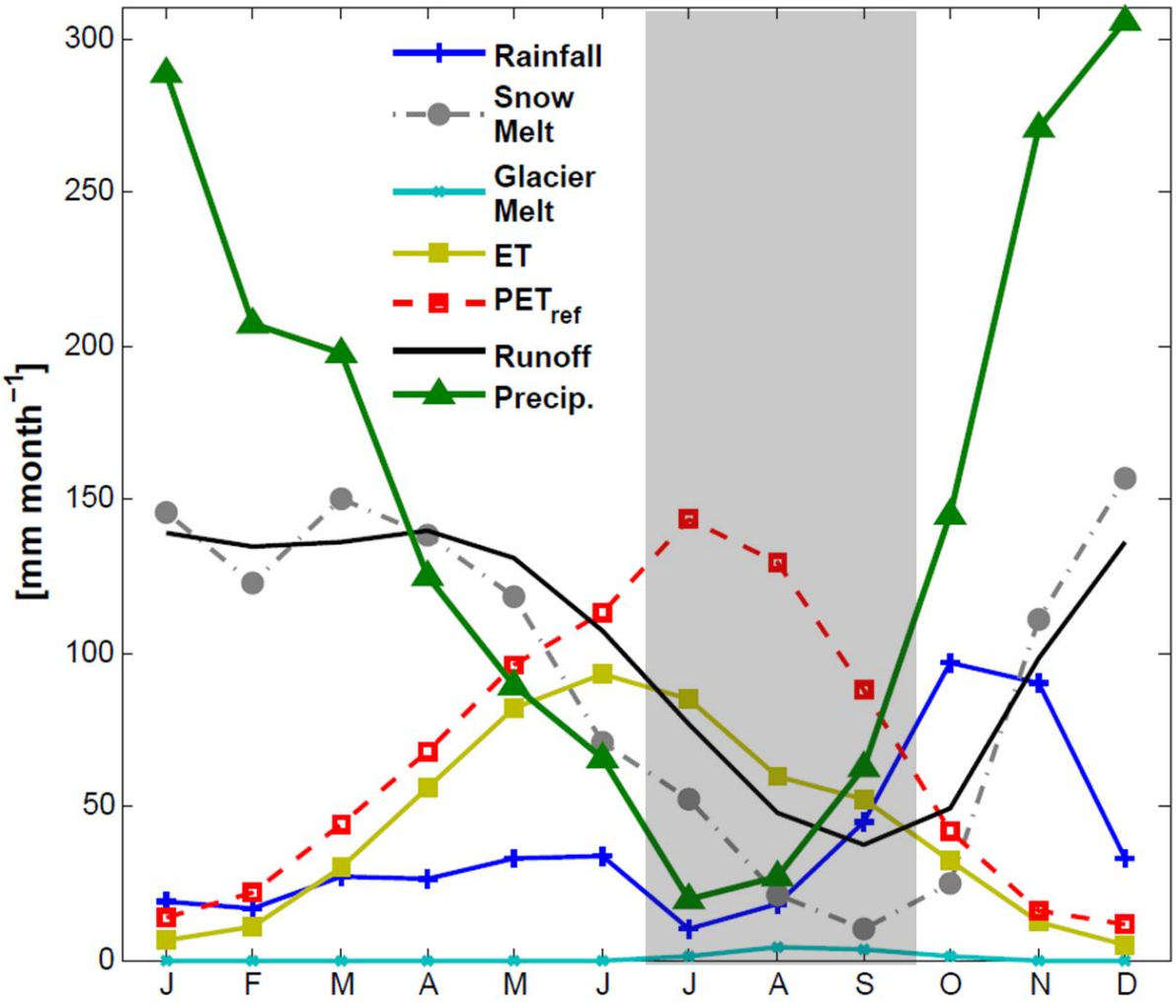

Figure 4: Modeled mean monthly hydrological fluxes spatially aggregated across the basin over the period of 1916-2005. The dashed box indicates a critical period where snowmelt and rain are at a minimum and soil moisture limitation is at maximum (as indicated by the difference between PET and ET).

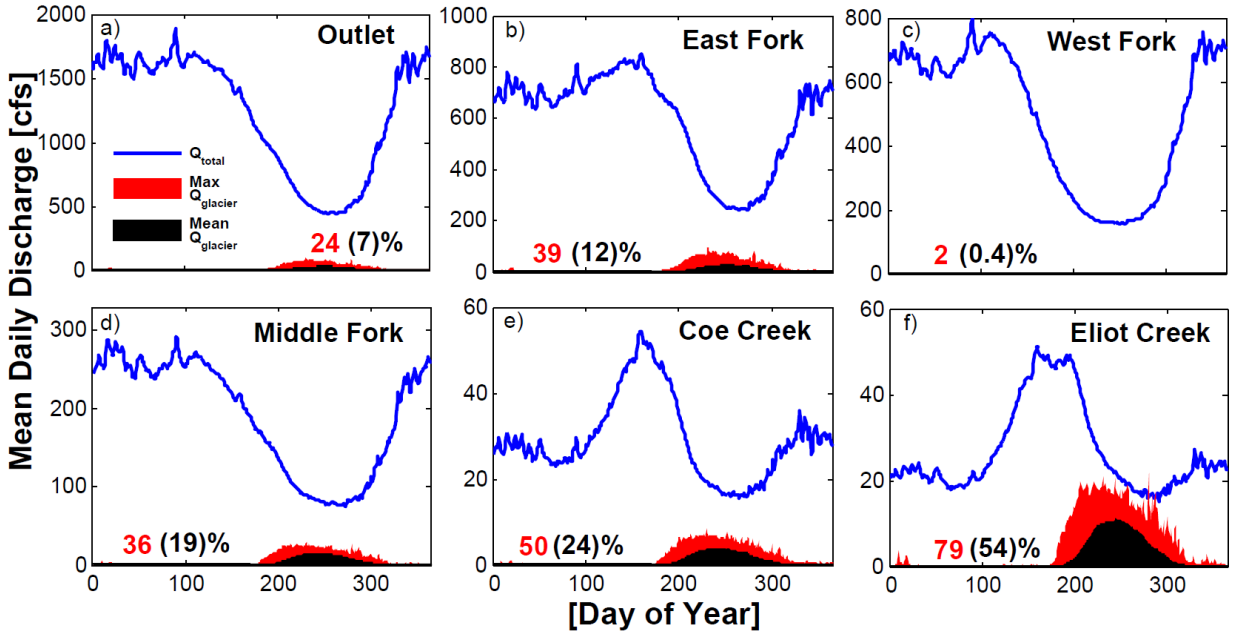

Figure 5: (a-f) Mean daily total discharge (blue), per day of year 1916-2005 for different stream locations in the basin (Fig. 1). Mean discharge from glacier melt is shown in black. The maximum daily mean discharge from glacier melt over the time period for each day is shown in red. The maximum daily contribution through the entire period is labeled with red text while the mean annual daily maximum glacier contribution is denoted with black text.

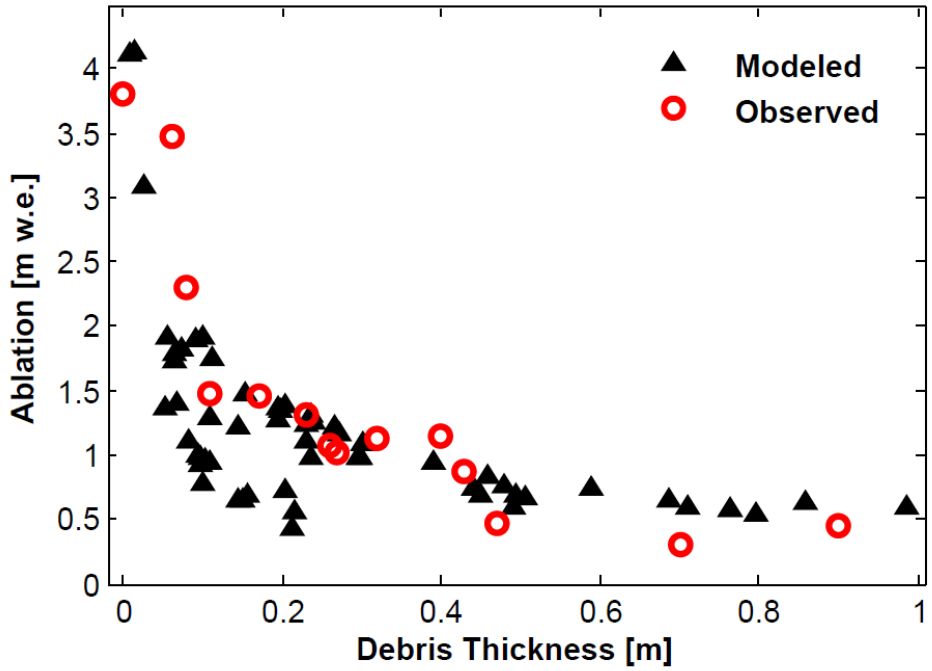

Figure 6: Observed and modeled ablation on the debris covered ablation area of Eliot glacier between 9-24-2004 and 7-28-2005 with varying range of debris thickness. Observations represent the ablation stake measurements of *Jackson and Fountain* [2007] while modeled values are presented for all debris covered grid cells on Eliot glacier.

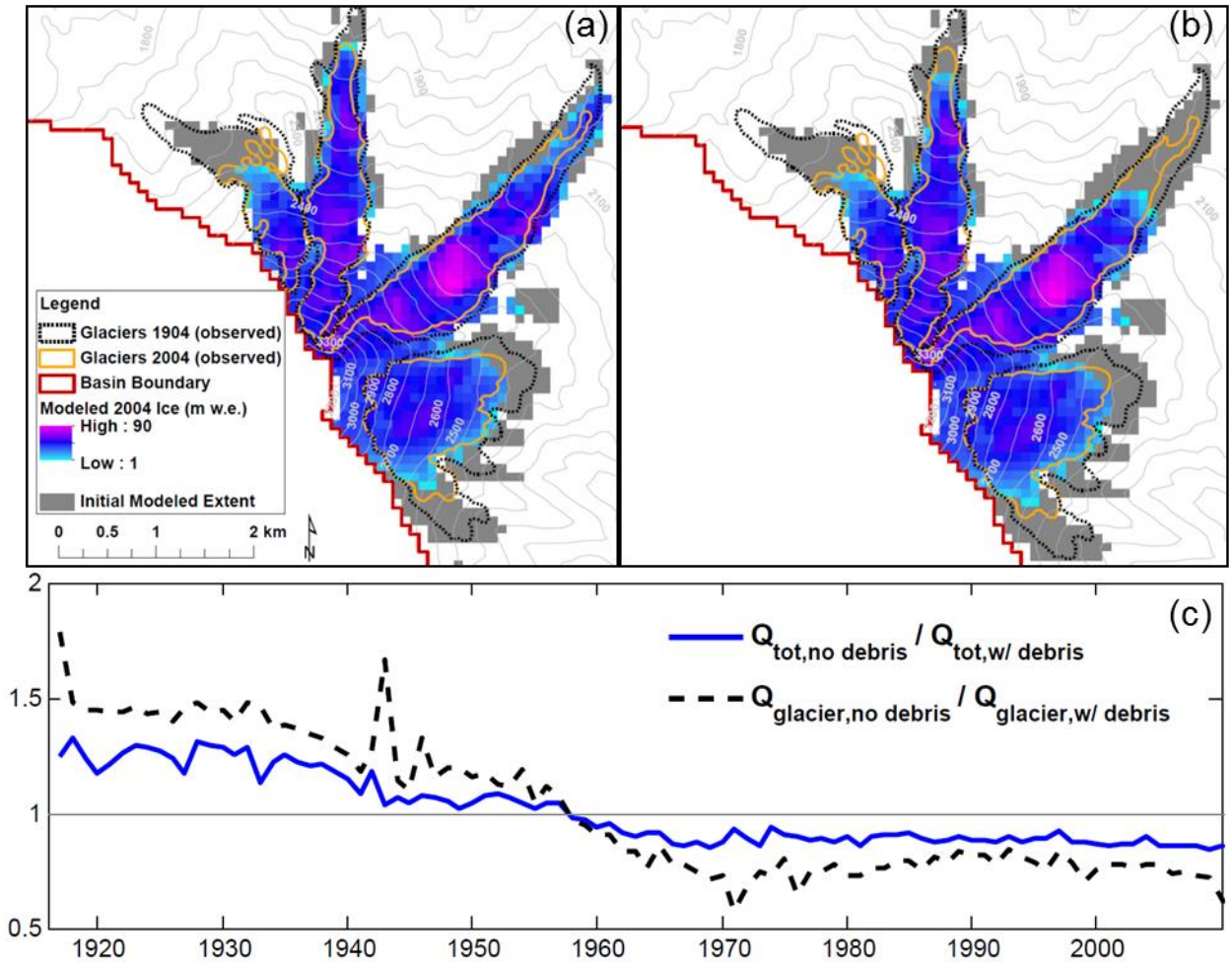

Figure 7: Experimental model simulations demonstrating the influence of surface debris on glacier area (a) with debris cover and (b) without debris at water year 2004. For reference outlines of historical estimates of glacier area from observations (Jackson and Fountain, 2007) are shown in addition to the initial extent used in the model simulations. (c) The progression of the ratio of modeled total discharge and glacier melt during the month of September using debris SEB algorithms to model results that do not consider debris is shown for the diversion location below Eliot glacier on Eliot Creek (Fig. 1).

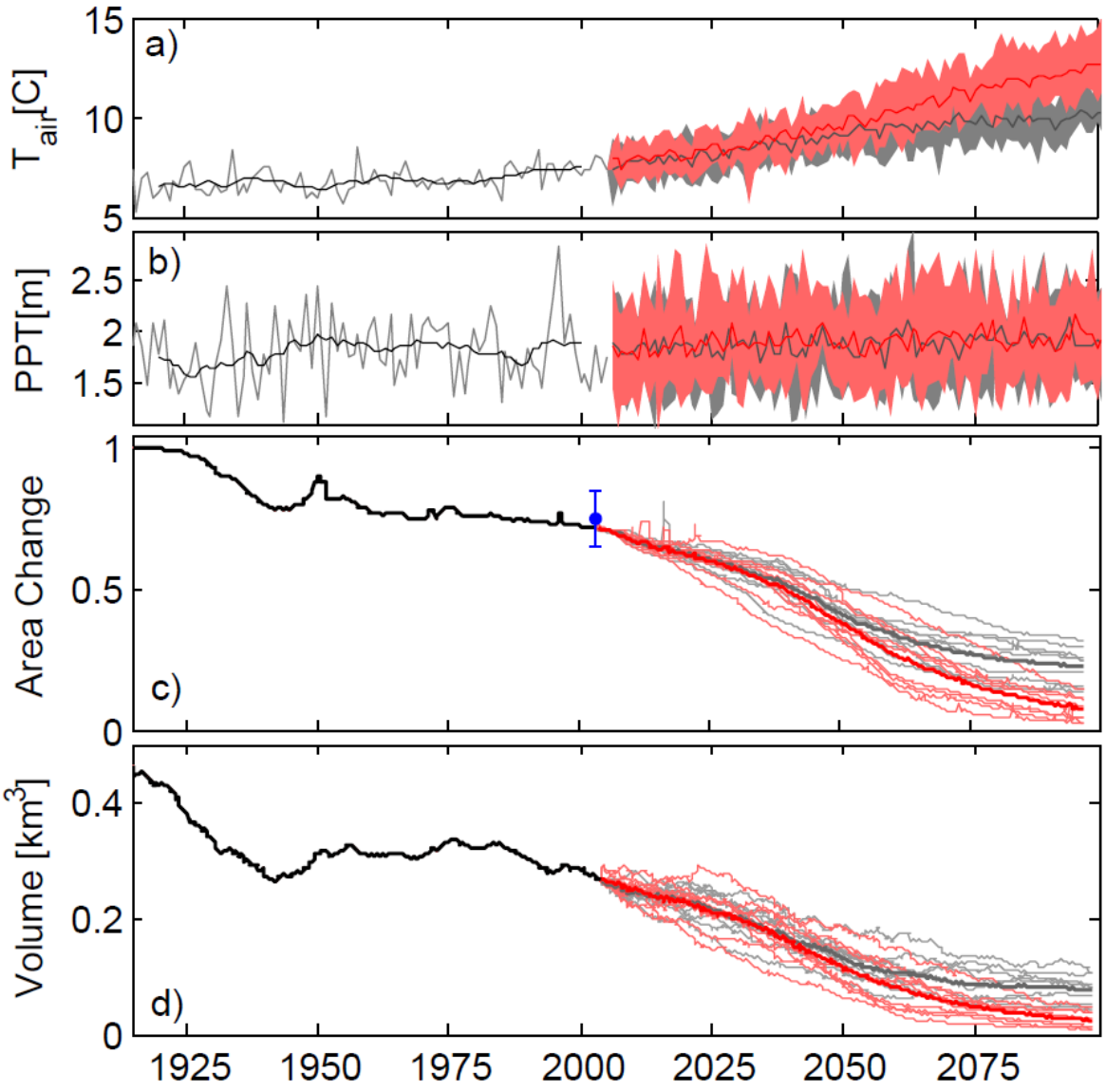

Figure 8: (a) Mean annual temperature and (b) precipitation spatially aggregated across the basin. The black line denotes 10-year center mean over the historical period. In the future period the range of projections of RCP4.5 are indicated in gray and RCP8.5 in red while the dark lines denote the ensemble mean. Modeled progression of glacier (c) area (relative to initial area early in the 20th century) and (d) volume over this historical (black) and future RCP4.5 (gray), RCP8.5 (red) climate scenarios. Observed estimates of glacier area change at 2004 (Jackson and Fountain, 2007) are indicated with the blue circle and whisker bars.

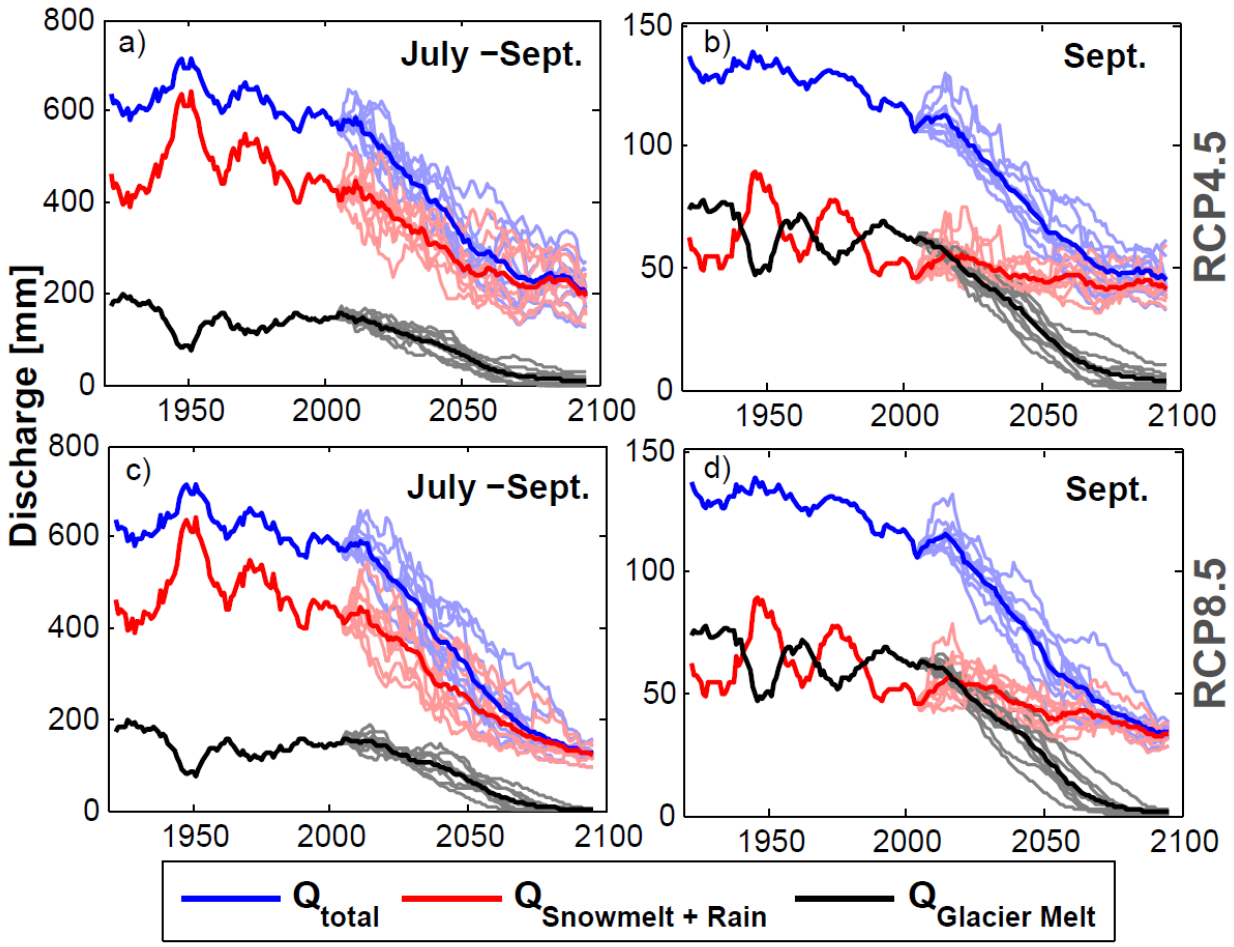

Figure 9: Historical and future (a,c) dry season (July – Sept) and (b,d) September discharge volume for CMIP5 (a,b) RCP4.5 and (c,d) RCP8.5 emissions scenarios.

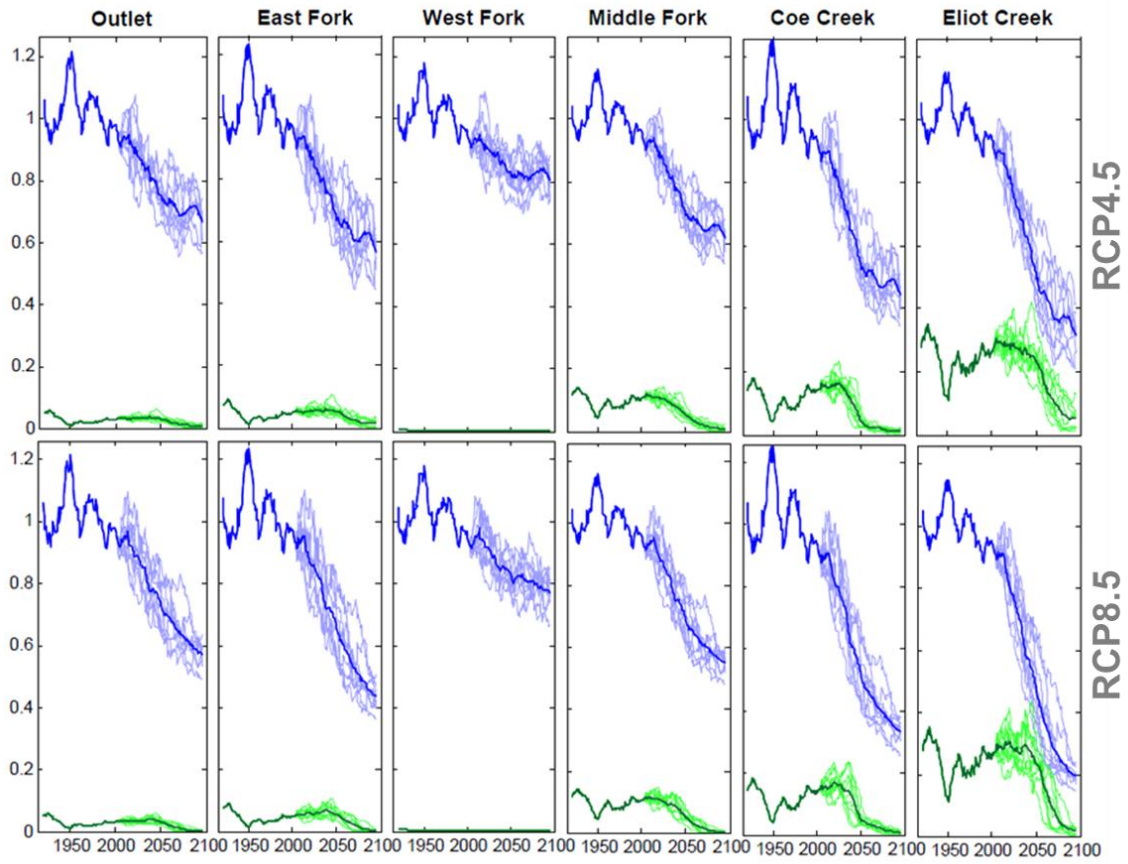

Figure 10: Projected changes in July-Sept. discharge volumes relative to the mean discharge for the period of 1916-1950 (blue) for the six locations in the basin. The relative glacier contribution to total discharge is plotted in green. Lighter colors indicate projections of individual GCMs where darker colors represent the ensemble mean and the historical period.

CHAPTER 4: EVOLVING PATTERNS OF GLACIO-HYDROLOGICAL PROCESSES IN THE PACIFIC NORTHWEST UNITED STATES

Abstract

The Pacific Northwest remains the only region in the conterminous United States with a sizable regional distribution of glaciers. Mountain glaciers in this region have displayed ubiquitous patterns of retreat since the 1980's partly in response to warming air temperature. Glacier melt in partially glacierized river basins in the region provides water for downstream anthropogenic systems (e.g., agricultural water supply, hydroelectricity generation) and sensitive ecological systems (e.g., fisheries, upland riparian habitat). While the changes in glacier area have been observed and characterized across the region over an extended period of time, the relative consequences of these changes are not fully understood. The hydrological response to glacier recession is often a multi-phased phenomenon and is highly dependent on the hydro-climatological attributes of a given river basin. To investigate the relative role of glaciers in river basins across the PNW and to determine how they have responded and will continue to respond to glacier recession we applied a regional modeling approach. This approach used regional gridded historical and projected future meteorological data, distributed observations of glacier mass and area, observations of river discharge, and an advanced glacio-hydrological simulation model for predictions of evolving hydrological processes at fine spatial scales for extended periods of analysis. Model applications in a sample of six river basins across the region are used to characterize the regional response.

Our modeling analysis encompassing a 140 year period (1960-2099) shows that while the rate of glacier recession is predicted to persist and increase, the amount of glacier melt and its contribution displays both positive and negative trends in time depending on the setting of the river basin. Elevation is found to be the dominant factor controlling the hydrological response while climatic factors play a secondary role. In high elevation river basins enhanced glacier melt provides a buffer to strong declines in seasonal snowmelt derived late summer streamflow for some time. Conversely, in lower elevation basins reductions in glacier melt exacerbates these negative trends.

4.1 Introduction

Glaciers and their hydrologic behavior are a significant component of many high alpine hydrological systems. Over the past several decades pervasive patterns of mass loss and retreat in response to recent warming temperatures have been observed in mountain glaciers across the globe. Partially glacierized watersheds have complex multi-phased patterns of hydrological response to increasing atmospheric temperatures and reductions in glacier mass [e.g., *Moore et* al., 2009; *Baraer et al*., 2012]. Following increasing air temperature, discharge sourced from glaciers initially increases as the result of an increase in the rate of ablation per unit of glacier area. Once the glacier area has been reduced to a threshold extent where the effects of losses in glacier area exceed increased rates of ablation, runoff sourced from glacier melt decreases as a function of further glacier recession. Irrespective of the trend direction in glacier derived discharge, its relative contribution can increase for some time as other seasonal sources and losses of water (i.e. seasonal snow accumulation and melt, evapotranspiration) respond to increasing temperatures in parallel as described in chapter 3. These patterns of response vary greatly as a function of the rate of change in climate, particulars of the local and regional climatology, initial relative glacier cover (spatial scale of analysis), and the timescales for which analyses are focused (annual, seasonal).

The hydrological response of river basins to glacier recession is not fully understood due to the long timescales at which it occurs, the limited number of observational datasets in high elevation areas, and the limited number of methodologies that are appropriate for capturing the parallel response of both non-glacierized and glacierized areas of river basins to increasing air temperature. Furthermore, natural and decadal climate variability is often superimposed on these responses to warming trends. Recently, observational and modeling research efforts have been developed and applied to further our understanding of these processes. These efforts have largely been focused on individual river basins where water is valued as a socioeconomic or ecological resource or in locations that contain extensive observational networks. Few studies have comprehensively characterized the response of glacierized river basins at regional scales.

Using a regional glacier dynamics model *Clarke et al.* [2015] predict nearly 2 centuries of changes in glacier mass, area, and melt across western Canada. The *Clarke et al*. work represents a major advance in the prediction of future glacier change at a regional scale; however, the analysis is limited to glacierized areas and does not consider the relative role of

changing melt patterns in conjunction with non-glacierized areas at the river basin scale. *Stahl and Moore* [2006] applied statistical trend analyses to streamflow records across western Canada and found decreasing late summer discharge in basins with high relative glacier cover. Statistical trend analyses do not describe the mechanisms of these changes; whether declines are linked to seasonal snowmelt, glacier melt, or both.

The PNW remains the only region in the conterminous United States with a sizable regional distribution of glaciers. Glacier melt water is important for water supply and hydroelectricity infrastructure, maintaining streamflow for fisheries, and there are growing concerns about increased risk of landslides and ecosystem succession following glacial recession. To begin to address a number of these issues in the PNW a regional glacio-hydrologic modeling study is necessary.

This chapter presents a modeling study with specific emphasis on the following research objectives: (1) characterize how hydrological response to glacier recession varies within a region; (2) identify vulnerable downstream locations in space and time; and (3) quantify at which spatial scales glacier melt is a significant contributor to discharge patterns. The aforementioned objectives can only be addressed with a regional modeling approach that uses regional gridded historical and projected meteorological data, distributed observations of glacier mass and area, observations of river discharge, and an advanced glacio-hydrological simulation model for predictions of evolving hydrological processes at fine spatial scales for extended periods of analysis. We predict the long-term coupled glacio-hydrological response for six watersheds that span sharp climatic gradients (maritime to continental), a range of temperate northern latitudes (45-49°), and varying local physiological attributes (e.g., range of elevations, wind/leeward) in the Pacific Northwestern United States (PNW).

4.2 Conterminous Pacific Northwest United States

This study examines catchments in the mountainous region of the states of Oregon and Washington where many river basins originate in partially glacierized headwater catchments. The climate of the region is defined by distinct seasonal temperature and moisture patterns. The majority of precipitation occurs during the winter and spring (November to March) from Pacific cyclonic systems while little precipitation falls during summer (June to September). Variability in the climate is largely controlled by variability in the sea surface temperature (SST) of the

North Pacific Ocean, described by the Pacific Decadal Oscillation index (PDO, *Mantua et al.*, 1997), the principal component of North Pacific SST variability. During positive PDO phases, warm SST of the Pacific promotes warm temperatures in the Northwest while negative phases lead to cooler temperatures.

The topography of the region is characterized by two mountain ranges that are aligned perpendicular to the atmospheric flow from the Pacific Ocean: the Olympic range on the coastal Olympic Peninsula of Washington and the interior Cascade Range that extends from Northern California to British Columbia, Canada. Over the period of 1900-2009 glacier area of the Olympic Range was observed to decrease 52% [Spicer et al., 1986; Riedel et al., 2015] and the North Cascades subregion lost 50% of its glacier area [Dick, 2013]. Glacierized stratovolcanoes mark the topography in the Cascade Range. Among these, Mount Baker, Mount Rainier, and Mount Hood lost 30% [*Brown*, 2010], 22% [*Nylen*, 2002], and 33% [*Jackson and Fountain*, 2007] of glacier area, respectively, during the 20th century.

Long term changes in glacier area have been documented at coarse time scales through historical aerial imagery and topographic maps in the PNW; however, the hydrological consequences of these changes are not well understood. *Pelto* [2008] report a 27% decline in summer streamflow in the North Cascades subregion over the period 1946-2005 and found that in the most glacierized drainages these declines were less than 10% due to increased glacier melt. Using the recent hypsometry of glaciers in the Olympic range and a positive degree-day melt model *Riedel et al.* [2015] estimated that the contribution of melting of ice, snowmelt, and firn from glacier areas represents 3-15.4% of summer (May-Sept) discharge in 3 basins during water years 2009 and 2010.

To characterize the hydrological implications and driving factors of changes in glacier area we selected six river basins (Figure 1, Table 1) that span the longitudinal maritime to continental climatic gradient. The drainage areas of these basins range from 270 to 879 km^2 while the historical relative glacier cover ranged from <1 to 13.6%. Mean annual precipitation ranges from 1.7 -3.8 meters based on the 1981-2010 PRISM climatology [*Daly et al.*, 1994]. End member basins included in this analysis include the Hoh River basin where high precipitation enables the lowest elevation glaciers of the region and the Nisqually River basin whose headwaters extend to the highest elevations in the region on the southern flanks of Mount Rainier.

4.3 Regional to Local Scale Glacio-Hydrological Modeling Methodology

4.3.1 Glacio-hydrological model

We used the distributed hydrology soil vegetation model (DHSVM; *Wigmosta et al*., 1994; 2002) for the numerical simulation of glacio-hydrological processes in each river basin selected for the study. DHSVM has been widely applied in the mountainous western United States for snowmelt [e.g., *Cristea et al*., 2014; *Jost et al*., 2009] and climate change applications [e.g., *Elsner et al*., 2010; *Cuo et al*., 2011]. Several model developments have been integrated to improve the representation of glaciers. First, a glacier dynamics model [*Clarke et al*., 2015] based on a shallow ice approximation of the continuum mechanics equations governing ice deformation and sliding was integrated into the model to simulate the lateral movement of ice [*Naz et al*., 2014]. The representation of ice flow is required to evolve the distribution of glacier ice in response to surface accumulation and ablation (Chapter 2). The presence of supraglacial debris greatly affects rates of ablation. As described in chapter 3, we integrated a representation of the energy dynamics of supraglacial debris cover (storage and conduction of heat) based on the algorithms of *Reid and Brock* [2010]. Lastly, in steep mountainous terrain snow is redistributed through avalanching. This can be a significant source of mass accumulation for valley glaciers and play a significant role in runoff generation [*Ragettli et al*., 2015]. To incorporate the effects of the gravitational redistribution of snow we integrated the empirical "snowslide" model of *Bernhardt and Schulz,* [2010]. In this model all accumulated snow in a model element is transported to downslope elements when local snow depth exceeds a snow holding depth threshold (SHD). SHD decreases exponentially with local snow surface slope:

$$SHD = P1 \times \exp[-slope \times P2] \qquad (1)$$

Snow depth and snow surface slope is calculated at each model time step to redistribute snow downslope as it accumulates. Parameters $P1$ and $P2$ were determined by manual adjustment to recreate observed late summer snow patterns through visual comparison with National Agriculture Imagery Program (NAIP) aerial imagery where available at the study catchments.

The model was implemented at a spatial resolution of 50 m. Hydrological model parameters (elevation, soil, vegetation) were resampled from their native resolution to 50 m (bi-linearly). The sources of geospatial data used as model input are listed in table 2.

4.3.2 Gridded Meteorological Data

We used the gridded historical meteorological dataset of *Livneh et al.* [2013] to force historical glaciological simulations. The data consist of minimum (Tmin) and maximum (Tmax) 2 meter air temperature, precipitation, and wind at a daily time interval at a spatial resolution of 1/16° (~6 km). We selected this dataset as it is used as historical training data to downscale an ensemble of global climate model output of the Coupled Model Inter-Comparison Project 5 (CMIP5) using the Multivariate Adaptive Constructed Analogs (MACA) statistical downscaling methods [*Abatzoglou and Brown*, 2011] as part of the Integrated Scenarios of the Northwest Environment project (http://pnwcirc.org/projects/integrated-scenarios/). In conjunction, the historical dataset and downscaled future projections allowed us to run model simulations for 185 years (1915-2099).

In the generation of this historical dataset *Livneh et al.* [2013] used a constant temperature lapse rate (-6.5 $^\circ\,\mathrm{km}^{-1}$) to interpolate Tmin and Tmax between weather station locations (Ben Livneh, personal communication). This assumption was tested by comparing the local climatology of each grid cell with that of the Parameter Regressions of Independent Slopes Model (PRISM, Daly et al., 1994) climatology (resampled to 1/16°). In areas with high vertical relief and low station density (mountains) the historical data had significant cold biases as compared with the PRISM 1981-2010 climate normals. Figures 2 and 3 show the biases in Tmin and Tmax as a function of elevation for the domain bounded by latitude (46.53125 - 49.28125) and longitude (-124.46875 - -120.03125). At high elevations cold biases are pervasive throughout the year in Tmin and during winter months in Tmax. To remove these biases we corrected the historical data using a delta method [e.g., *Watanabe et al*., 2012] for monthly Tmin and Tmax derived from the comparisons with the PRISM data:

$$T_{bc,i} = T_{Livneh,i} + (\bar{T}_{PRISM,Month} - \bar{T}_{Livneh,Month}) \quad (2)$$

Where $T_{bc,i}$ is the bias corrected value of the daily Livneh temperature value at day i in the time series. The difference between the PRISM climatological mean ($\bar{T}_{PRISM,Month}$) and the Livneh et al. climatological mean ($\bar{T}_{Livneh,Month}$) for the corresponding month are used for bias correction. We applied the bias correction factors to the future data as well as they were trained on the original uncorrected dataset.

The bias corrected daily historical and future data were disaggregated to a 3-hourly time interval and incoming longwave and shortwave radiation and relative humidity were estimated using the Mountain Microclimate Simulation Model (MTCLIM) algorithms [*Thornton and Running*, 1999] as implemented in *Bohn et al.* [2013]. The locations of the centroids and the mean elevations of each 1/16° grid cell were used to distribute temperature to the 50 m model resolution using calibrated temperature lapse rates. The calibration procedure is outlined in the following section.

Precipitation was spatially distributed from the centroid locations of the regional Livneh et al [2013] dataset to each 50-m model grid cell based on the relative distributions of the local PRISM precipitation normals at each model grid cell,

$$P_{x,y} = P_{centroid} \times \left(PRISM_{x,y,month} / PRISM_{x_{centroid}, y_{centroid}, month} \right) \quad (3)$$

where the precipitation at a local grid cell ($P_{x,y}$) is calculated using the precipitation of the Livneh et al. data ($P_{centroid}$) and the relationship between the local PRISM precipitation normal value for the current month ($PRISM_{x,y,month}$) with the PRISM precipitation normal value for location of the centroid ($PRISM_{x_{centroid}, y_{centroid}, month}$). In this manner the relative spatial patterns of PRISM are used to spatially distribute the coarser Livneh data. In the model shortwave radiation is distributed based on a solar geometry model that accounts for sloped surfaces and terrain shading for each time of the day and month of the year. Bi-linear interpolation was used to assign spatial weights to each station for each local grid cell.

4.3.3 Observational Data

Confidence in the model predictions depends on how well the model reproduces historical hydrological and glaciological patterns. To constrain the model to accomplish this, we relied heavily on several observational datasets; primarily on historical glacier mass balance and glacier extent at each site. Observations of glacier mass typically consist of point measurements of accumulation and ablation that are typically conducted twice a year to capture peak accumulation and total ablation at the end of the melt season. These point observations (the number varies depending on the glacier and monitoring program) are interpolated across a glacier's area to calculate net annual changes in mass. We used observations of glacier mass of individual glaciers in the Nisqually, Thunder Creek and Stehekin River basins collected and

archived by the U.S. National Park Service [*Riedel and Larrabee*, 2011a]. Observations for these glaciers in the North Cascades began in the early 1990's and early 2000's on Mount Rainier [*Riedel and Larrabee*, 2011b]. The United States Geological Survey (USGS) has been monitoring mass fluctuations of South Cascade Glacier (Cascade River) since the 1950's. Measurements and estimates of net mass balance of Blue glacier (Hoh) were compiled for the period of 1956-1999 [*Conway et al.*, 1999].

Various sources of glacier area estimates were used to characterize patterns of recession. Where available we use databases of glacier area compiled by the glacier research group at Portland State University [*Nylen*, 2002; *Dicks*, 2013; *Spicer*, 1985; *Granshaw and Fountain*, 2006]. These glacier area estimates are derived from analyses of historical aerial imagery and topographic maps. During recent decades, in basins where these data were not available, we relied on estimates of glacier area from Landsat satellite imagery. Glacier area was classified from atmospherically corrected Landsat images using the Normalized Difference Snow Index (NDSI) methodology described in *Burns and Nolin* (2014). Landsat images were taken from dates at the end of the melt seasons of anomalously dry years to avoid mapping seasonal snow. To calibrate and test modeled discharge we used USGS streamflow gauge data (waterdata.usgs.gov/nwis/rt).

4.3.4 Steps in Glaciological and Hydrological Calibration

To increase robustness of applications of glacio-hydrologic models, selection of model parameters that govern climatic distributions and hydrological processes and that are able to capture both glaciological and hydrological patterns is paramount (Chapter 2). To select parameters that constrain model predictions we divided the calibration and initialization procedure into three steps: (1) cryospheric calibration, (2) watershed calibration, and (3) the initialization of the historical distribution of glacier ice. These steps were followed for all basins except for the Hood River where different sources of observational data were used in calibration and testing (e.g., observations of sub-debris glacial ablation; geochemical sampling). The Hood River calibration is described in detail in Chapter 3.

This study focused on the evolving contribution of glaciers to runoff production; hence we first started by selecting climate and surface energy balance model parameters that govern the accumulation and ablation of snow and ice at high elevations in the river basins. In this step, we

used observations of glacier mass on individual glaciers and observed estimates of glacier area. Each river basin in the sample contains a glacier where a record of net mass fluctuations exists. We used measurements of winter balance, summer balance, and net annual balance for Sandalee, (Stehekin River), N. Klawatti (Thunder Creek), South Cascade (Cascade River), and Nisqually (Nisqually River) glaciers. Reconstructed mass balance observations on Blue Glacier (Hoh River) were limited to net annual mass changes.

Using narrow physically plausible ranges of model parameters, we used an automatic multi-objective calibration technique (MOCOM-UA, Yapo, 1999) to sample and evaluate different parameter sets in recreating seasonal and annual observations of mass balance. The objectives that were minimized were RMSE of winter, summer, and net mass balance, and the absolute error in cumulative mass balance at the end of the calibration period. The time period for calibration was selected based on the length of observation and was limited to a time period where the area of the glacier did not fluctuate significantly. Thus, in the model the glacier area is fixed to the observed extent so that the calibrated parameters only reflect surface mass balance and the area is consistent with what was used to calculate observed net mass balance. For example, the observed record of mass balance at South Cascade Glacier starts in 1953; however the glacier area reduced considerably during the entire period of mass balance observations (44%, 1958-2010). Thus to only consider the effects of surface mass balance on net balance calculations we limited the calibration period to 1990-2011, excluding the earlier record. Temperature lapse rates and precipitation multipliers were used as local climate calibration parameters. SEB parameters used for calibration included the maximum snow albedo used in snow albedo decay functions [*Laramie and Schaake*, 1972; *Wigmosta et al*. 2002], glacier albedo, and a constant for the aerodynamic roughness length over snow and ice surfaces.

Next, we applied the calibrated parameters from each individual glacier to estimate the mean annual mass balance distributed throughout each respective river basin. Because mass balance observations are only available for a small number of locations, we rely on simulated patterns of positive mass balance (annual positive net accumulation of snow and ice) and observed glacier area to infer the suitability of the calibrated parameters across a larger area. Additionally, in step 3 of calibration and initialization a field of mean annual mass balance that realistically represents accumulation and ablation processes is used in conjunction with the glacier dynamics model to spin-up the glaciers up to a steady state condition (Chapter 2). In this

step we estimated mean annual mass balance by running the snow/ice SEB model for the entire domain of each river basin for a period spanning several recent decades. In this simulation ice was available to melt at every grid cell when no snow was present. The net balance throughout the time period was summed and divided by the number of years of simulation to calculate a distribution of mean annual net mass balance.

We compared the distribution of positive mean annual mass balance with recent observations of glacier area to determine the applicability of the calibrated parameters for glaciers across the entire river basin. We assumed that the calibrated parameter that varies the most in space at broad scales, and that would justifiably need local manipulation, was the precipitation multiplier. Hence, in areas where the mean annual mass balance was positive for a large amount of area outside of glaciers the precipitation multiplier was decreased. On the other hand, in areas where medium to large glaciers (>0.5 km^2) are currently observed and mean annual mass balance was entirely negative, the precipitation multipliers were increased. This process relies on the major assumption that precipitation and its variability has first order control on spatial patterns of mass balance. Temperature was bias corrected using PRISM normals and has much less variability in space than precipitation; hence it was not adjusted in calibration. In most cases where mass balance was positive outside of glaciers, the simulated annual discharge volume at downstream locations used in in the watershed calibration step (next step) was also overestimated. This confirmed that precipitation was likely the driver behind over estimations of net positive mass balance.

Next, we ran model simulations for each river basin to evaluate the suitability of the calibrated parameters for reproducing discharge patterns at seasonal timescales. Additionally, in this step soil parameters that govern subsurface flow, surface runoff generation, and storage of water in the soil column were adjusted to improve timing of streamflow at day to week timescales. We evaluated model performance by comparing distributions of monthly flows, the Nash Sutcliffe statistic (NSE) of flows at multiple temporal intervals, and flow duration curves with observations. During this step in calibration the glacier areas remained fixed to the observed extent. The time period for calibration was limited to periods where significant fluctuations of glacier area were not observed. In cases where positive biases in annual flow volumes that exceeded 10% were observed, further precipitation multipliers were applied to low elevation centroids to reduce the precipitation forcing. These were applied to low elevation Livneh

centroids as to not offset the calibrations from the previous step. Application of precipitation multipliers in this step was required in the Thunder Creek basin to correct over predictions in annual flow volumes. In other basins the use of precipitation multipliers during the mass balance calibration simultaneously reduced streamflow bias.

The final step in initializing the model for coupled long term glacio-hydrological simulations was to estimate the distribution and initial thickness of ice across each river basin. This spin-up procedure used calibrated mean annual mass balance fields (described above) and offline simulations with the glacier dynamics model (separate from the hydrology model). The spin-up procedure is detailed in Chapter 2.

4.4 Results

4.4.1 Historical Model Calibration

We first report the optimal parameter values found through calibration to mass balance observations of individual glaciers. Optimal parameter values for each observed glacier are shown in table 3. The optimal parameter values reflect logical physical relationships. For example, the strongest temperature lapse rates and high maximum snow albedo were found to be optimal in more dry continental environments of the northern interior (Sandalee, N. Klawatti, South Cascade). In contrast, in more moist maritime environments weaker temperature lapse rates were optimal (Blue, Nisqually). Precipitation multipliers in excess of 1% were required to capture mass balance at two of the observed glaciers. The multiplier required for Sandalee glacier was very high (3.47). The precipitation of the $1/16^\circ$ grid cell at the location of this glacier was anomalously low as compared with surrounding grid cells; hence, it represented an extreme local bias and the precipitation multiplier was not used for other locations in the basin.

Comparisons of calibrated modeled glacier mass balance and observed mass balance are shown in Figure 4. For the larger glaciers with longer records of observation the model does reasonably well at reproducing observed time series of net annual mass fluctuations (r^2 = 0.81, South Cascade and North Klawatti). For the smallest glacier (Sandalee) and for the glacier with the shortest record of observation (Nisqually) the model performance is low (r^2=0.31-0.75). In these two glaciers secondary accumulation and ablation processes (e.g., glacier ice avalanching, debris covered ice) have a larger influence on net mass changes (Jon Riedel, NPS, personal communication) which makes their mass more difficult to model and measure. The model is able

to reproduce the general pattern of mass fluctuations of Blue glacier; however overestimation of mass accumulation in the highest events was observed in the early 1970's which was found to be linked to biases in the precipitation forcing data.

Next we illustrate model performance in predicting stream discharge by comparing monthly streamflow and flow duration curves in each basin for a selected calibration period in each basin (Fig. 5). For reference we report mean monthly precipitation during the period of calibration (Fig. 5 a-d). The seasonal timing of precipitation is ubiquitous, while the Hoh River receives the greatest amount and the Stehekin River the least. The distributions of observed and modeled monthly discharge volumes are plotted in panels f-g and the statistical distributions of daily discharge volumes are shown as exceedance probabilities in panels k-o. In general the model captures seasonal discharge patterns and monthly variability well (NSE = 0.76-0.9). Discharge is well simulated at the time of year with the largest glacier contribution to discharge, late summer (Aug.-Sept.). A notable shortcoming of the model is evident in January and February low flows in the Cascade River basin. This is likely attributed to our use of a constant non-seasonally varying temperature lapse rate (-8.6 C/km). This strong temperature lapse rate can result in more precipitation falling as snow; hence, there is a complimentary overestimation of June-July discharge. Situated on the west side of the cascade range it is probable that winter temperature lapse rates are weaker [*Minder et al.,* 2010].

4.4.2 Historical Model Testing

To test the model's performance we compared modeled and observed discharge outside of the period for which the calibration was conducted. The test period for the basins ranged from 17-28 years based on available observations. The model results are taken from glacio-hydrological simulations conducted for the entire historical period (presented and analyzed in a later section). The model performance is consistent with the performance during the period of calibration (NSE = 0.78-0.85, Table 4).

Next we compare the hypsometry of modeled and observed glacier area and its change over the course of the historical time period (Figure. 6). For each of the six river basins we composited modeled and observed glacier area into 100 meter elevation intervals for a year early in the historical period (1904-1985) and a recent year (2004-2010). The earliest year was determined by the availability of extent estimates for every glacier in each river basin. For

instance in the Hoh basin estimates of glacier area are available for individual glaciers in the middle of the 21st century (e.g., Blue, Hoh); however, estimates for all glaciers are not available until 1985. The overall shapes of modeled and observed vertical distributions of glacier area compare well (Figure 6). The higher the symmetry in the vertical plots, the better the model performance becomes in predicting glacier area. The total glacier area is reported in the dashed boxes and filled areas for the historical and recent date, respectively. A notable discrepancy is observed in the distribution of glaciers in the Stehekin River basin. While the total area is in agreement (within 1 km^2) the modeled glacier area is greater at lower elevations. The relative amount of modeled area change in each basin shows agreement with the observations, with the largest disagreement seen in the Nisqually River. The largest loss of glacier area occurs in the Nisqually and Hood river basins; however this is due to the longer period of analysis. The least amount of recession is observed and modeled in the Thunder Creek basin, the northern most and highest elevation basin in the sample that does not include a volcano. The lowest elevation basin, the Hoh River, shows a large amount of recession over a relatively short amount of time (1985-2010). This indicates that although it receives more precipitation than the other basins, its elevation profile (hypsometry) made it more sensitive to late 20^{th} century warming.

4.4.3 Historical Role of Glacier Melt

After the model was calibrated and tested against observations, we used the modeling methodology to identify the relative contributions of glaciers in dry season discharge patterns in all of the river basins. We define the glacier contribution to include the melting of glacier ice only (not including snowmelt on glacier surfaces). For consistency, when analyzing patterns of glacier melt and discharge we have limited the beginning of our analysis to 1960, as 1955-1960 is the earliest point of glacier estimates for most of the basins in the sample. Table 5 reports the modeled mean and maximum contribution of glacier melt discharge to summer (July-Sept.) and September only streamflow discharge. The values reported represent discharge ratios at the outlet that we have defined for each basin (Table 5) based on USGS gauging station locations. On average the relative contribution of glacier melt to summer discharge is modest at the basin scale in most cases (2-14%) with the largest contribution of 14% in the Nisqually basin. During September after much of the seasonal snow has melted, the relative contribution increases (6-28%). The maximum contribution to September discharge modeled during this time period is

nearly double the mean value in most cases and was as high as 63% in the Thunder Creek basin. The years of maximum contribution occurred in the late 1980's and early 1990's and for water year 2005. The relative glacier contribution for each basin closely follows the relative glacier cover (Table 1).

The contribution of glacier melt at the basin scale for some of the basins is small, however the contribution is large in upstream tributaries. Figure 7 displays the mean contribution to September discharge volume along the stream network for each of the basins during the period of 1960-2010. The thickness of each stream network segment is scaled by its discharge volume relative to the discharge volume modeled at the outlet of each basin. Glacier contribution increases from warmer to cooler colors starting with red (no glacier contribution) and ending with blue. On average in upstream locations the glacier contribution to September discharge is as high as 66%. This number may appear low because our definition of the glacier contribution is limited to the melting of glacier ice only; seasonal snowmelt still represents a sizable fraction of runoff in high elevation locations in September. There is also strong inter-annual variability in glacier contribution. In years with cold temperatures and high precipitation the relative glacier contribution can be close to zero as the glaciers are covered with snow for most of the year whereas in warm years the limited amount of seasonal snowmelt can increase the relative glacier contribution up to 90% of discharge.

We further the analysis of glacier contribution to September streamflow by relating the relative glacier contribution at each stream network location to the upstream glacier area fraction. We define the upstream glacier area of each network segment using the earliest observed glacier extent estimates and drainage area defined using the DEM. Figure 8 shows the relationship between maximum and mean glacier contribution to September discharge for each stream segment for each of the basins. To emphasize the contribution of glacier melt input in higher order channels that drain sizable areas, stream segments of order 4 or higher are plotted with a larger symbol. The relationship between glacier contribution and upstream area fraction can be broadly described as having two parts. Generally speaking, there is a nonlinear and relatively rapid increase in glacier contribution for area fractions 0-0.2, and a relatively constant slope as upstream glacier area fraction gets larger. The nonlinear portion of the relationship is more pronounced for maximum glacier contributions modeled in September except for the Nisqually Basin.

4.4.4 Projected Glacio-hydrological change: 1960-2099

To identify regional patterns of temporal shifts of glacio-hydrological response over the historical period and to infer how these patterns will evolve through the 21st century we analyzed glacio-hydrology model simulations that encompass the period of 1960-2099. Simulations were initialized from 1915 for the Nisqually and Hood River basins because observed glacier area estimates were available early in the 20th century; however discharge comparisons are limited to the same period as the other basins. For the future period we use projections of 10 CMIP5 global climate model outputs downscaled to the resolution of our historical forcing data ($1/16^\circ$) using the MACA methodology. The GCM models were selected based on the model skill rankings of *Rupp et al.* (2013) who evaluated CMIP5 model outputs for the PNW region. We evaluated two emissions pathway scenarios: RCP4.5, a moderate warming scenario in which emissions stabilize by the end of the 21st century, and RCP8.5, a scenario in which emissions continue to increase through the 21st century. An envelope of predictions for each emissions scenario was developed for each basin through simulations using each downscaled GCM output as model forcing. For regional comparisons we use the mean of the ensemble of predictions to make comparisons between basins. In the following analyses the mean of the ensemble of glacio-hydrologic predictions were normalized for comparisons between basins. Glacier area was normalized to the area in the year 1960 and discharge was normalized to the historical mean (1960-2010).

Figure 9 shows the changes in the annual temperature and precipitation relative to the means of 1960-2010 for scenarios RCP4.5 (solid) and RCP8.5 (dashed). The mean of the ensemble of GCM projections is shown for the future period. The data were smoothed using a 20 year centered mean for clarity. Temperature is projected to increase steadily through the 21st century with the largest changes predicted for the interior basins (Cascade, Thunder, Stehekin) up to 6^{o} C under RCP8.5 by the end of the century. The maritime Hoh river basin is projected to warm the least. In all of the basins precipitation is projected to increase steadily throughout the 21st century. The ensemble of GCM projections indicates increases of up to 10% of historical amounts under both warming scenarios for all basins except the Nisqually and Hood River. The Hoh river displays a strong drying trend over the historical period which is linked to a positive

bias in the meteorological forcing data in the late early 1970s which was also observed in the simulation of glacier mass balance (Section 4.4.1).

In section 4.4.2 we showed that the model was able to capture net changes in glacier area over the historical period. We now show the modeled long-term trajectory of glacier area through 2099 for RCP4.5 and RCP8.5 (Figure 10). The two basins that were modeled starting earlier in the 20th century, Hood and Nisqually, show rapid losses of glacier area until ~1950. This is consistent with observations of glacier area reported in *Jackson and Fountain* (2007) for Mount Hood. In addition to a transitioning of glacier masses away from the glacier states at the end of the Little Ice Age (LIA), this period was also characterized by a warm positive phase of PDO. At mid-century the PDO phase shifted to a cooler, wetter climate and gains in mass and area are modeled in all basins to some extent. After 1980, glacier area declines are pervasive in all basins. The most rapid retreat is observed in the glaciers of the Hoh River basin. The highest elevation basins (Nisqually, Thunder Creek, Hood) display the slowest retreat until 2040 when the retreat increases rapidly. The smallest loss of glacier area is modeled for the Nisqually Basin, the highest of the glaciers studied, located on south-west face of Mt. Rainier (4,392 m).

Next we analyzed the consequences of climate change with respect to summer discharge volumes at the basin scale. We focus on August and September discharge volumes and consider the total amount, the amount from snowmelt and rain to characterize the source of non-glacial water input, the amount from glacier melt, and the relative contribution of glacier melt. The data was normalized to the 1960-2010 mean. Additionally, we used a 20-year centered mean to smooth the modeled time series. RCP4.5 is shown with a solid line and RCP8.5 a dashed line. Continuous declines in total discharge from 1980-2099 are evident in all of the basins (Fig. 11 a,e). The reduction in total discharge is highest in the Stehekin, Cascade, and Thunder basins. This is largely linked to continuous declines in non-glacial sources (snowmelt+rain, Fig. 11 b,f) as these basins have the strongest seasonal snowmelt signature (Fig. 5f-h). The largest decrease in total discharge predicted by the end of the 21st century is during August in these basins under RCP8.5 (~80%).

A more complex pattern is observed in the evolution of glacier melt (Fig. 11 c,g). Toward the end of 1980s, modeled glacier melt begins to decline in the Hoh, Stehekin, and Cascade River basins in both August and September. The slopes of these negative trends are interrupted intermittently until 2030-2040, after which the rate of decline is negative. Glacier

melt in the Hood river basin is predicted to increase until early in the 21st century and decrease thereafter; however its relative contribution is small at the basin scale (Fig. 10 d,h). In the basins at the highest elevations with high initial glacier cover (Nisqually, Thunder) glacier melt decreases in the near future and continuously rises until peaking at mid-century. In the near future (2010-2030) the slowing of declines in glacier melt in the Hoh, Stehekin, Cascade and Hood basins and the reduction in glacier melt in the Thunder and Nisqually is linked to the projected increase in precipitation (Fig. 9). Initially, increased precipitation buffers the effects of moderate amounts of warming projected during this time period. After this period the amount of warming overcomes the increased precipitation and glacier melt continues to decline at a rapid rate for the Cascade, Stehekin, and Hoh basins and increases in the Thunder and Nisqually basins until reaching peaks at mid-century.

Changes in the relative contribution of glacier melt do not always mimic the direction of changes in glacier melt itself. Despite declines in glacier melt in the Hoh, Hood, Stehekin, and Cascade river basins the relative contribution of glaciers increases (remains steady) until about mid-century during August (September) due to more rapid declines in seasonal snowmelt. The relative contribution in August is sustained longer due to the glaciers being exposed earlier in the year following the shifting of the melt season with increasing temperature.

To facilitate comparisons between the basins that are independent of initial upstream glacier cover we analyzed projected September discharge at selected locations in the stream network in each basin with the same upstream glacier cover. The Thunder Creek basin had the highest upstream glacier cover (13.6%, Table 1), hence we selected an upstream network location in each of the 5 other basins with glacier area approximately equal to ~13% of the upstream drainage area. Glacier melt and its contribution declines the fastest in the lowest latitude basin (Hood) and the lowest elevation basin in the northern interior (Cascade; Fig. 11b,c) Interestingly, in the lowest elevation basin in the entire sample (Hoh, Table 1) the reduction the glacier melt and its contribution is moderate until 2040 and 2060 respectively. This basin has the highest amount of precipitation (Table 1) and is projected to experience the least amount of warming (Fig. 9). As noted in the basin scale analysis, glacier melt and its relative contribution in the basin at the highest elevation (Nisqually), and the highest elevation northern basin (Thunder) are projected to increase until after mid-century (2040-2060).

To further demonstrate the multiphased hydrologic response to glacier recession and its effect on trends in discharge, we analyzed the response of modeled September total discharge volumes within the Thunder Creek basin. This basin showed clear increases and decreases in glacier melt through the 21st century (Fig. 11 c,g; Fig. 12 b). Demonstrating the effect of increasing and decreasing amounts of glacier melt we calculated linear trends of total discharge for each stream segment in the basin (Fig. 7) for a period leading to the peak in glacier melt (2011-2050; Fig, 13 a,c) and a period after the peak in glacier melt (2051-2099; Fig. 13 b,d). We used the Sen's slope estimator (Sen, 1968) to calculate trend magnitude and the Mann-Kendall statistic to test statistical significance (p-value < 0.05). The modeled trends for each GCM output simulation are plotted as a function of upstream glacier area. Early in the 21st century negative trends are modeled in segments with low upstream glacier cover (up to ~ -4% yr^{-1}) and increasing trends are modeled in stream segments with the highest upstream glacier cover (up to +2% yr^{-1}; Fig. 13 a,c). During this period increasing discharge from highly glacierized areas offsets and buffers decreasing discharge from areas with low glacier cover. This can be observed in the modeled trajectory of total September discharge (Fig. 11e; 12a). In the second half of the century after glacier melt peaked (Fig. 11c,g; Fig. 12b). Declining glacier melt drives negative trends in total discharge for stream segments with high glacier cover (up to -6% yr^{-1}; Fig. 13 b,d). This analysis provides an example of how changes in glacier melt discharge can both buffer and exacerbate negative trends from declining non-glacial sources (seasonal snowmelt) in high elevation northern basins.

We have focused the analysis on predictions of discharge during the end of the melt season (August, September) when glaciers have the largest contribution at the basin scale and at upstream locations in each basin. However, significant changes are predicted throughout the year as the result of changes in seasonal snowmelt as well as increased precipitation. Figure 14 shows the change in mean monthly discharge composited to three future 30 year time periods (2011-2040, 2041-2070, 2071-2099) for the two emissions pathway scenarios considered. The reported changes in monthly discharge are relative to the modeled mean of 1960-2010 and represent basin scale discharge. The ranges of GCM predictions and the ensemble means are shown. For reference, the historical magnitudes of monthly discharge volumes are presented in Figure 5. The projected changes in discharge are greatest for basins that historically had the largest seasonal snowmelt contribution (Thunder, Cascade, Stehekin). Basins that have more rain derived

discharge (Hood, Nisqually, Hood) show a smaller response. For example, winter flows in the Stehekin basin which were historically low (Fig. 5) are greatly amplified as more winter precipitation occurs as rain. In all basins November-March discharge is predicted to increase as more snow falls as rain, and July – September discharge is predicted to decrease following decreasing seasonal snowmelt and glacier melt. The largest changes to low flows occur in July and August.

4.5 Discussion

We used a physically complex modeling approach to estimate the relative contribution of glaciers to basin scale streamflow over the historical period in select basins of the Pacific Northwest. The relative contribution of glacier melt to streamflow in river basins in the region has also been estimated using simpler observation based approaches. In Chapter 3 we demonstrated agreement between model results and estimates of glacier contribution using geochemical sampling in the Eliot Creek tributary of the Hood River basin [*Nolin et al*., 2010]. In the Hoh River basin *Riedel et al.* (2015) compared the estimated loss of glacier volume over a 23 year period with mean observed discharge and estimated that glacier ice melt represented 7% of Aug.-Sept. discharge on average. In their estimate glacier volume loss was calculated by comparing recent elevation profiles of the lower reaches of 4 glaciers measured by GPS to a USGS DEM representing surface topography in 1987. During this period our model application predicts a higher average relative glacier contribution of 15 (3-30)% in the Hoh River. This difference is likely linked to the model's ability to track and quantify smaller ice masses that would not be well captured in volume estimates reconstructed by comparing a historical DEM with recent spatially sparse ice surface measurements.

The relative glacier contribution has also been estimated in the North Cascades subregion. Using an empirical model that calculates ablation as a function of elevation *Riedel and Larrabee* (2011b) estimated the contribution of glaciers to summer (May – Sept.) discharge to be 32 (21-48)% and 11 (5-23)% for the Thunder Creek, and Stehekin river basins, respectively. In their work, the empirical model was developed based on using point measurements of ablation at 4 glaciers in the North Cascades. Our Thunder Creek and Stehekin River hydrological model applications predicted 7 (2-13)% and 2(1-3)% glacier contribution for May-Sept. streamflow, respectively. The relative contribution estimated by *Riedel and Larrabee*

(2011b) is substantially greater than that predicted by our model. Their estimates include seasonal snowmelt that occurs within the glacier areas which is a large source of water for the period of May-Sept. Our definition of glacier melt is limited to the melting of glacier ice.

Comparing glacier contribution estimates that use different methods highlights a large potential for disagreement between studies. Differences can be attributed to the definition of glacier melt contribution, the period of the year analyzed, spatial representativeness and uncertainty of observations, or uncertainty in numerical model parameters and meteorological input. A major limiting factor of all methods that estimate the relative glacier contribution is that they rely on a limited amount of sparsely measured data to describe processes in these remote high elevation locations. The comparisons between estimates using different methods demonstrate the need for a clear definition of the glacier contribution, as well as a thorough description of data sources and related uncertainties when reporting an estimate of the relative glacier contribution within a river basin.

Few approaches have been applied to predict the consequences of glacier recession on watershed hydrology for century length timescales [e.g. *Immerzeel et al*. 2013; *Ragettli et al*. 2013; *Jost et al*. 2012]. Most hydrological modeling approaches rely on empirical formulations of watershed and snowmelt processes and simplified glacier ice flow or offline predictions of glacier area. Compared to other hydrological modeling approaches, we used more complex representations of watershed hydrology, snow and ice accumulation and melt, and glacier dynamics at a fine spatial resolution. The combination of these complexities provides a more complete representation of the modeled processes and increases the computational demand, required input data, and need for local meteorological calibration. For these reasons, this analysis relied on well calibrated model applications for a small sample of basins to describe the hydrological response of glacierized river basins of the region. Simpler approaches would be more appropriate for hydrological predictions at coarser spatial scales that are spatially continuous across the entire region. However, in the PNW region many of the glaciers are relatively small (average glacier area in the North Cascades was estimated to be 0.35 km^2; Granshaw and Fountain, 2006) and many of the glaciological and topographic features that influence ablation would be lost with applications with simpler models used at coarse spatial resolutions. With ongoing advances of hydrological models of varying complexity, future research should compare different modeling approaches to identify the level of complexity

required for the purpose of the prediction of long-term runoff production of partially glacierized river basins.

4.6 Conclusions

The role of glacier melt in the hydrology of glacierized PNW river basins varies greatly in space and time. Seasonally, glacier melt is highest during the month of September. In years with low seasonal snowmelt and warm summer temperatures, the relative contribution of glacier melt to summer discharge can more than double. The relative contribution of glaciers to dry season discharge is significant even with relatively low glacier cover (~2%). Spatially, within river basins the contribution of glacier discharge increases with increasing upstream glacier area cover until the upstream glacier area is ~15% of the drainage area. With further increase in upstream glacier area fraction, the increase in glacier melt contribution to streamflow becomes relatively small.

Historically glacier area across the PNW US has shown a slow pervasive decline with intermittent slowing and some advances linked with climate variability driven by positive phases of PDO. In the 21st century as the climate continues to warm the frequency and magnitude of these intermittent periods of slower retreat and advance are predicted to decrease and a strong negative trend in glacier area is predicted to be ubiquitous throughout the region. However, these losses in glacier area do not always translate to reductions in glacier melt in the hydrology of river basins across the region. Glacier melt in river basins at high elevations with relatively higher initial glacier cover (e.g., Thunder, Nisqually) is expected to increase well into the 21st century. Elevation and latitude play a dominant control on the characteristic response of river basins to glacier recession as the higher glacier areas will respond later in time.

Irrespective of changes in glacier area, seasonal snowmelt is predicted to decrease commensurate with increases in temperature across the region. In drainage areas that originate in at high elevations with high upstream glacier cover, increased glacier melt and its amplified relative contribution has the potential to buffer the effects of declining seasonal snowmelt on late summer streamflow for some time. However, further downstream in most glacierized river basins declines in glacier melt will further exacerbate negative trends in summer streamflow driven by reductions in seasonal snowmelt.

References

Abatzoglou JT, Brown TJ. 2012. A comparison of statistical downscaling methods suited for wildfire applications. *International Journal of Climatology* **32**(5), 772-780. doi:10.1002/joc.2312

Baraer M, Mark BG, McKenzie JM, Condom T, Bury J, Huh K, Portocarrero C, Gómez J, Rathay S. 2012. Glacier recession and water resources in Peru's Cordillera Blanca. *Journal of Glaciology* **58**, no. 207 (2012): 134-150.

Bernhardt, M., and K. Schulz (2010), SnowSlide: A simple routine for calculating gravitational snow transport, Geophys. Res. Lett., **37**, L11502, doi:10.1029/2010GL043086.

Bohn TJ, Livneh B, Oyler JW, Running SW, Nijssen B, Lettenmaier DP. 2013. Global evaluation of MTCLIM and related algorithms for forcing of ecological and hydrological models. *Agricultural and Forest Meteorology*, **176**, 38-49.

Burns, P. and A. Nolin (2014), Using atmospherically-corrected Landsat imagery to measure glacier area change in the Cordillera Blanca, Peru from 1987 to 2010, Remote Sens. of Environ., 140, 165-178.

Clarke, G. K., A.H. Jarosch, F. S. Anslow, V. Radić, and B. Menounos. 2015. Projected deglaciation of western Canada in the twenty-first century. *Nature Geoscience*, **8**, 372-377, doi:10.1038/ngeo2407.

Cuo L, Beyene TK, Voisin N, Su F, Lettenmaier DP, Alberti M, Richey JE. 2011. Effects of mid-twenty-first century climate and land cover change on the hydrology of the Puget Sound basin, Washington. Hydrological Processes, 25(11), 1729-1753, doi: 10.1002/hyp.7932.

Conway, H., Rasmussen, L. A., & Marshall, H. P. (1999). Annual mass balance of Blue Glacier, USA: 1955–97. Geografiska Annaler: Series A, Physical Geography, 81(4), 509-520.

Cristea, N. C., Lundquist, J. D., Loheide, S. P., Lowry, C. S., & Moore, C. E. (2014). Modelling how vegetation cover affects climate change impacts on streamflow timing and magnitude in the snowmelt‐dominated upper Tuolumne Basin, Sierra Nevada. Hydrological Processes, 28(12), 3896-3918.

Daly C, Neilson P, Phillips DL. 1994. A statistical-topographic model for mapping climatological precipitation over mountainous terrain. *Journal of Applied Meteorology* **33**: 140–158.

Dick, Kristina Amanda, Glacier Change in the North Cascades, Washington: 1900-2009. 2013. Dissertations and Theses. Paper 1062. http://pdxscholar.library.pdx.edu/open_access_etds/1062

Elsner MM, Cuo L, Voisin N, Deems JS, Hamlet AF, Vano JA, Mickelson K, Lee SY, Lettenmaier DP. 2010. Implications of 21st Century climate change for the hydrology of Washington State. *Climatic Change* **102**(1-2) 225-260, doi:10.1007/s10584-010-9855-0

Granshaw, F. D., & Fountain, A. G. 2006. Glacier change (1958–1998) in the north Cascades national park complex, Washington, USA. *Journal of Glaciology*, **52**(177), 251-256.

Immerzeel, W. W., Pellicciotti, F., & Bierkens, M. F. P. 2013. Rising river flows throughout the twenty-first century in two Himalayan glacierized watersheds. *Nature Geoscience*, **6**(9), 742-745.

Jackson KM, Fountain AG. 2007. Spatial and morphological change on Eliot Glacier, Mount Hood, Oregon, USA. *Annals of Glaciology* **46**(1), 222-226.

Jost G, Moore RD, Weiler M, Gluns DR, Alila Y. 2009. Use of distributed snow measurements to test and improve a snowmelt model for predicting the effect of forest clear-cutting. *Journal of Hydrology*, **376**(1), 94-106.

Jost, G., Moore, R. D., Menounos, B., & Wheate, R. 2012. Quantifying the contribution of glacier runoff to streamflow in the upper Columbia River Basin, Canada. *Hydrology and Earth System Sciences*, **16**(3), 849-860.

Laramie, R. L., & Schaake, J. D. (1972). Simulation of the continuous snowmelt process. Ralph M. Parsons Laboratory for Water Resources and Hydrodynamics, Massachusetts Institute of Technology.

Livneh, B,. Rosenberg, A., Lin, C, Nijssen, B., Mishra, V., Andreadis, K.M., Maurer, E.P. and Lettenmaier, D.P. 2013. A long-term hydrologically based dataset of land surface fluxes and states for the conterminous United States: Update and extensions. *Journal of Climate* **26**, (23) : 9384-9392.

Mantua NJ, Hare SR, Zhang Y, Wallace JM, Francis RC. 1997. A Pacific inter-decadal climate oscillation with impacts on salmon production. *Bulletin of the American Meteorological Society* **78**(6), 1069-1079.

Moore RD, Fleming SW, Menounos B, Wheate R, Fountain A, Stahl K, Holm K, Jakob, M. 2009. Glacier change in western North America: influences on hydrology, geomorphic hazards and water quality. *Hydrological Processes* **23**, 1: 42-61.

Naz BS, Frans CD, Clarke GKC, Burns P, Lettenmaier DP. 2014. Modeling the effect of glacier recession on streamflow response using a coupled glacio-hydrological model. *Hydrology and Earth System Sciences* **18**(2), 787-802.

Nylen, T. Spatial and Temporal Variations of Glaciers on Mount Rainier between 1913 and 1994. (2004) (Master's thesis, Portland State University)

Pelto MS. 2008. Impact of climate change on North Cascade alpine glaciers, and alpine runoff. *Northwest Science* **82**(1), 65-75.

Pouyaud, B., M. Zapata, J. Yerren, J. Gomez, G. Rosas, W. Suarez, and P. Ribstein. 2005. On the future of the water resources from glacier melting in the Cordillera Blanca, Peru, *Hydrological Science Journal*, 50(6), 999–1022.

Ragettli, S., Pellicciotti, F., Bordoy, R., & Immerzeel, W. W. 2013. Sources of uncertainty in modeling the glaciohydrological response of a Karakoram watershed to climate change. *Water Resources Research*, **49**(9), 6048-6066.

Ragettli, S., F. Pellicciotti, W. W. Immerzeel, E. S. Miles, L. Petersen, M. Heynen, J. M. Shea, D. Stumm, S. Joshi, and A. Shrestha. 2015. Unraveling the hydrology of a Himalayan catchment through integration of high resolution in situ data and remote sensing with an advanced simulation model. *Advances in Water Resources* **78** (2015): 94-111.

Reid TD, Brock BW. 2010. An energy-balance model for debris-covered glaciers including heat conduction through the debris layer. *Journal of Glaciology* **56**(199), 903-916.

Riedel, J.L., Larrabee, M.A., 2011a. Mt. Rainier National Park Glacier Mass Balance

Monitoring Annual Report, Water Year 2009. North Coast and Cascades Network, National Park Service, Natural Resource Stewardship and Science, Natural Resource Technical Report NPS/NCCN/NRTR-2011/484, Fort Collins, Colorado.

Riedel, J.L., Larrabee, M.A., 2011b. North Cascades National Park Glacier Mass Balance Monitoring Annual Report, Water Year 2009. North Coast and Cascades Network, National Park Service, Natural Resource Stewardship and Science, Natural Resource Technical Report NPS/NCCN/NRTR-2011/483, Fort Collins, Colorado

Riedel, J., Wilson, S., Baccus, W., Larrabee, M., Fudge, T., and Fountain, A. (2015). Glacier status and contribution to streamflow in the Olympic Mountains, Washington, USA. *Journal of Glaciology*, **61**(225).

Sen, P. K. 1968. Estimates of the regression coefficient based on Kendall's tau. *Journal of the American Statistical Association*, **63**(324), 1379-1389.

Spicer RC (1986) Glaciers in the Olympic Mountains, Washington: present distribution and recent variations. (PhD thesis, University of Washington)

Stahl K, Moore RD. 2006. Influence of watershed glacier coverage on summer streamflow in British Columbia, Canada. *Water Resources Research* **42**(6).

Thornton PE, Running, SW. 1999. An improved algorithm for estimating incident daily solar radiation from measurements of temperature, humidity, and precipitation. *Agricultural and Forest Meteorology* **93**(4), 211-228.

Watanabe, S., Kanae, S., Seto, S., Yeh, P. J. F., Hirabayashi, Y., & Oki, T. (2012). Intercomparison of bias‐correction methods for monthly temperature and precipitation simulated by multiple climate models. Journal of Geophysical Research: Atmospheres (1984–2012), 117(D23).

Wigmosta, M. S., L. W. Vail, and D. P. Lettenmaier (1994), A distributed hydrology-vegetation model for complex terrain, Water Resour. Res., 30, 1665–1679.

Wigmosta, M.S., B. Nijssen, P. Storck, and D.P. Lettenmaier, 2002: The Distributed Hydrology Soil Vegetation Model, In Mathematical Models of Small Watershed Hydrology and Applications, V.P. Singh, D.K. Frevert, eds., Water Resource Publications, Littleton, CO., p. 7-42.

Yapo, P. O., H. V. Gupta, S. Sorooshian, Multi-objective global optimization for hydrologic models. 1998. *Journal of Hydrology*, 204, 83–97.

Tables

Table 1: Characteristics of the river basins included in the regional analysis.

Basin	Drainage Area [km^2]	M.A.P. [mm]	Mean Elev. [m]	Max Elev. [m]	Glacier Area [km^2]	Glacier Cover [%]
Cascade	440	2370	1270	2660	16.3 (1960[3]) – 11.9 (2010[4])	2.7-3.7
Hoh	640	3830	775	2370	23.7 (1985[5]) – 18.0 (2009[2])	2.8-3.7
Nisqually	360	2300	1240	4380	26.4 (1913[6]) – 18.2 (2009[4])	5.0-7.3
Stehekin	830	1700	1630	2110	24.2 (1960[1]) – 18.7 (2010[2])	2.3-2.9
Thunder	270	2220	1570	2740	36.8 (1960[1]) – 32.1 (2010[7])	11.9-13.6
Hood	880	1800	927	3400	6.7 (1904[8]) - 4.6 (2004[7])	<1

[3] Granshaw and Fountain
[4] Landsat NDSI derived
[5] Spicer, 1985
[6] Andrew Fountain, unpublished
[7] Dick, 2013
[8] Jackson and Fountain (2007)

Table 2: Data utilized as model input and for model verification.

Data	Organization/Description	Data Source
Model Input		
Digital Elevation Model	Shuttle Radar Topography Mission (SRTM) 30m	http://www.opentopography.org/
Soil Texture	NRCS STATSGO2	http://www.nrcs.usda.gov/
Vegetation	National Land Cover Database (NLCD 2011)	http://www.mrlc.gov/nlcd2011.php
1981-2010 Precipitation Normals	800 m, PRISM Climate Group	http://www.prism.oregonstate.edu/
Historical Meteorological Data	Livneh et al. (2013)	http://maca.northwestknowledge.net
Future Meteorological Data	MACA Downscaled CMIP5 GCM Output	http://maca.northwestknowledge.net
Model Verification		
Glacier Area	Glacier Research at Portland State University	Dick (2013); Nylen (2002); Spicer (1986)
Glacier Area	Landsat CDR NDSI derived Snow/Ice Extent	http://earthexplorer.usgs.gov/
Glacier Mass Balance	National Park Service	Riedel and Larrabee (2011)
Glacier Mass Balance	United States Geological Survey	http://www.usgs.gov/climate_landuse/clu_rd/glacierstudies/default.asp
Glacier Mass Balance	University of Washington	http://earthweb.ess.washington.edu/Glaciology/projects/blue_glac/mass_balance.htm
Discharge	United States Geological Survey Stream Gauging	http://waterdata.usgs.gov/nwis/
Snow Water Equivalent	NRCS Snow Telemetry (SNOTEL)	http://www.wcc.nrcs.usda.gov/snow/
1981-2010 Temperature Normals	800 m, PRISM Climate Group	http://www.prism.oregonstate.edu/

Table 3: Optimal Parameters found through mass balance calibrations of individual glaciers. P. Multi is the precipitation multiplier, MaxSnow α is the maximum albedo of snow used in temporal decay curves**,** Glacier α is glacier albedo, and Rl is the aerodynamic roughness length over snow and ice.

Glacier	**Basin**	**P. Multi**	**Tlapse** [°C km^{-1}]	**MaxSnow** α	**Glacier** α	**Rl [mm]**
South Cascade	Cascade	1.00	-8.6	0.88	0.36	0.91
N. Klawatti	Thunder	0.99	-9.8	0.88	0.33	1.50
Sandalee	Stehekin	3.47	-7.2	0.9	0.42	2.02
Nisqually	Nisqually	1.01	-4.4	0.81	0.32	7.17
Blue	Hoh	1.34	-6.2	0.87	0.39	3.81

Table 4: Performance of modeled discharge during outside of the calibration period. Nash Sutcliffe Efficiency (NSE) was calculated on monthly interval time series.

Basin	**NSE**	**Period**
Cascade	0.78	1962-1979
Thunder	0.85	1961-1989
Stehekin	0.85	1961-1989
Nisqually	0.85	1961-1991
Hoh	0.84	1989-2010

Table 5: Mean and maximum modeled glacier contribution to summer (July-September) and late summer (September) discharge volumes for the period 1960-2010.

	July-September		***September***	
Basin	$\text{mean}(Q_g / Q_{tot})$	$\max(Q_g / Q_{tot})$	$\text{mean}(Q_g / Q_{tot})$	$\max(Q_g / Q_{tot})$
Cascade	0.05	0.13	0.15	0.54
Hoh	0.09	0.22	0.14	0.39
Nisqually	0.14	0.28	0.24	0.42
Stehekin	0.04	0.11	0.12	0.36
Thunder	0.12	0.27	0.28	0.63
Hood	0.02	0.07	0.06	0.11

Figures

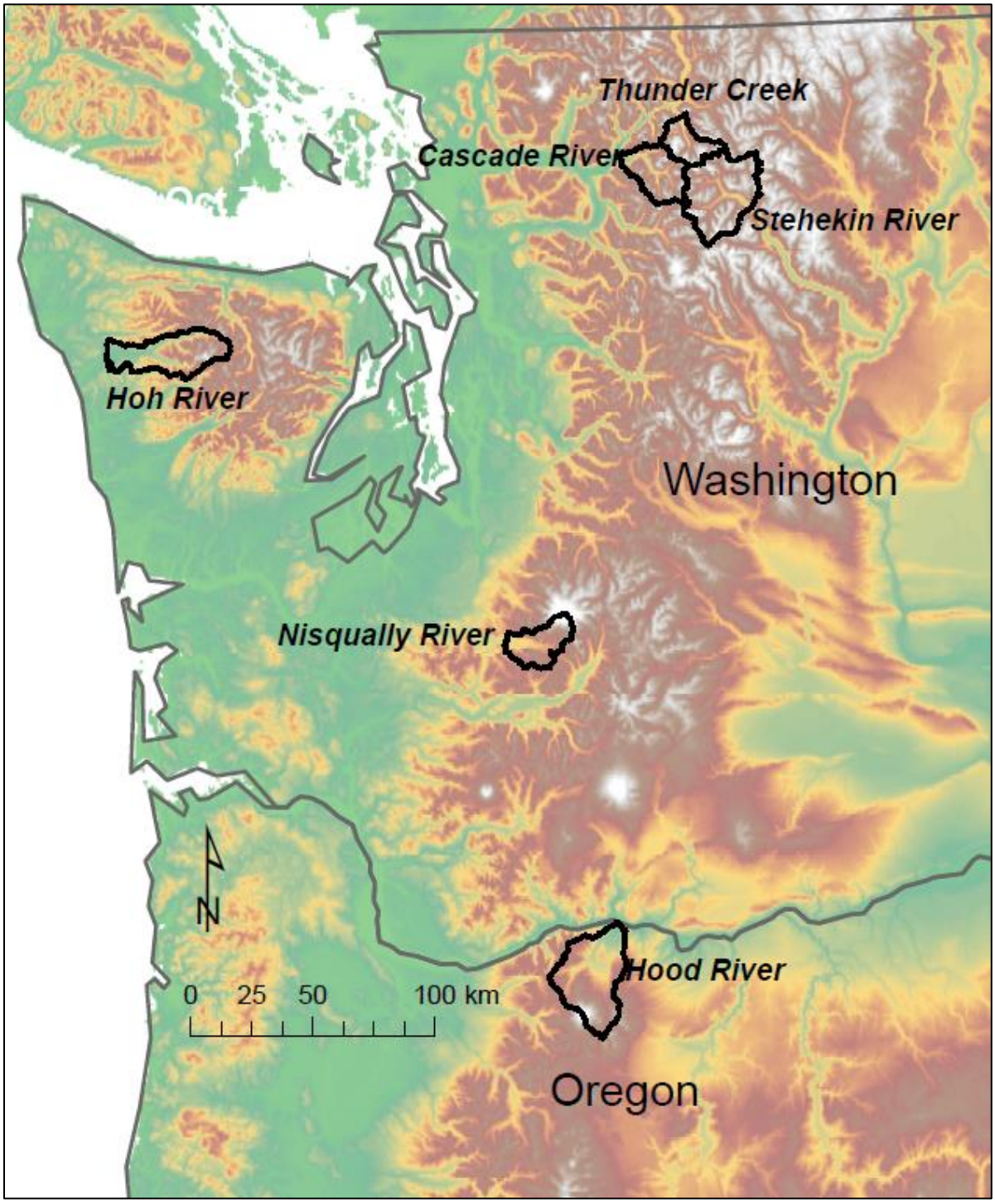

Figure 1: Location of river basins included in the regional analysis. The basin drainage areas are defined with black lines.

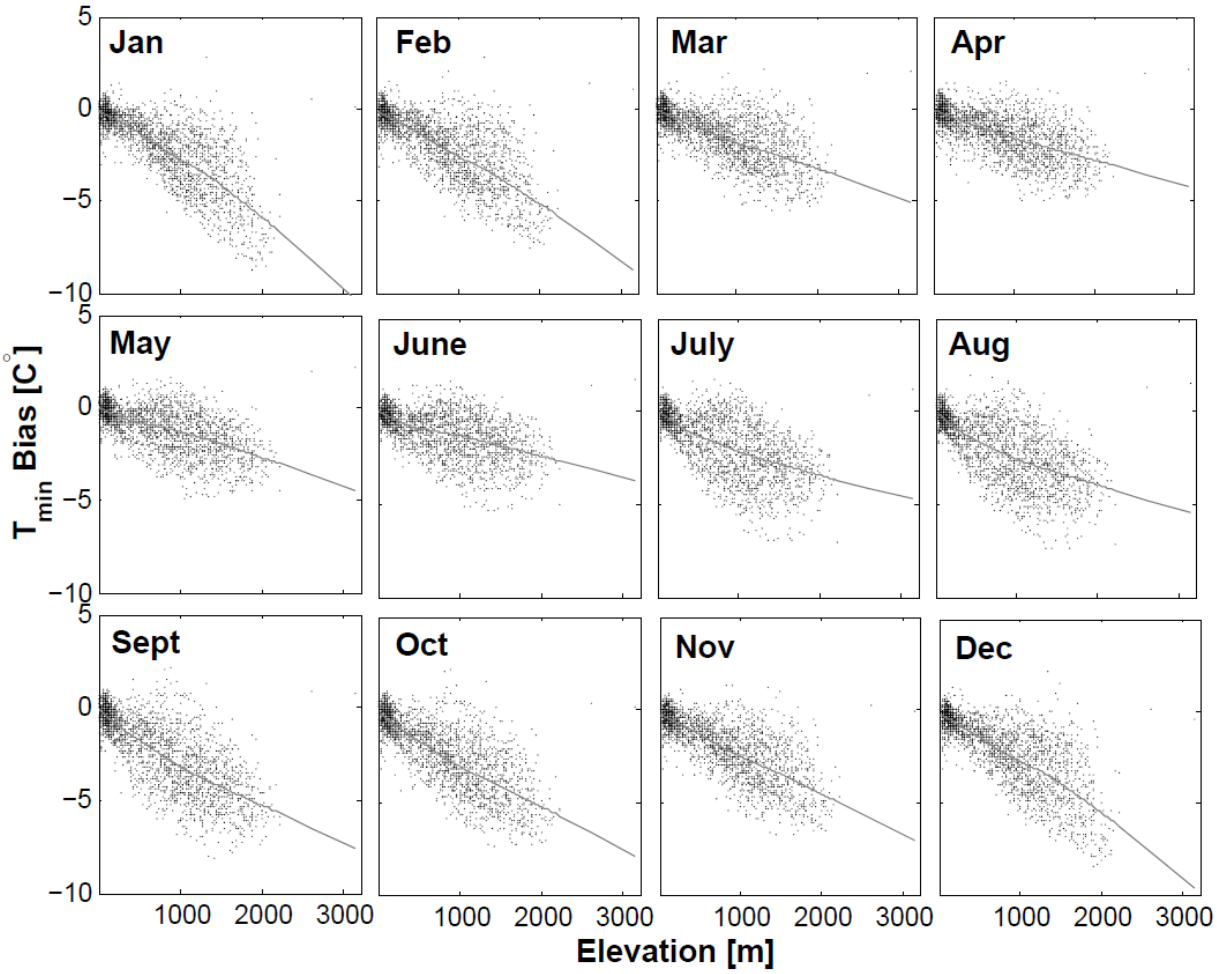

Figure 2: Bias as a function of elevation of Livneh et al. (2013) 1981-2010 monthly mean minimum air temperature as compared to PRISM normals for the domain bounded by latitudes 46.53125,49.28125 and longitude -124.46875,-120.03125. LOWESS fit is shown with a solid gay line.

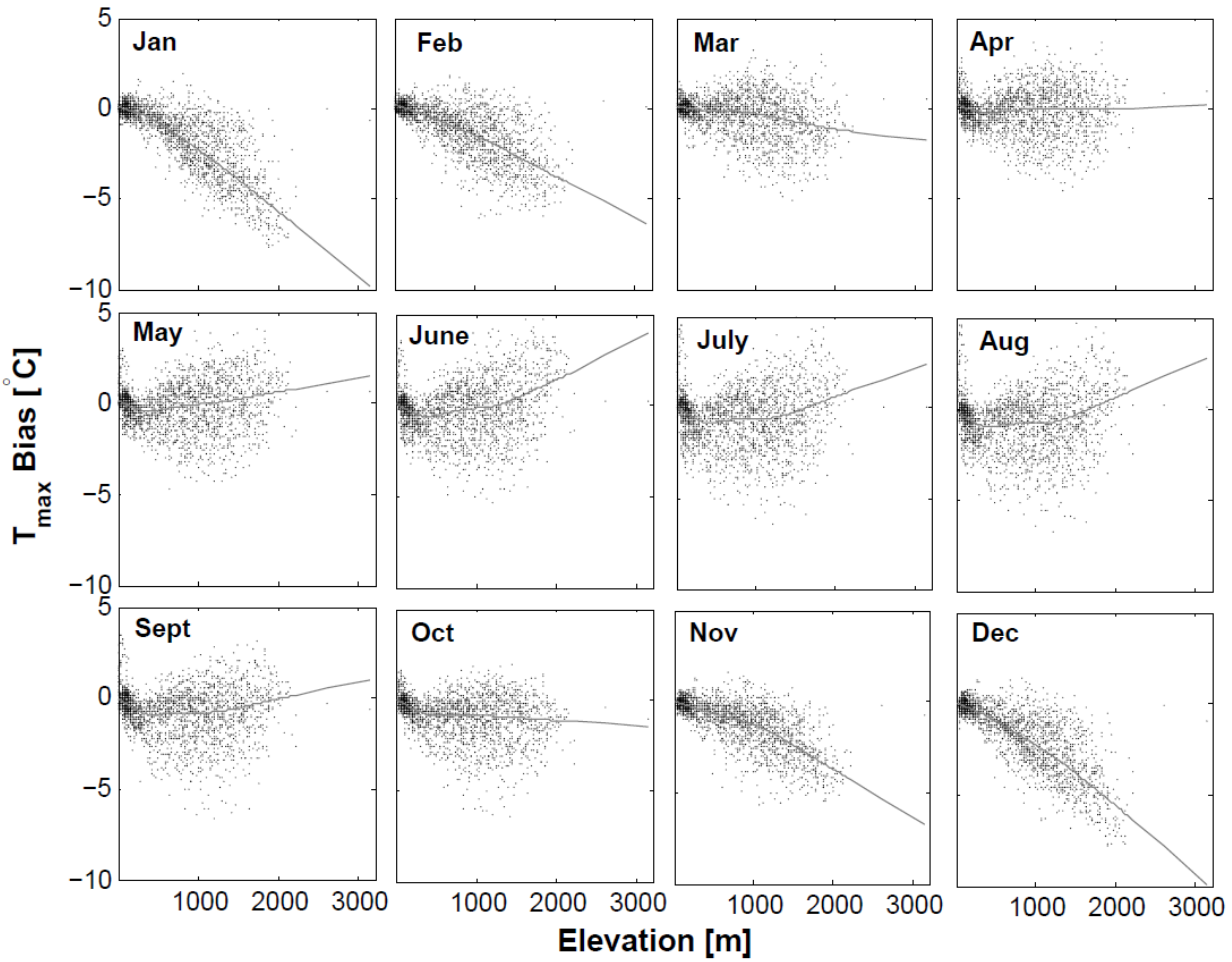

Figure 3: Bias as a function of elevation of Livneh et al. (2013) 1981-2010 monthly mean maximum air temperature as compared to PRISM normals for the domain bounded by latitudes 46.53125,49.28125 and longitude -124.46875,-120.03125. LOWESS fit is shown with a solid gay line.

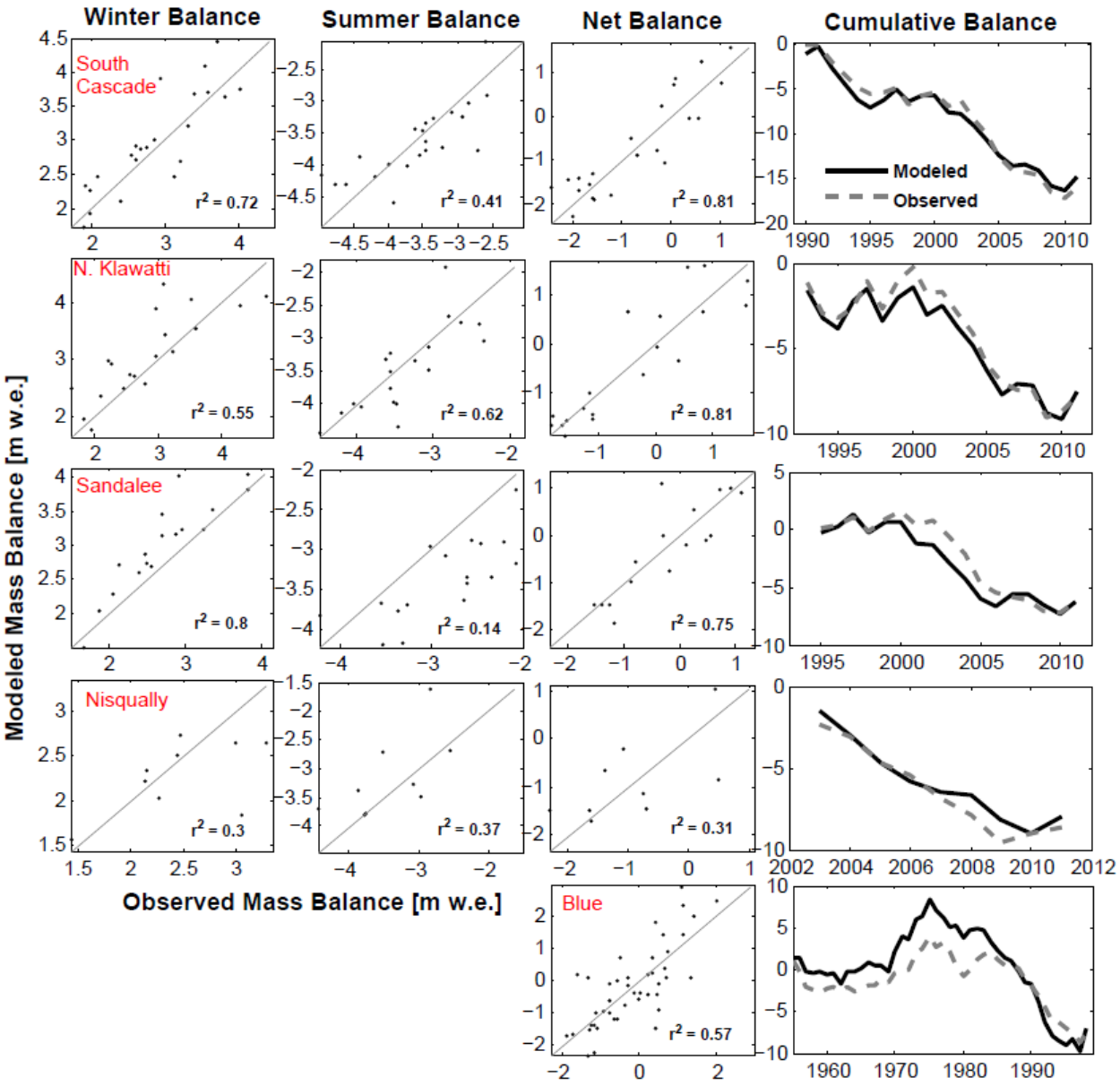

Figure 4: Simulated and observed glacier mass balance during the calibration time periods.

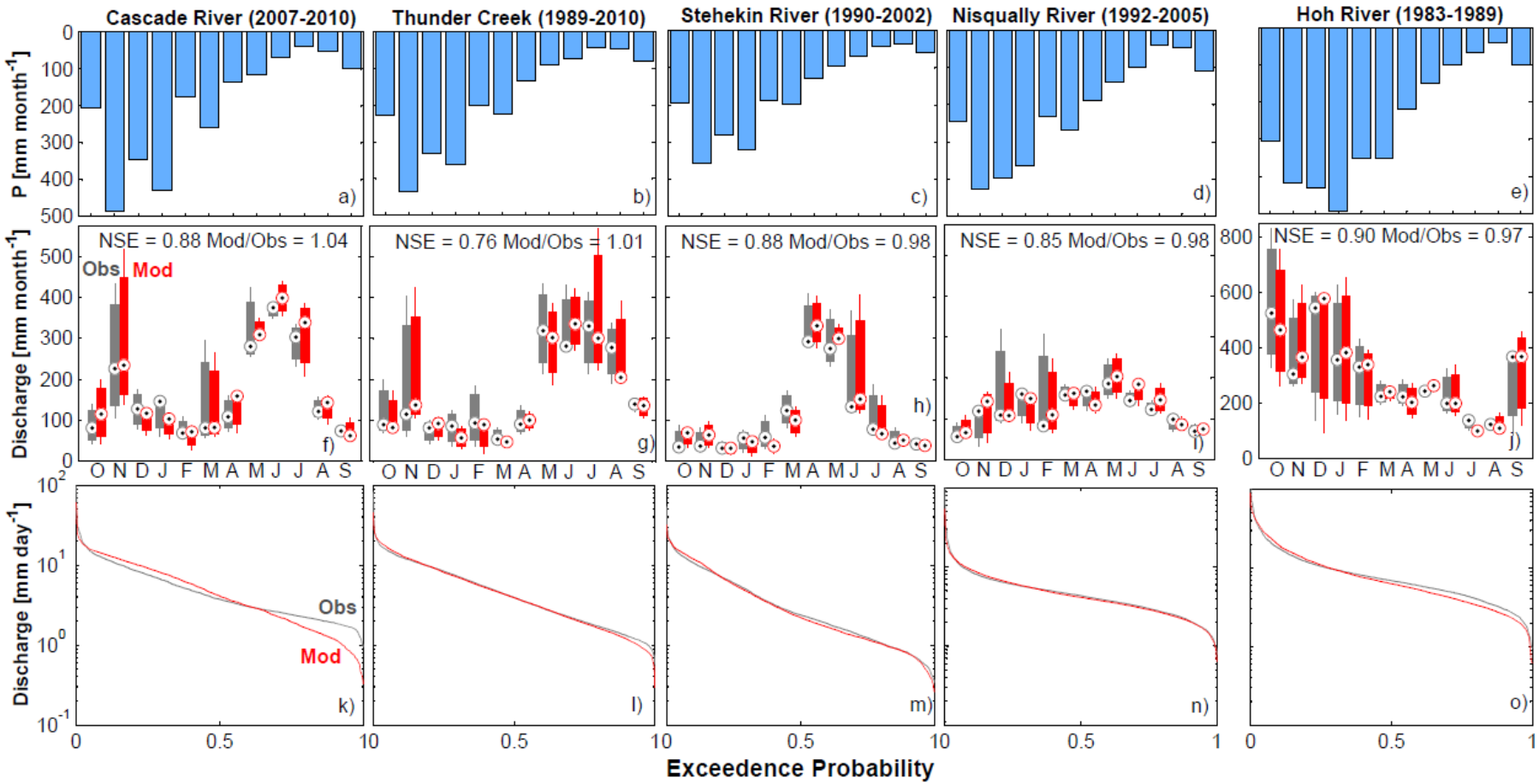

Figure 5: (a-e) Monthly mean precipitation, (f-j) modeled and observed monthly distributions of discharge, and (k-o) modeled and observed exceedance probabilities of daily discharge for each river basin during the calibration periods.

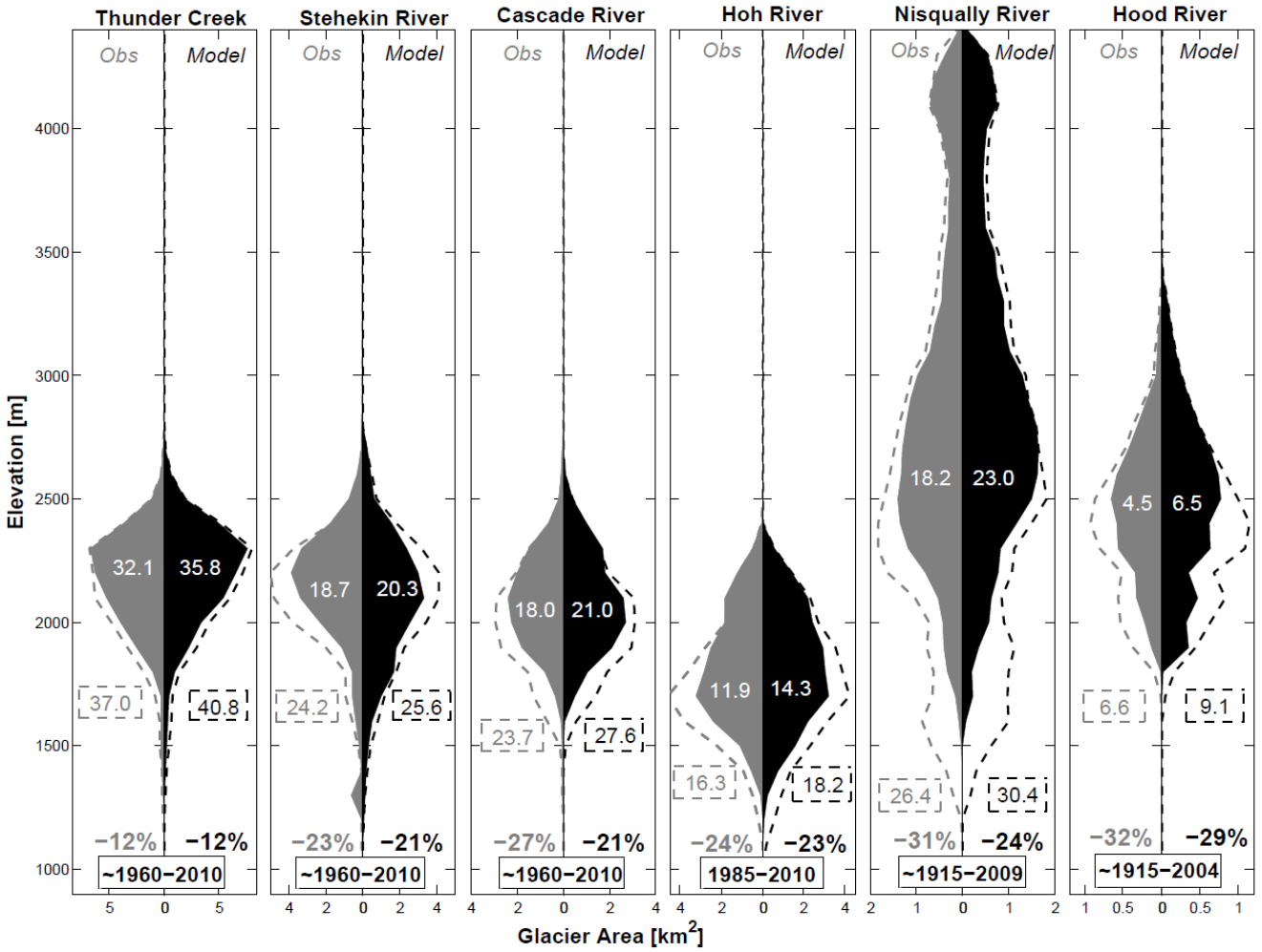

Figure 6: Observed and modeled distributions of glacier area with elevation for historical (dashed) and recent (filled) periods of time. The period of analysis varies between basins and is reported at the bottom of each plot. For reference the historical and recent total glacier area (km ^{2}) is reported in the dashed boxes and filled areas, respectively. The relative change in in glacier area is reported as a % over the period of analysis at the bottom of each plot.

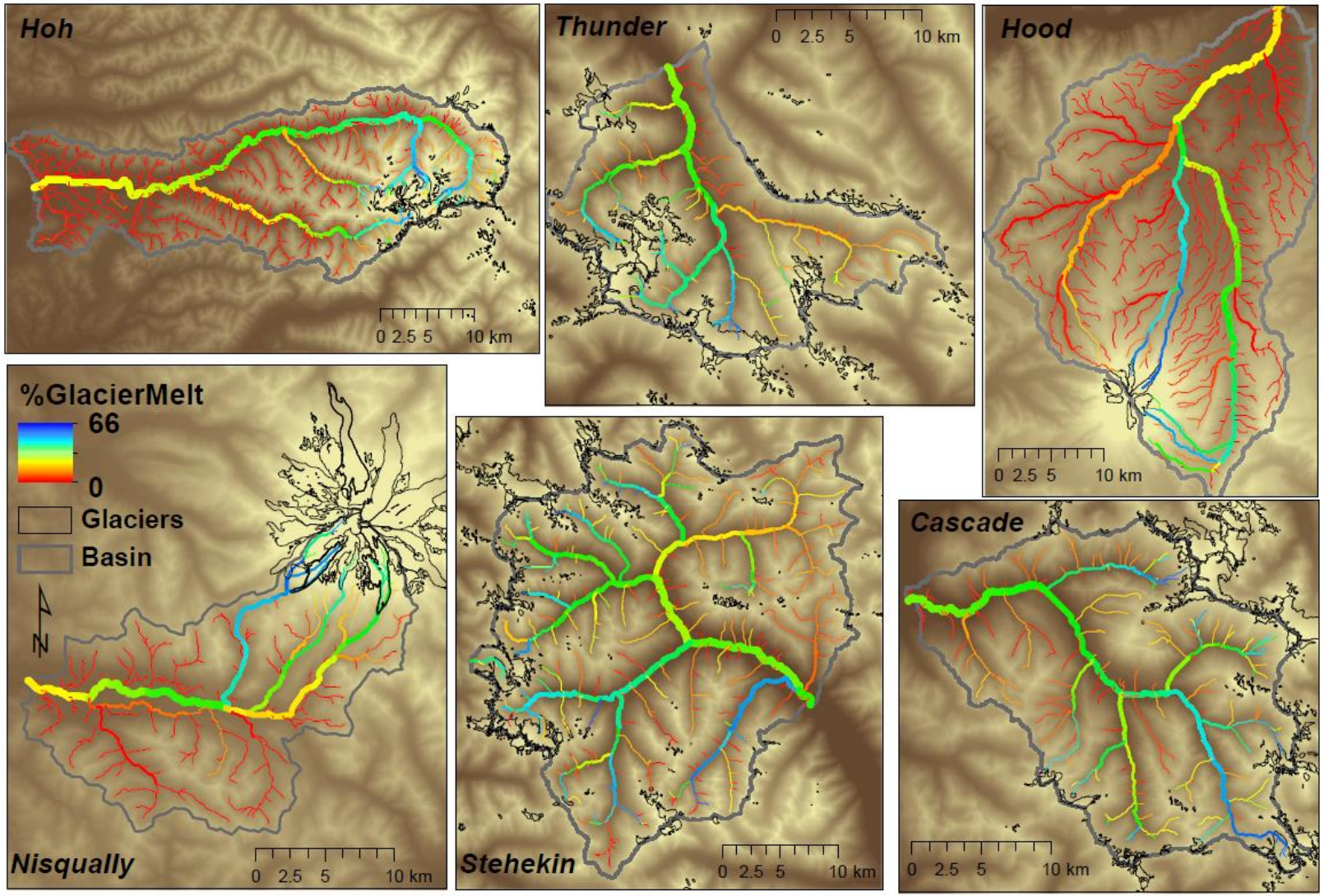

Figure 7: Mean percent glacier contribution to streamflow in September along the stream network of each basin the sample. Network segment width is scaled by its discharge volume relative to discharge at the outlet.

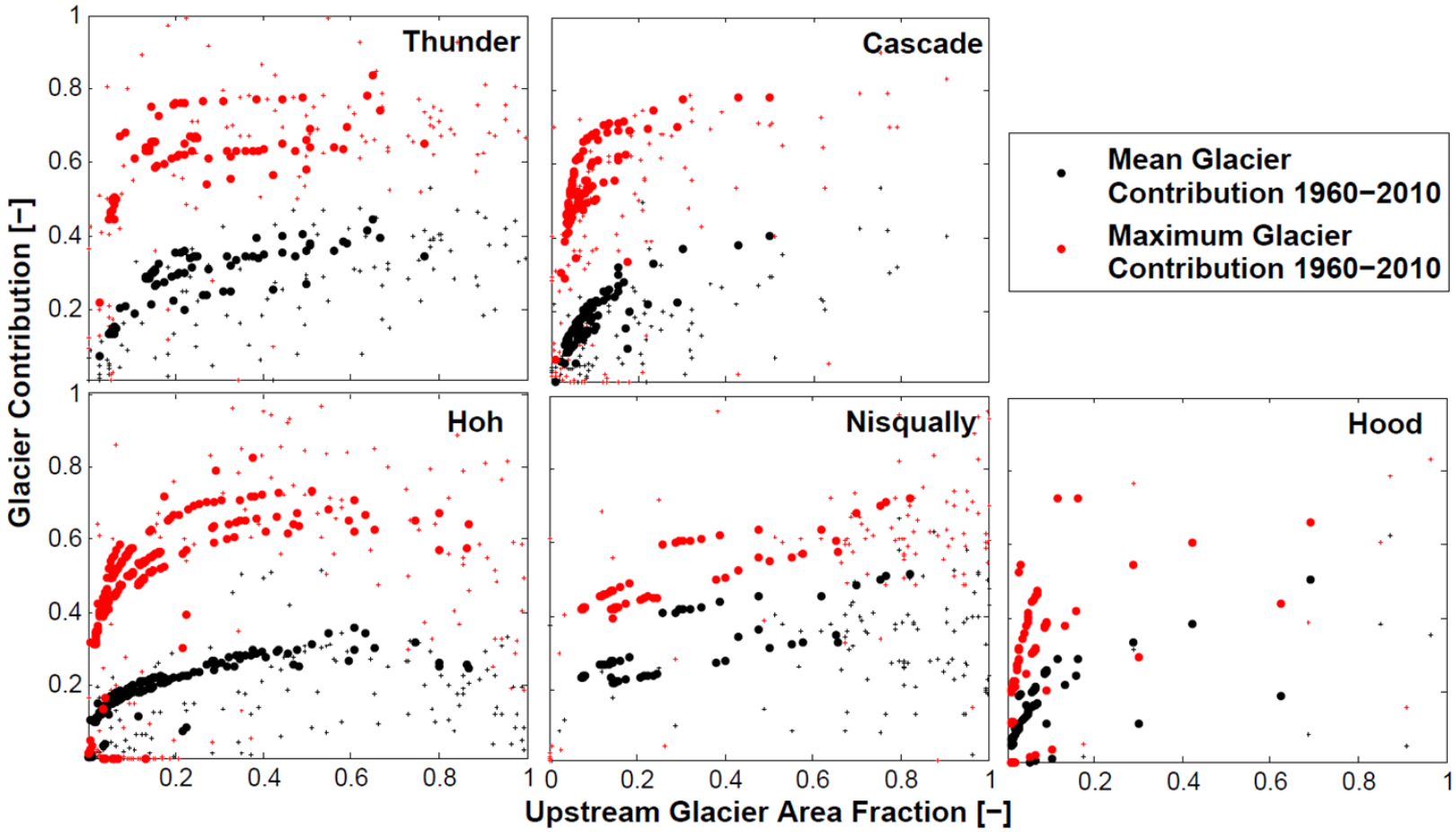

Figure 8: The mean and maximum glacier contribution to September discharge for each stream network segment as a function of upstream glacier area. The upstream glacier area is defined from the earliest observed estimate during the period of analysis. Stream segments with order greater than 4 are shown with large circles.

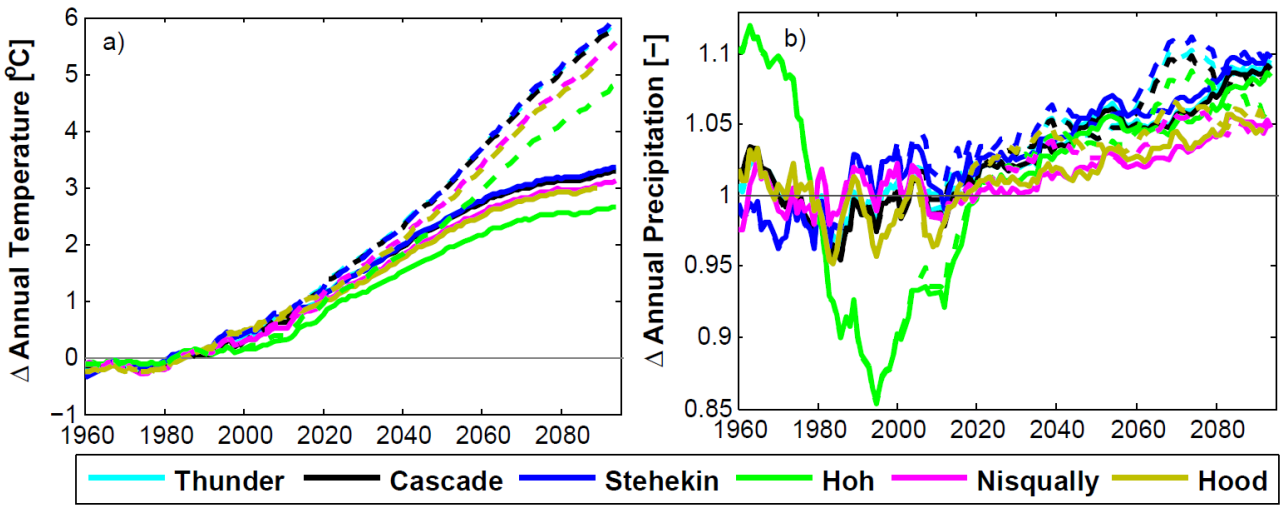

Figure 9: Historical and projected changes in (a) annual temperature and (b) precipitation with respect to the 1960-2010 mean presented as a 20 year centered mean. The ensemble mean of 10 downscaled GCM model outputs is shown for clarity. RCP4.5 is represented with solid lines and RCP8.5 is shown with dashed lines.

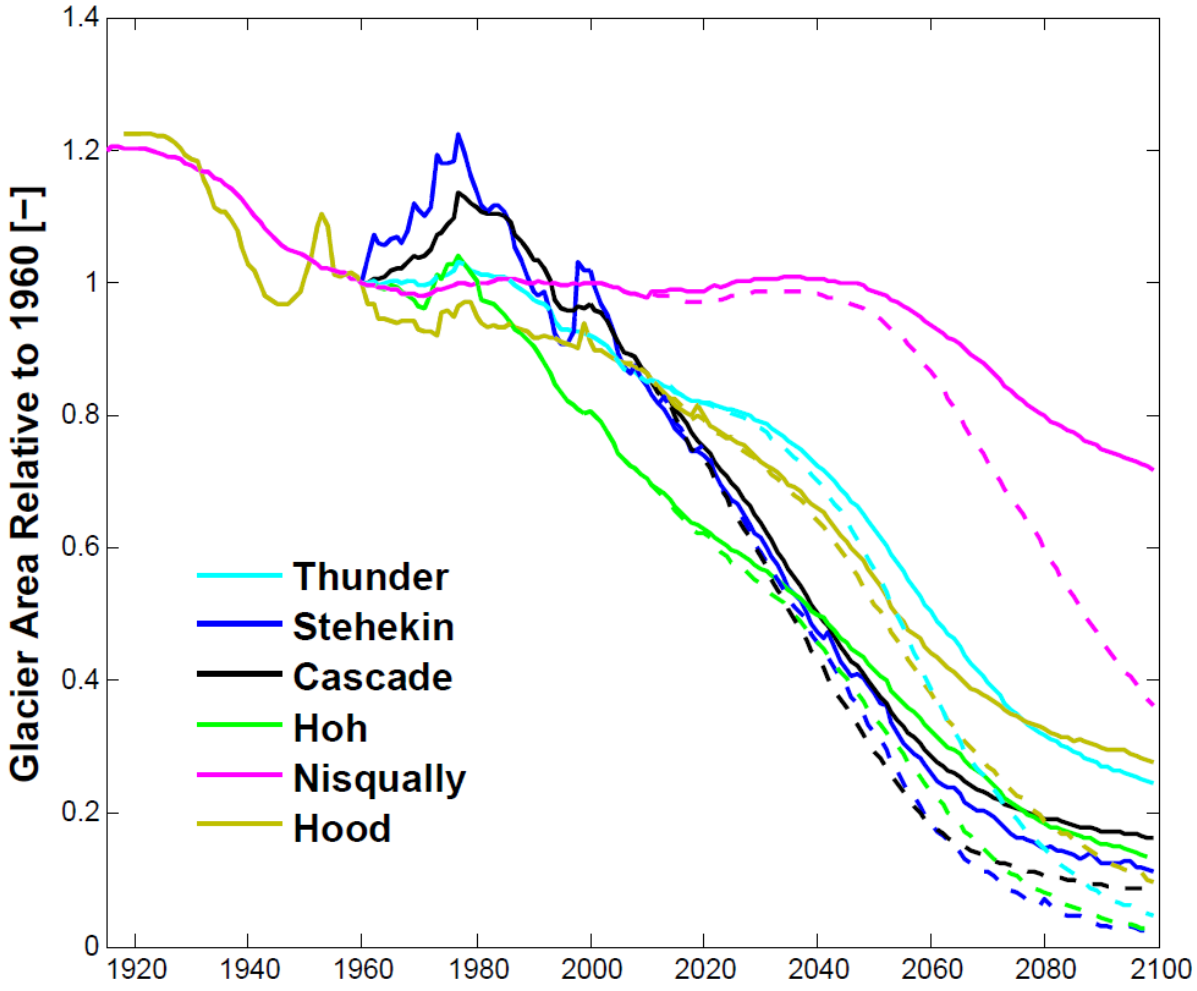

Figure 10: Modeled glacier area for the river basins. Solid lines represent the historical and ensemble mean of RCP4.5 scenario and the dashed lines represent the ensemble mean of RCP8.5.

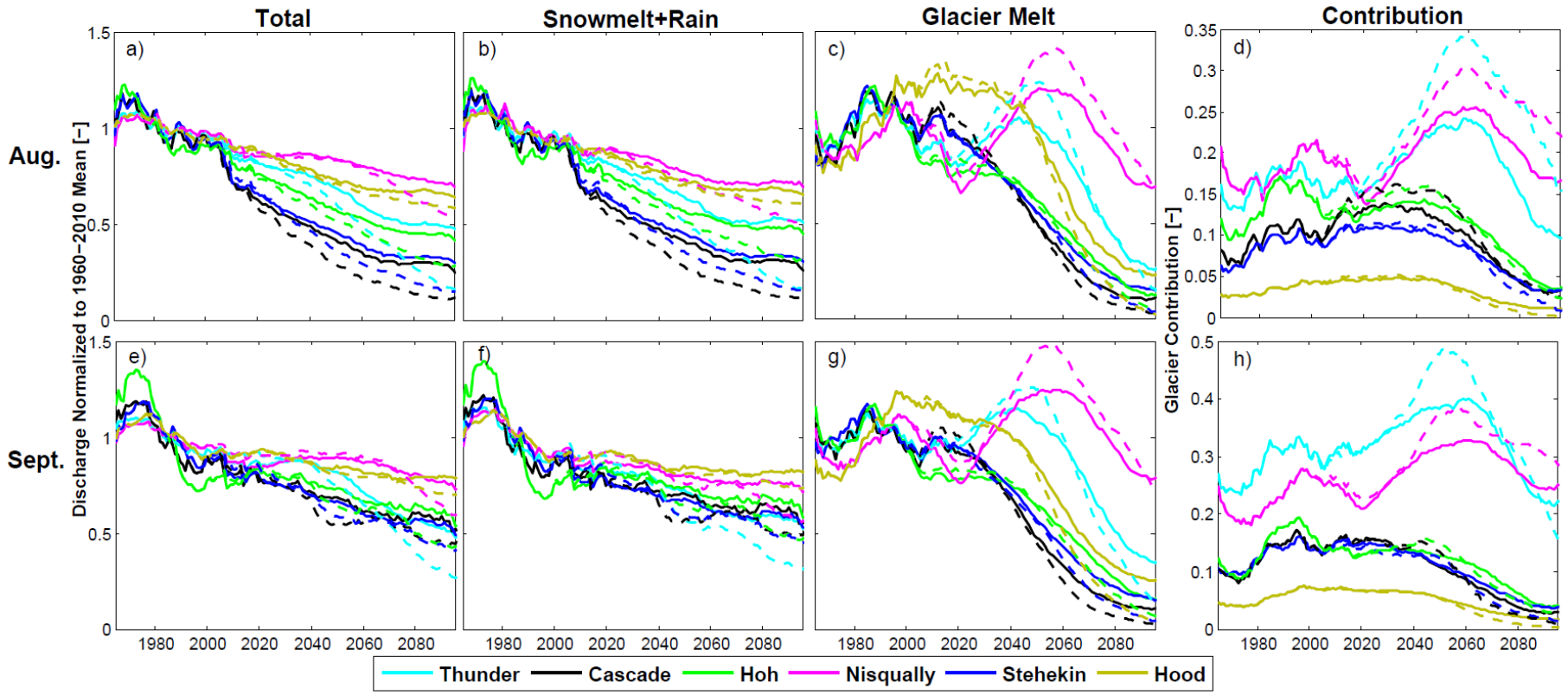

Figure 11: 20-year centered mean of (a,e) modeled total discharge, (b,f) Sum of Snowmelt and Rain normalized to 1960-2010 mean, (c,g) glacier melt, and (d,h) the relative contribution of glacier melt. Solid lines represent the historical and ensemble mean of RCP4.5 scenario and the dashed lines represent the ensemble mean of RCP8.5.

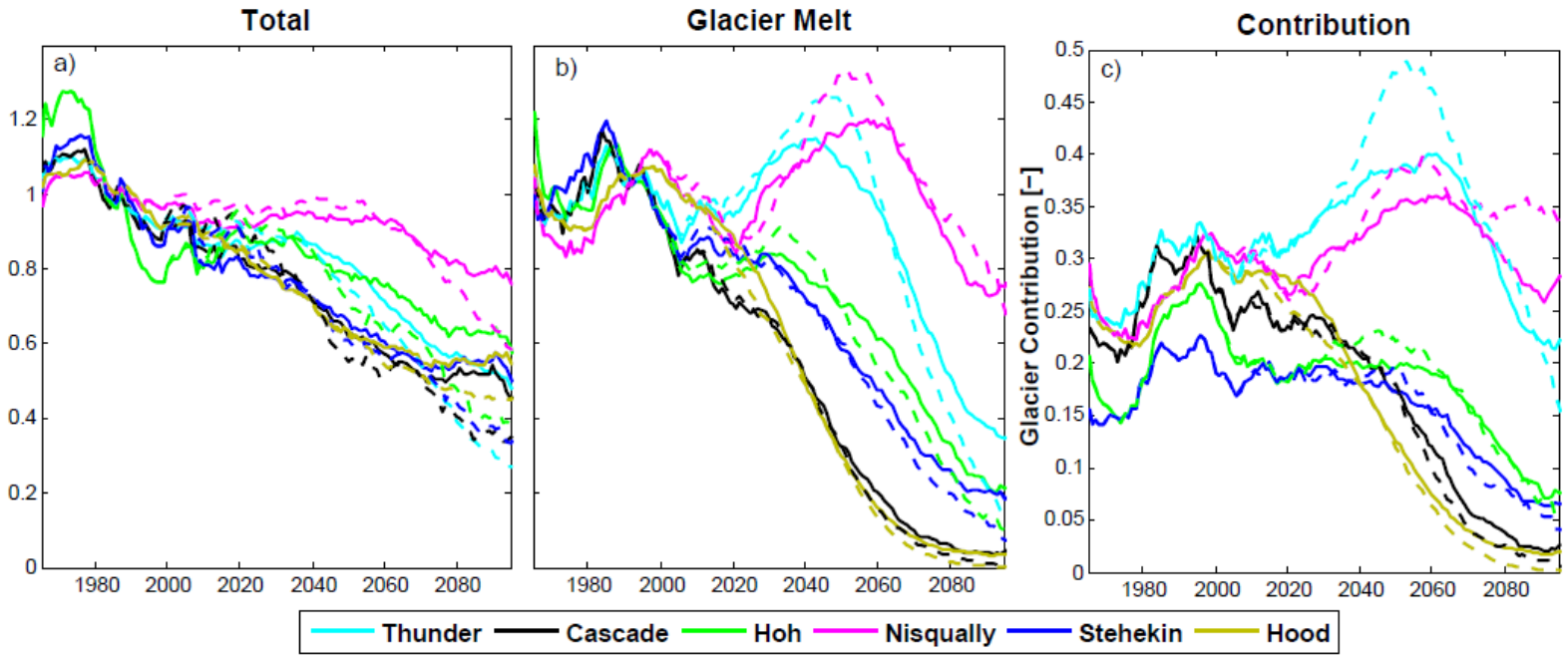

Figure 12: (a) Projected total discharge, (b) glacier melt, and (c) glacier contribution for a stream location on the main channel in each basin that had ~13% initial glacier cover.

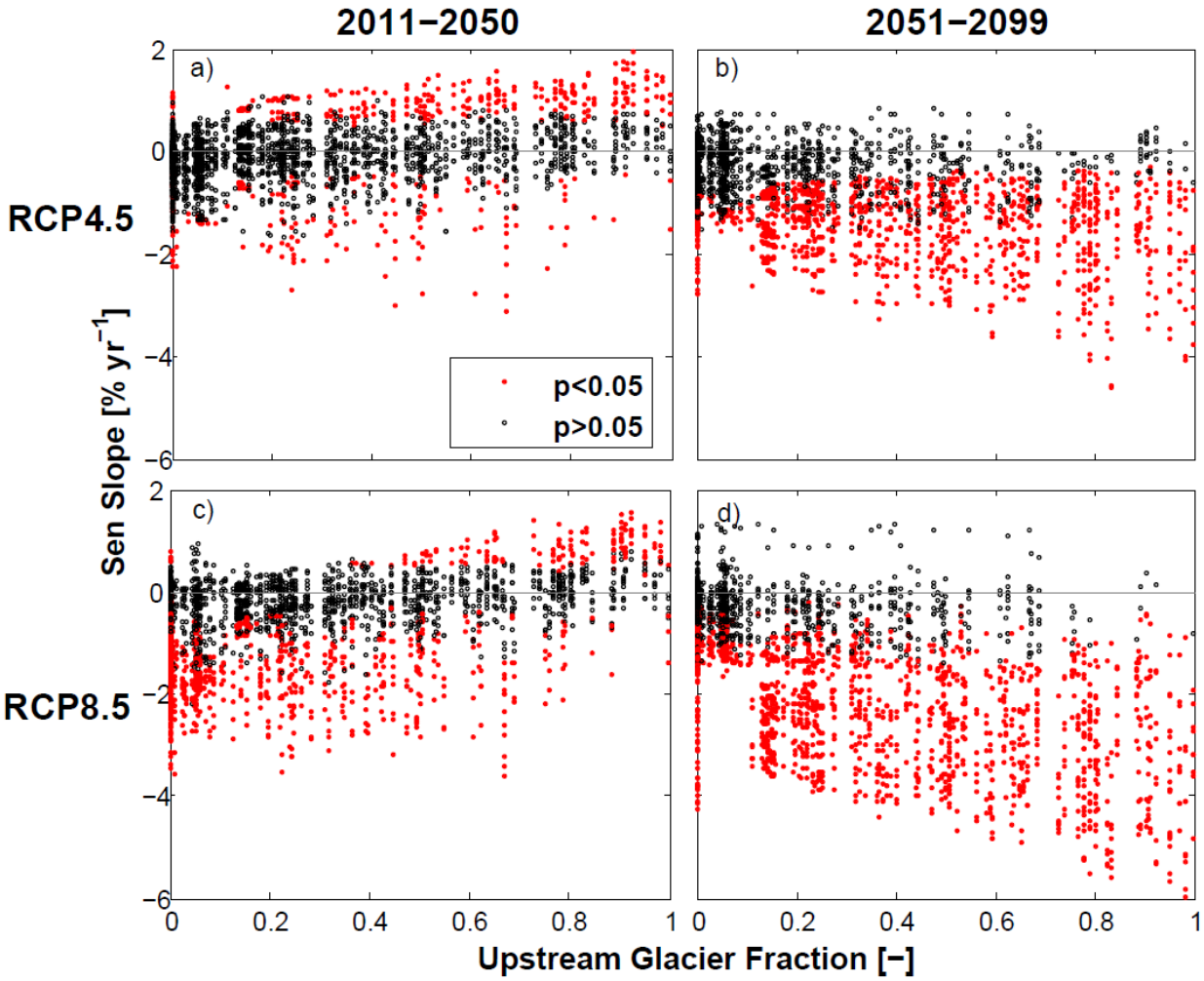

Figure 13: Linear trends in modeled September discharge volumes in each stream network segment in the Thunder Creek Basin for each of the 10 GCM model scenarios as a function of upstream glacier area. Trends were calculated using the Sen's slope estimator for the periods of (a,c) 2011-2050 and (b,d) 2051-2099. Trends with statistical significance (p-value < 0.05) are denoted with filled red circles and trends that are not statistically significant (p-value > 0.05) and shown with hollow black circles. Historical observed glacier area (~1960; Dick, 2013) was used to index upstream glacier area.

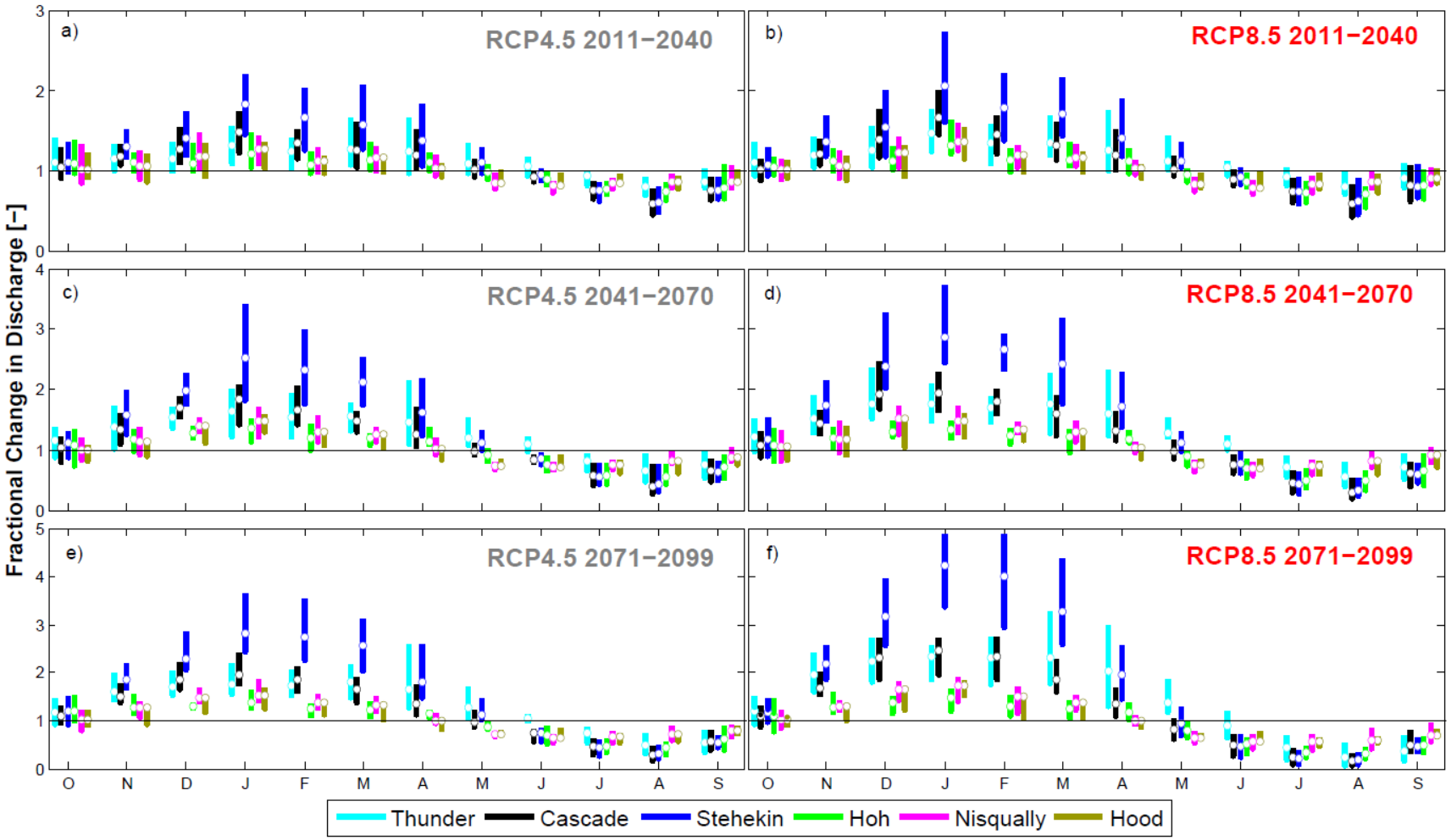

Figure 14: Projected changes in monthly discharge volume. The relative change in discharge is presented as a fraction of the modeled mean value of 1960-2010. The range of GCM scenarios is depicted with vertical lines and the ensemble mean with hollow circles.